FEBRUARY 1961 VOLUME 10 (1961) No. 2

GREGG M. SINCLAIR LIBRARY
UNIVERSITY OF HAWAII
8-7-63

NUCLEAR INSTRUMENTS & METHODS

A JOURNAL ON ACCELATORS, INSTRUMENTATION AND TECHNIQUES IN NUCLEAR PHYSICS

EDITOR: K. SIEGBAHN - UPPSALA

CONTENTS

H. FAUSKA, J. W. ORTH and F. H. SCHMIDT, Fixed frequency cyclotron operation with a regulator for dee voltage stabilization 73

A. V. COHEN, J. A. COOKSON and J. L. WANKLING, A magnetic particle spectrometer for use with a 12 MeV tandem electrostatic generator 84

L. HÖGBERG and K. VOGEL, Experiments with electrodeless generation and acceleration of plasma rings 95

LUDWIG MEYER, Die Bildungsgeschwindigkeit von Nebelspuren in der Nebelkammer . . . 108

R. BENAROYA and W. J. RAMLER, Deflection coil for an external accelerator beam 113

J. CSIKAI, E. MOLNAR and B. SCHLENK, Investigations about the critical radius of the BF_3 counters 121

ÅKE SVANHEDEN, A cold cathode ion source for a synchrocyclotron 125

TORBJÖRN WESTERMARK, A double-focusing magnetic spectrometer for studies of energy losses in matter of electrons from a 5 MeV betatron 129

TORBJÖRN WESTERMARK, Energy distribution and energy stability of the electron beam from a 5 MeV betatron 145

BENT ELBEK and MICHIYUKI NAKAMURA, Multichannel detector for use in particle spectrometers 164

NORTH-HOLLAND PUBLISHING COMPANY — AMSTERDAM

NUCLEAR INSTRUMENTS AND METHODS

A journal on accelerators, instrumentation and techniques in nuclear physics

EDITOR: K. SIEGBAHN, UPPSALA

EDITORIAL BOARD:

J. B. ADAMS (CERN)
F. A. ALSINA (Buenos Aires)
E. AMALDI (Rome)
H. L. ANDERSON (Chicago)
K. T. BAINBRIDGE (Cambridge, Mass.)
P. R. BELL (Oak Ridge)
R. E. BELL (Montreal)
A. BERTHELOT (Saclay)
H. BRINKMAN (Groningen)
E. H. COOKE–YARBOROUGH (Harwell)
S. DE BENEDETTI (Pittsburgh)
M. DE HEMPTINNE (Louvain)
A. DE-SHALIT (Rehovoth)
M. DEUTSCH (Cambridge, Mass.)
S. DU TOIT (Pretoria)
B. S. DŽELEPOV (Leningrad)
W. GENTNER (Heidelberg)
P. C. GUGELOT (Amsterdam)
H. HALBAN (Paris)
O. HAXEL (Heidelberg)
P. HUBER (Basel)
S. KIKUCHI (Tokyo)
J. KOCH (Copenhagen)
M. S. KOZODAEV (Moscow)
S. LIVINGSTON (Cambridge, Mass.)
E. M. MCMILLAN (Berkeley)
M. G. MEŠČERJAKOW (Moscow)
P. B. MOON (Birmingham)
M. L. OLIPHANT (Canberra)
W. PAUL (Bonn)
A. S. RAO (Bombay)
G. SALVANI (Rome)
P. SAVIĆ (Belgrade)
P. SCHERRER (Zürich)
CH. SCHMELZER (CERN)
R. TANGEN (Oslo)
D. TAYLOR (Northampton)
V. I. VEKSLER (Moscow)
G. VON DARDEL (CERN)
O. WERNHOLM (Stockholm)
R. R. WILSON (Cornell)
S. D. WINTER (Saclay)

INSTRUCTIONS FOR CONTRIBUTORS

Contributions may be sent to the Editor, Professor K. Siegbahn, Institute of Physics, University of Uppsala, Sweden, either directly or through the intermediation of one of the members of the Editorial Board. Contributions may be written in English, French or German but should always, except for very short papers, be supplied with a brief abstract in English. Figures should be inked original drawings or glossy prints and they should be sufficiently large. Contributors should make sure that important details in drawings and photographs will show up clearly in the diminished copy used by the publisher.

Books for review should be sent to Professor Siegbahn.

Objective and descriptive material on endeavours and product developments from the industry for the section "Spotlight on Industry" should be sent directly to the publishers, North-Holland Publishing Company, P.O. Box 103, Amsterdam.

Nuclear Instruments and Methods is published monthly. The subscription price of a volume of about 360 pages is $ 17.00 (130 s), postage free.

Subscriptions should be sent to the publishers, North-Holland Publishing Company, P.O. Box 103, Amsterdam, or to any subscription-agent.

No part of this issue may be reproduced in any form, by print, photoprint, microfilm or any other means without written permission from the publisher.

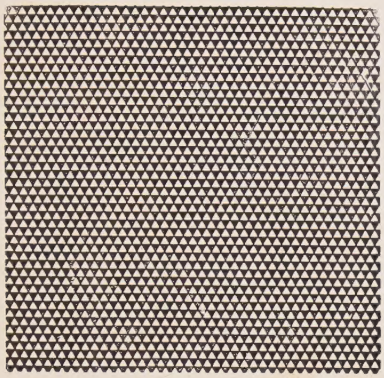

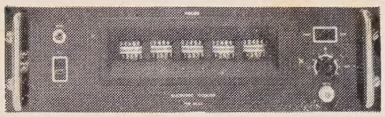

PW 4032

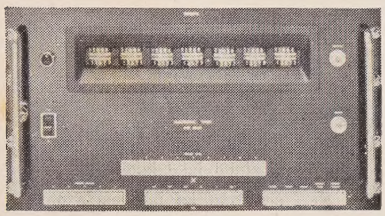

PW 4062

PW 4022

Pre-set count / pre-set time scaler for direct connection of G.M.-counters, scintillation- or proportional detectors

COUNTING CAPACITY: 5 decimal scaling stages; 2 binary pre-scalers. Total indicated counts: 400 000.
RESOLVING TIME: 0.5 μsec (first binary scaler).
INPUT SENSITIVITY: G.M.-counters: 0.5 $V_{p\text{-}p}$; Scintillation detectors: via built-in amplifier with adjustable attenuators: 5 $mV_{p\text{-}p}$.
PRE-SET TIME SETTING: (1-2-3...9) x (10^{-1}-1-10-10^{2}-10^{3}) sec.
PRE-SET COUNT SETTINGS: (1-2-4)x(10-10^{2}-10^{3}-10^{4}-10^{5}) counts.
TIME REGISTERING CAPACITY: 0.001-10 000 sec. in millisecond intervals.
H.V. RANGE: 300-2500 V in steps of 22 V.

PHILIPS

nuclear equipment

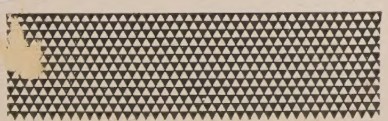

N.V. PHILIPS' GLOEILAMPENFABRIEKEN - EINDHOVEN - HOLLAND

Particle accelerators - Reactor control instrumentation - Health protection and monitoring equipment - Radiation measuring and detection equipment - Geiger-Müller counters - Photomultipliers - Radio-active isotopes.

SCINTILLATION COUNTING

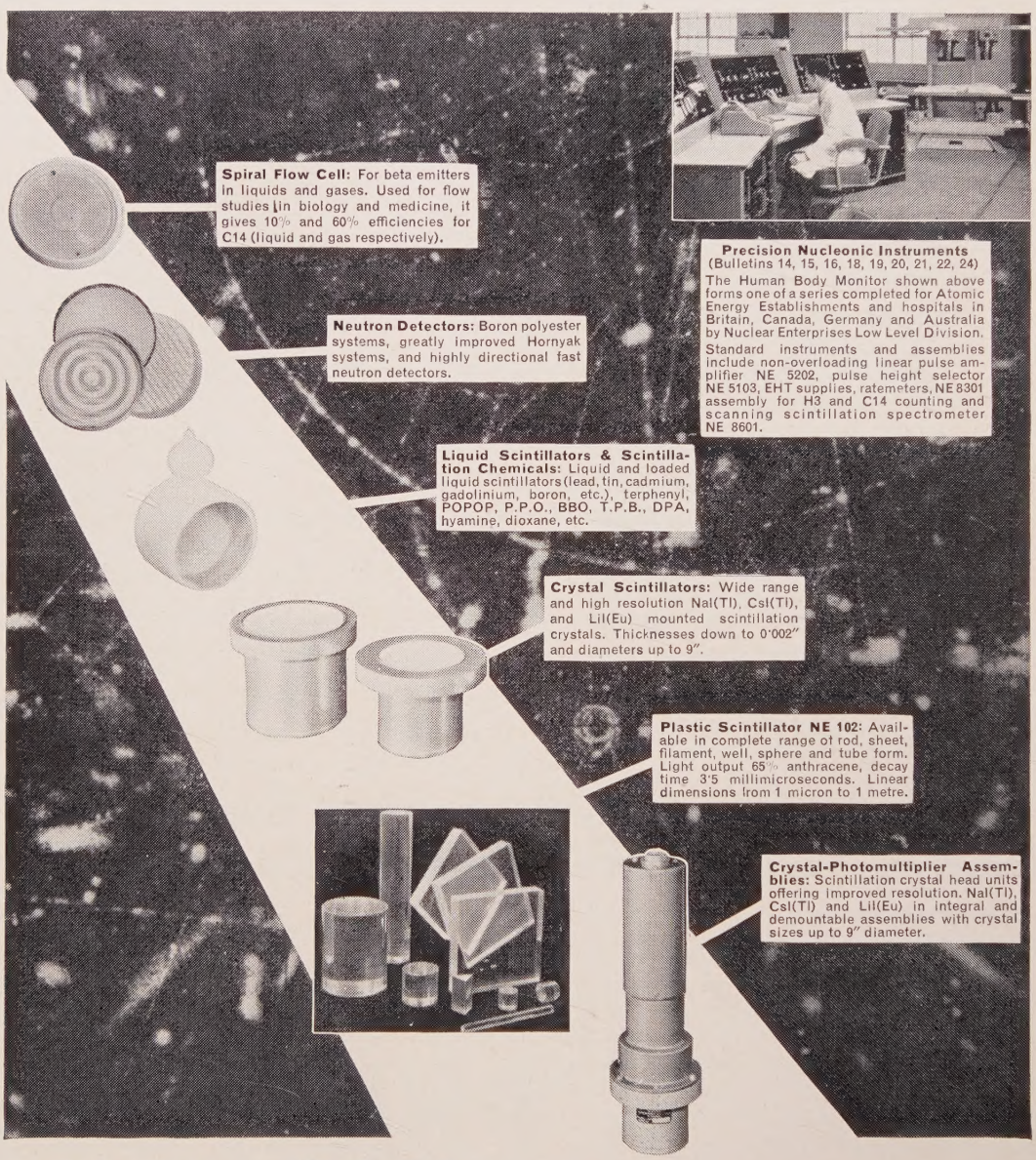
Spiral Flow Cell: For beta emitters in liquids and gases. Used for flow studies in biology and medicine, it gives 10% and 60% efficiencies for C14 (liquid and gas respectively).
Neutron Detectors: Boron polyester systems, greatly improved Hornyak systems, and highly directional fast neutron detectors.
Liquid Scintillators & Scintillation Chemicals: Liquid and loaded liquid scintillators (lead, tin, cadmium, gadolinium, boron, etc.), terphenyl, POPOP, P.P.O., BBO, T.P.B., DPA, hyamine, dioxane, etc.
Crystal Scintillators: Wide range and high resolution NaI(Tl), CsI(Tl), and LiI(Eu) mounted scintillation crystals. Thicknesses down to 0·002" and diameters up to 9".
Plastic Scintillator NE 102: Available in complete range of rod, sheet, filament, well, sphere and tube form. Light output 65% anthracene, decay time 3·5 millimicroseconds. Linear dimensions from 1 micron to 1 metre.
Crystal-Photomultiplier Assemblies: Scintillation crystal head units offering improved resolution. NaI(Tl), CsI(Tl) and LiI(Eu) in integral and demountable assemblies with crystal sizes up to 9" diameter.

Precision Nucleonic Instruments
(Bulletins 14, 15, 16, 18, 19, 20, 21, 22, 24)

The Human Body Monitor shown above forms one of a series completed for Atomic Energy Establishments and hospitals in Britain, Canada, Germany and Australia by Nuclear Enterprises Low Level Division.

Standard instruments and assemblies include non-overloading linear pulse amplifier NE 5202, pulse height selector NE 5103, EHT supplies, ratemeters, NE 8301 assembly for H3 and C14 counting and scanning scintillation spectrometer NE 8601.

SCINTILLATORS

The unique scintillation service afforded by Nuclear Enterprises (G.B.) Ltd. includes the highly efficient NE 102 plastic scintillator, liquid scintillators, neutron detectors, scintillation chemicals and an extensive range of crystals & crystal-photomultiplier assemblies.

NEW NE 150 plastic phosphor for pulse shape discrimination techniques and NE 160, a special high temperature plastic scintillator.

For full details write for Technical Bulletins (Nos. 9, 11, 12, 13, 23, and 25) & Catalogue to the Sales Division, Edinburgh.

Nuclear Enterprises (G.B.) Ltd.

Sighthill, Edinburgh 11, Scotland.—Tel.: Craiglockhart 5262

Associate Company: Nuclear Enterprises Ltd.
550. Berry Street, Winnipeg 21. Canada.

ndh 8161

the first portable, "desk-top" 400-channel pulse height analyzer

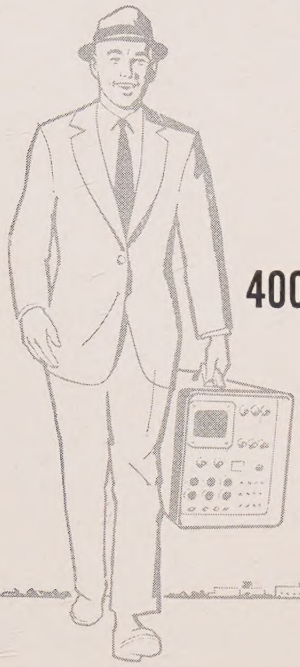

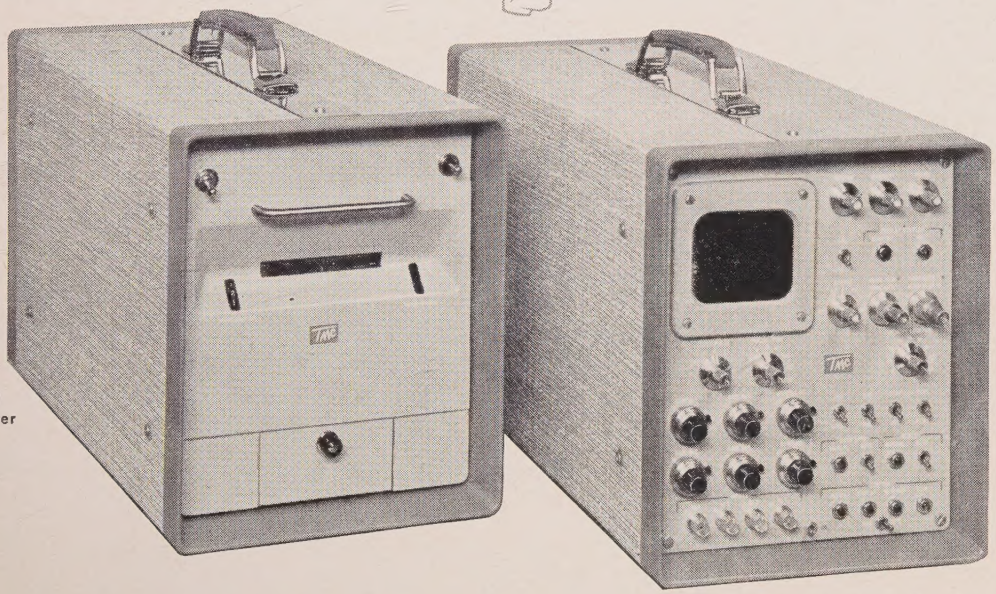

Model 500
decimal printer

Model 404
pulse height analyzer

— the TMC Model 404

The new TMC Model 404 is the most portable pulse height analyzer you can own. Take it and use it anywhere. With its all-transistor, printed circuitry and 400-channel memory in a package just over a cubic foot, this analyzer is small enough to operate on your desk. *All* the instruments needed for an experiment can be carried easily by one person.

The Model 404 has a magnetic core memory that can be used in sub-groups of two or four; four separate inputs and associated amplifiers; internal pulse routing circuitry; pushbutton data transfer and display overlap; very low power requirements and many "system" advantages. And it can be used with the new solid state detectors.

For readout, use its companion unit, the Model 500 Decimal Printer; a high speed paper tape punch; strip chart or X-Y recorders; or an IBM electric typewriter.

LITERATURE ON REQUEST

TMC TECHNICAL MEASUREMENT CORPORATION

441 WASHINGTON AVENUE NORTH HAVEN, CONNECTICUT

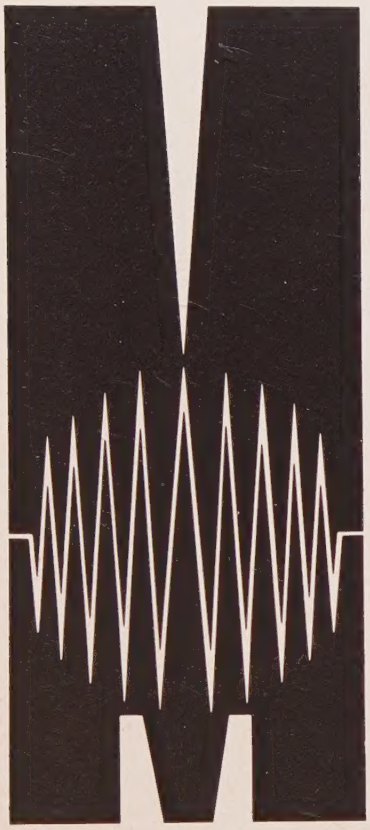

PARIS FROM MAY 9TH TO MAY 17TH 1961

MESUCORA

INTERNATIONAL EXHIBITION
MEASUREMENT - CONTROL - REGULATION - AUTOMATION
AND 58TH EXHIBITION OF THE
"SOCIÉTÉ FRANÇAISE DE PHYSIQUE"

- First French Exhibition exclusively devoted to these techniques, the most important and the most international one realized in Europe.
- International Congress, the subject of which will be "Recent progress in the fields of Measurement Control and automatic Regulation, resulting from the cooperation of the Techniques (electric, electronic, mechanical)".
- 700 Exhibitors - 14 nations - 35.000 square meters.
- The most recent discoveries and appliances of the theoretic and experimental research.
- Most refined measurement and control equipments, materials and methods; their applications to regulation and automation in the fields of the industry and of the public services.
- An unprecedented gathering, an international confrontation of the highest technical value which

ALL the responsible persons in industry and the public services
ALL engineers and research workers
ALL teachers and students of the technical and scientific Upper Teaching

MUST VISIT

centre national des industries et des techniques

Call on: MESUCORA - Service Propagande - 40, rue du Colisée - Paris 8e - Tél. BALZAC 77-50
FRANCE for the complete documentation, stating if you want it in French, German or English

DYNAMITRON ELECTRON ACCELERATOR . . .
featuring high power (up to 30 KW)
and industrial reliability.

DYNAMITRON POSITIVE ION ACCELERATOR . . .
featuring wide voltage range (up to 3 MEV),
constant potential and the high
current Dynamag ion source.

DYNAMITRON ACCELERATORS . . .
have won international acceptance in
research and industrial applications.

Sales Agencies

WESTREX CO.	VICKERS	C. ITON & CO., LTD.
Paris	Research, Ltd.	2-4 Honcho
France	Sunninghill, Berks	Nihon Bashi
Brussels	England	Chuo-Ku
Belgium		Tokyo, Japan

RADIATION DYNAMICS, INC.

Westbury Industrial Park
Westbury, Long Island, N. Y.

CABLE ADDRESS: RADYNE, WESTBURY, N.Y.

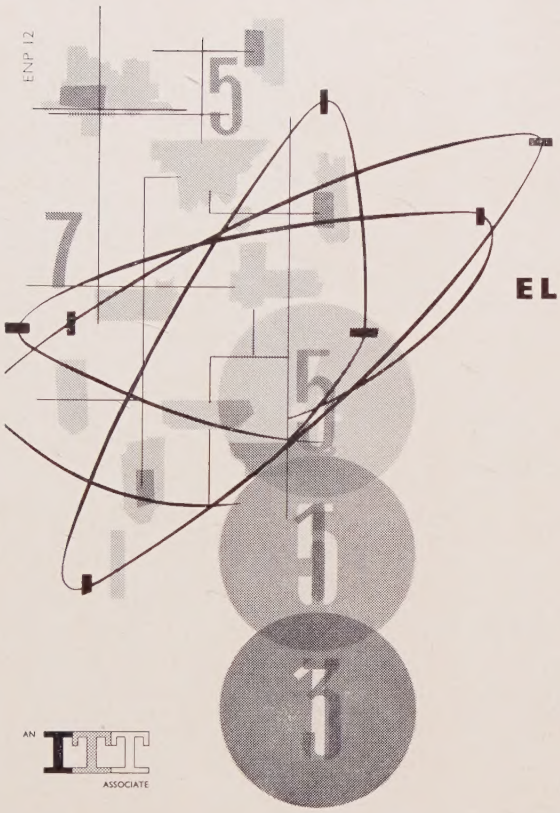

ELECTRONICS FOR NUCLEONICS

SCALER CHRONOSCOPE

Bell Telephone scaler chronoscope gives you top quality reproduction of automatic counting and printing.
It is so constructed that from a small stock of basic modules a wide scope of performances can be covered. This type normally supplied in a metal case is also available for rack mounting

- preset time
- preset count
- result printing facilities
- interchangeable modules
- in line read out
- fully transistorized

Our staff is always available to answer your inquiries.

Bell Telephone Mfg Co

"Nuclear Energy division"
33, Berkenrodelei
HOBOKEN-Antwerp-BELGIUM

NANOSECOND PULSES? - MICROSECOND PULSES?

MODEL 414

CALIBRATION PULSER

Decay Times	*Ranges*
0.003 microseconds	0 - 1 millivolts
0.01 microseconds	0 - 5 millivolts
0.03 microseconds	0 - 10 millivolts
0.1 microseconds	0 - 50 millivolts
0.3 microseconds	0 - 100 millivolts
1. microseconds	0 - 500 millivolts
3. microseconds	0 - 5 Volts
10. microseconds	0 - 10 Volts
100. microseconds	0 - 50 Volts
	0 - 100 Volts

Dual purpose- manual or motor driven slider.
Dual 50 ohm output permits coincidence circuit applications.
Internal standard cell calibration.
Polarity switch for positive or negative pulses.
0.1% helical potentiometer.
High pressure hermetically sealed mercury relay.

Write for details

$ 785 f.o.b. factory

RADIATION INSTRUMENT CO.

P.O. BOX 733

SILVER SPRING, MARYLAND, U.S.A.

NORTH-HOLLAND BOOKS

Paul Ehrenfest

COLLECTED SCIENTIFIC PAPERS

XII + 632 pages

Guilders 45,00 (90s.)

This volume makes widely scattered publications readily available. All Dutch articles appear here in English; the German publications are in the original language.

Sole Agency for U.S.A.:

Interscience Publishers Inc. — New York

NORTH-HOLLAND PUBLISHING COMPANY - AMSTERDAM

CDC's PROVEN PERFORMANCE

100-CHANNEL PULSE HEIGHT ANALYZER

CHALK RIVER KICKSORTER

Manufactured by Computing Devices of Canada, Limited, from specifications prepared by Atomic Energy of Canada, Limited.

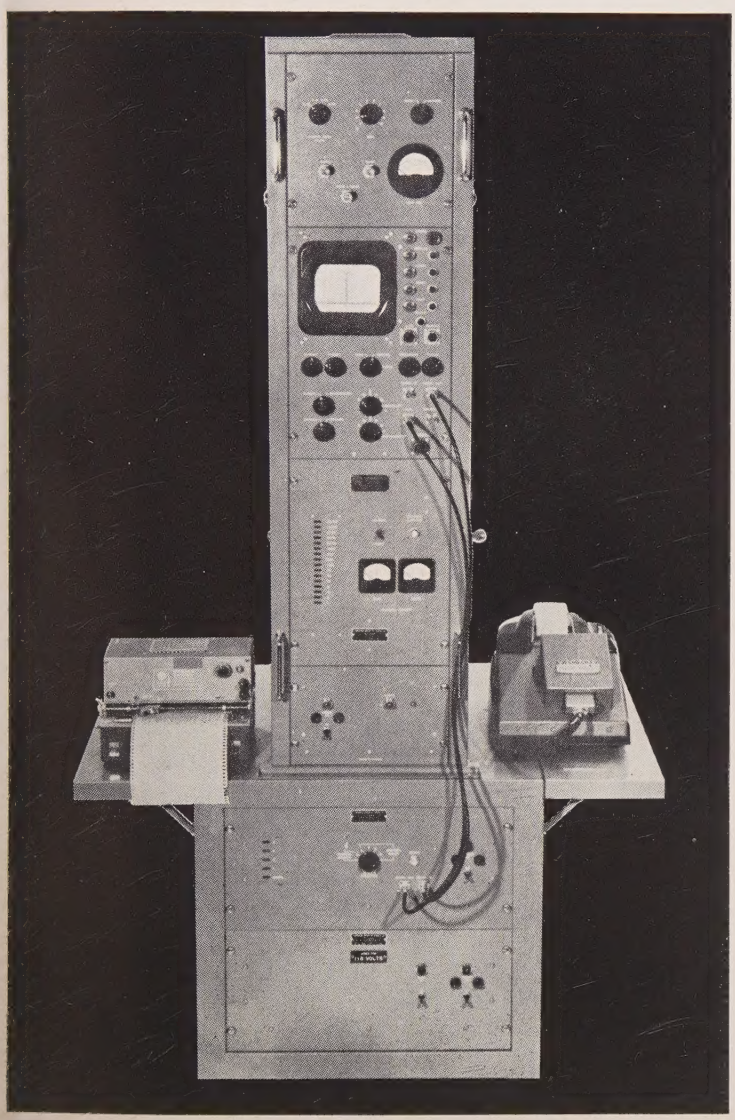

The convenience and speed of automatic printout can be obtained by adding a Decimal Scaler, a Print Control Unit, and an Electric Printer as accessories, shown with the Kicksorter. Provision is also made in the circuitry for the addition of a Pen Recorder for more accurate analog output.

88% TRANSISTORIZED

- Printed Circuitry
- Low Maintenance—High Reliability
- Low Power Consumption—120 Watts
- No Ventilation or Cooling Problems

VERSATILE DATA PRESENTATION

- Oscilloscope Display
- Binary Manual count readout allows the count on any channel to be displayed in digital form.
- Magnetic Core Memory—65,535 counts can be stored per channel.
- Permanent Count Storage—sixteen magnetic cores for each of the 100 channels.
- Highly Versatile—can be modified to accommodate most applications which require additional features.

The Chalk River "Kicksorter" is designed to span random pulses of various amplitudes and shapes, sort them according to amplitude into 100 channels, and store a record of the counted pulses in a magnetic core memory. This computer, with its magnetic core memory and versatile data display system, makes it possible to observe the pulse amplitude spectrum as it accumulates or after it has accumulated.

In addition to its wide use in gamma spectroscopy, the "kicksorter" has many applications in medical research, neutron time-of-flight studies, radioactive fallout studies, shielding studies, oil well and uranium logging, neutron activation analyses, measuring of radioactivity in humans, and other areas.

The analyzer is designed so that information accumulated may be displayed or read out in various ways. Data may be observed on the oscilloscope, or information already accumulated in the memory core may be displayed on the screen, plotted on a strip chart recorder, or printed out in decimal form on an automatic printer.

For additional information, wire or write to:

Bendix International

DIVISION OF THE BENDIX CORPORATION
205 East 42nd Street
New York 17, N. Y., U.S.A.
Cable Address: "Bendixint"

Sales Representative for Great Britain

NUCLEAR ENTERPRISES (G.B.) LTD.

BANKHEAD MEDWAY, SIGHTHILL,
EDINBURGH 11, SCOTLAND

SALES AND SERVICE AVAILABLE THROUGHOUT THE WORLD

Van de Graaff®
Accelerators
0.4 to 15 Mev Energy
Electrons:
up to 1 ma at 3 Mev
Positive Ions:
up to 400 μa at 3 Mev
Neutrons:
up to 10^{12} n per sec

For Research
In Nuclear Physics
Biology & Medicine
Solid State Physics
Radiation Chemistry
Reactor Kinetics

For Application
In Polymerization
Sterilization — Therapy
High Energy Radiography
Catalysis
Nuclear Engineering
and Teaching

LINACS
Microwave Linear Electron Accelerators
4 to 150+ Mev Energy
Peak Pulse Current:
up to 1 ampere
in 0.3 μsec pulses
Neutrons:
up to 10^{16} n per sec
during pulse

160 cm
Electromagnetic Isotope Separator
10 μa of most abundant isotope in mass range 1 to 400
(Resolving Power: 400)
Ion Sources
Duoplasmatron—200 ma protons
Neutral and Negative Ion Sources

Cockcroft-Walton Accelerators
40 to 800 kev Energy
Beam Current:
up to 2 ma
Neutrons:
up to 10^{11} n per sec
Electromagnetic Accelerator
100 to 600 kev Energy
Current Capacity:
up to 8 ma

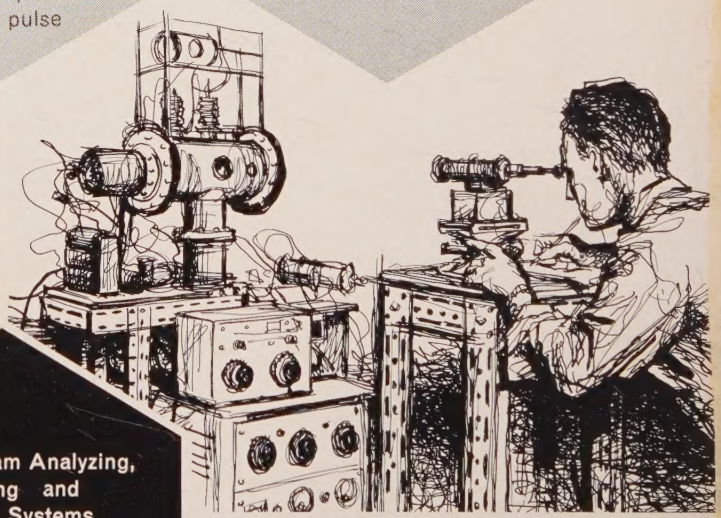

Beam Pulsing Equipment
Van de Graaff:
1.0 millimicrosecond
up to millisecond
Linacs:
0.1 to 30 μsec pulses

Magnetic Beam Analyzing, Stabilizing and Switching Systems
Ion Lens Systems
Electron Scanners
5″ to 30″

PERFORMANCE SPECIFICATIONS ALWAYS GUARANTEED

More than 275 particle accelerators by High Voltage Engineering Corporation and Applied Radiation Corporation are now installed world-wide

Mass Spectrograph/ Spectrometers
for energy analysis of protons, deutrons, alpha particles
(Resolving Power: 10^{-3})

HVEC arc

HIGH VOLTAGE ENGINEERING CORPORATION
BURLINGTON, MASSACHUSETTS • U.S.A.
APPLIED RADIATION CORPORATION
WALNUT CREEK, CALIFORNIA, U. S. A.
HIGH VOLTAGE ENGINEERING (EUROPA)
AMERSFOORT, THE NETHERLANDS

NUCLEAR INSTRUMENTS AND METHODS **10** (1961) 73–83; NORTH-HOLLAND PUBLISHING CO.

FIXED FREQUENCY CYCLOTRON OPERATION WITH A REGULATOR FOR DEE VOLTAGE STABILIZATION†

H. FAUSKA, J. W. ORTH and F. H. SCHMIDT

University of Washington, Seattle, Washington

Received 29 September 1960

A severe time modulation of the beam from a 152 cm cyclotron was found to be caused by dee voltage fluctuations. To eliminate this difficulty, a series-type regulator has been constructed. The regulator controls the oscillator plate power voltage in order to maintain a constant and ripple-free potential on one dee. Under average conditions of use the dee voltage is constant to ± 0.15%. In addition to improving the beam time stability, the regulator introduces several unexpected features of cyclotron performance among which are the following: The deflected beam goes through pronounced peaks and valleys as the dee voltage is varied. The deflection efficiency is greater when the dee voltage is set on a beam maximum. Stability of the cyclotron against sparking is improved. The focussed beam image in a scattering chamber remote from the cyclotron is substantially smaller showing that the beam energy spread is less.

1. Introduction

It has been recognized for some time that for optimum operation the radio frequency applied to the dee electrodes of constant frequency cyclotrons of either the conventional type or the spiral shim isochronous type should be of constant and controllable amplitude[1]). Several regulator systems have been reported in the literature. In the course of their work with ion phase selecting slits at the center of the Canberra 30-inch cyclotron, Morton and Smith[2]) found that it was necessary to regulate the dee voltage to within ½%. They used a system involving grid modulation of the main oscillator tube. With larger cyclotrons involving power inputs of 75 to 100 kW or more, the problem becomes somewhat more severe, although a similar grid modulation system has been installed on an experimental basis on the 90-inch cyclotron at the Lawrence Radiation Laboratory at Livermore, California[3]). A regulator arrangement suitable for a crystal controlled oscillator-power amplifier system has been installed on the cyclotron at the Institute of Atomic Energy, Moscow[4]). This device holds the dee voltage on both dees constant to ± 1%.

For self-excited oscillators a chief source of dee voltage variation arises from the high voltage power supply. Most cyclotrons employ three phase full wave rectifiers which have an unfiltered 360 cycle ripple amplitude of about 5 percent. To reduce substantially this ripple by means of filters is expensive. In addition, filtering adds a source of stored energy which may damage the oscillator during periods of dee voltage breakdown.

Another source of dee voltage ripple arises from variable loading of the oscillator due to fluctuations in the ion source output. Slow variations of the dee voltage can be caused by ion loading, by heating of the internal dee structure, or by other similar secular changes of the oscillator system.

It is the purpose of this paper first to discuss

† Partially supported by the U.S. Atomic Energy Commission.

[1]) See for example, T. A. Welton, Conference on Sector Focused Cyclotrons, Publication 656, National Academy of Sciences-National Research Council, p. 192 (1959).

[2]) A. H. Morton and W. I. B. Smith, Nucl. Instr. and Meth. **4** (1959) 36;
W. I. B. Smith, Conference on Sector Focused Cyclotrons, Publication 656, National Academy of Sciences-National Research Council (1959) p. 183.

[3]) J. M. Peterson, private communication.

[4]) A. V. Antonov, Yu. V. Korshunov, E. A. Melefhko, V. S. Panayuk, Prib. i Tekhn. Eksper. No. 1 (1958) 41; and No. 6 (1959) p. 20.

the observations which motivated us to expend the effort and money to construct a regulator for the University of Washington Sixty-Inch Cyclotron[5]), second to describe the features of the regulator, and third to describe the features of cyclotron performance with the regulator. Although the initial motive for the regulator was to eliminate beam modulation, a number of other improvements resulted.

2. The Direct Need for Dee Voltage Regulation

For some time it was known that the external beam of our cyclotron was severely modulated by the 360 cps plate power supply ripple; however, the full nature of the modulation, especially into a distant scattering chamber, was not suspected until rather recently.

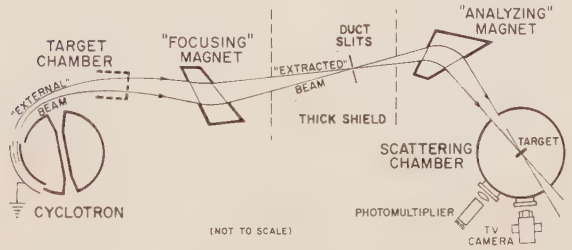

Fig. 1. Schematic diagram of the external beam system. The beam pattern and modulation was observed on a fluorescent target placed in the large scattering chamber and viewed by a T.V. camera and a photomultiplier.

About a year and a half ago, D. Drake and J. Orth observed a high frequency modulation of the beam current to several small probes placed immediately beyond the normal deflecting channel. The high frequency was tentatively ascribed as due to numerous individual cyclotron "turns" sweeping past the exit strip at a 360 cps rate[6]). Later, in the course of preparation for scattering experiments involving particle-gamma ray coincidences with very low counting rates, the time distribution of the beam into a distant scattering chamber was studied in detail. A schematic diagram illustrating the method is shown in fig. 1. The extracted beam is partially energy analyzed by a double focusing magnet and directed upon a slit about 10 meters distant from the cyclotron. After passing through the slit the remaining beam is deflected by a second double focusing magnet into a scattering chamber 1.5 meters in diameter. The latter is provided with numerous observation ports. A thin target of fluorescent material[7]) was fixed at the center of the chamber. A television camera was placed at one port, and a lens and photomultiplier at another. The output of the photomultiplier was connected to a Tektronix Type 541 oscilloscope. The portion of the beam image "seen" by the photomultiplier could be correlated with the image observed on the television monitor.

We found immediately that the beam was very severely modulated with a fundamental frequency of 360 cps. However, superimposed on the 360 cycle period was a remarkable complex pattern which was stable over many cycles. Moreover, the detailed pattern varied across the beam image. The best beams had a "duty cycle" of only about 20%; that is, for 80% of the time no beam existed[8]). The detailed time structure of the beam was highly sensitive to the dee voltage. In fig. 2 we show four oscillograms which illustrate the beam variations, each for a different dee voltage. Beneath the one at 83 kV is a sketch of the dee voltage ripple. The horizontal lines represent the several "eigenvoltages" which are capable of producing ions of exactly the correct energy and direction so as to pass through the external magnet and slit system. These show quite clearly that as the dee voltage rises (or falls) each beam current peak is produced by one less (or one more) number of cyclotron turns than the preceding peak. Moreover, one notes that the narrower peaks correspond to rapidly changing dee voltage. The fourth oscillogram, taken at a dee voltage well above cyclotron threshold, is complicated by aberrations in the focusing system as well as by changes in ion

[5]) F. H. Schmidt, G. W. Farwell, J. E. Henderson, T. J. Morgan and J. F. Streib, Rev. Sci. Instr. **25** (1954) 499.

[6]) F. H. Schmidt, Conference on Sector Focused Cyclotrons, Publication 656, National Academy of Sciences-National Research Council, (1959) p. 216.

[7]) Pilot "B" plastic phosphor, or fluorescent paint.

[8]) The "true" maximum duty cycle of a cyclotron is about 5% due to the rf bunching. The 20% figure refers to 20% of the 5%.

energies *vs* dee voltage. Hence, the "eigenvoltages" are not as clearly revealed, although the same general pattern is evident. The thickness of the horizontal base line in each oscillogram is caused by rf pickup in the oscilloscope signal lead. The wider beam "peaks" shown in fig. 2 have a half width of $\approx$ 2000 rf beam pulses,

3. Regulator Circuit

Fig. 3 shows a block diagram of our regulator system. When initially installed some eleven years ago the main plate power supply (which is located in a vault remote to the cyclotron proper) was grounded by a fortunate circumstance only at the anode transmission line of the

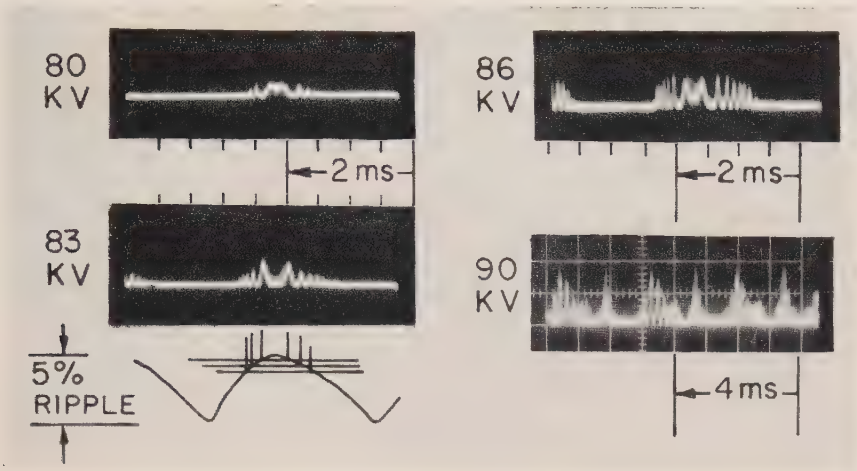

Fig. 2. Oscillograms of the time variations of the beam in the scattering chamber. Each photograph is for a different dee voltage. The interpretation in terms of the dee voltage modulation is schematically indicated below the 83 kV oscillogram. Each successive peak in the beam current corresponds to a change by one in the number of ion turns in the acceleration cycle. The average beam at 86 kV was $\approx$ 30 mμA.

the narrower ones $\approx$ 100 rf beam pulses. The equivalent spacing of the peaks is about 0.5 percent change in dee voltage. From these data we concluded that the dee voltage should be regulated to within $\approx$ 0.2% or better.

The somewhat surprising results discussed above provided a strong impetus to proceed as rapidly as possible with the construction of a suitable dee voltage regulator. At the same time it was decided to postpone experiments involving low coincidence counting rates. With the intense instantaneous current peaks evident in fig. 2 the chance that two scattering events can occur in the same rf beam pulse is significantly large. The background counting rate may then become intolerable[6]). Indeed, once it was known that the time-distribution of our beam into the scattering chamber was very poor, we were able easily to discern the "pile-up" pulses of scattered particles by visual observation of a scintillation counter output in an oscilloscope.

grounded-grid oscillator. It was therefore relatively simple to install a series regulator tube, a Machlett ML–6696, in the ground return circuit. The maximum plate dissipation of this tube is 60 kW. The grid is operated at 50–100 volts positive and draws from 70 to 200 milliamperes current. Operation with or without the regulator may be selected, as shown, by means of a shorting switch operable from the control desk.

We chose to regulate via the plate supply voltage rather than via the oscillator grid voltage for the following reasons: 1. Our oscillator incorporates a cathode bias resistor in lieu of a constant current network[5]). The output power therefore is relatively insensitive to grid bias. 2. The oscillator efficiency is a function of grid bias. It seemed to us unwise to alter this tuning parameter.

The principal regulating signal is derived from a pick-up loop which projects inside the cyclotron vacuum chamber. The loop is exposed to

the dee on the deflector side of the cyclotron. The rf appearing on the pick-up loop is rectified and a portion of the d.c. signal is compared with the potential of a 5651 voltage reference tube. The desired signal level, and hence the desired dee voltage, is adjusted by means of the ten turn helipot shown in fig. 3. To achieve sufficient

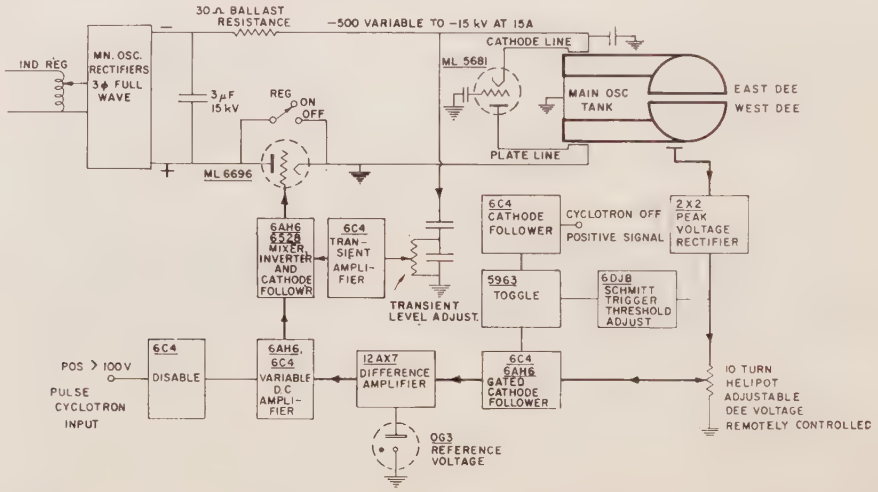

Fig. 3. Schematic diagram of the dee voltage regulator system featuring a large series tube in the plate supply. The path of the principal regulating signal from the dee system is indicated by heavy lines. An a.c. coupled "derippling" signal from the power supply is also fed to the regulator tube. The trigger and toggle circuits are required for proper response during dee to ground spark breakdowns.

sensitivity of control, the helipot is connected through a 10 to 1 reduction gear to a selsyn motor. The latter is operable from the cyclotron control desk. The difference voltage is amplified by a d.c. variable-gain amplifier and fed to the ML-6696 grid. The signal level at the helipot tap is 85 volts, and the d.c. gain from this point to the 6696 grid may be varied from 100 to 500. The phase shift up to 1000 cps is less than 8 degrees.

The cyclotron dee system has a "Q" of about 6000 when there is no ion load. If such a resonant circuit is subjected to an amplitude modulated driving signal the resultant current is also amplitude modulated, but with a smaller percentage modulation. In addition, the modulated wave lags in phase with respect to the input signal. Neither of the above statements may be obvious at first sight. The justification is as follows: We regard the dee system as being subjected to an exciting signal with an angular frequency ω_0 plus upper and lower sideband frequencies $\omega_0 \pm \omega_1$, where ω_0 is the resonant frequency of the system; i.e., that frequency for which the driving voltage and current are in phase. We assume that the self-excited oscillator operates at or near this frequency. Each of the three frequencies leads to independent steady-state solutions of the harmonic oscillator equations. The resultant current is the linear superposition of the three solutions. Two results of interest emerge: First, the percent modulation of the input signal is attenuated in the output by the factor $[1 + 4Q^2\,\omega_1{}^2/\omega_0{}^2]^{-1}$; second, the output modulation has a phase shift lag $\theta \cong \tan^{-1}(2Q\omega_1/\omega_0)$. Both results can be understood qualitatively on physical arguments.

The phase shift discussed above, when added to phase shifts introduced by the amplifier and other portions of the regulator feed-back circuit, can produce a sustained oscillation in amplitude of the dee voltage. The condition for which this will occur can be shown to be given by

$$-G\,[1 + 4Q^2\,\omega_1{}^2/\omega_0{}^2]^{-1}\cos(\theta_A + \tan^{-1} 2Q\omega_1/\omega_0) \geq 1$$

where G is the total loop gain of the system and must include the efficacy of the pick-up loop, the ratio of dee voltage generated to oscillator plate voltage, as well as the gains of the amplifier

and series regulator tube. The angle θ_A is the phase shift of the amplifier plus any other phase shifts in the regulator circuit. θ_A is a function of ω_1, the frequency of amplitude modulation. At the limiting condition, where the above expression is equal to one, we can in principle solve for the expected oscillation frequency $\omega_1 = \omega_{\text{critical}}$. With the parameters for our regulator ω_{critical} is approximately $2\pi \times 2500$ radians per second. Indeed, in practice we observe such an amplitude oscillation at ≈ 2500 cps when the amplifier gain exceeds about 400.

Although we have made no careful quantitative measurements it is interesting to point out that each quantity in the equation for sustained oscillations except "Q" can be found with reasonable precision. Thus, an observation of ω_{critical} can be used to determine the "Q" of the cyclotron.

At 360 cps, the principal ripple frequency of the power supply, the phase shift discussed above is $\approx 24°$. Hence, a feed-back signal derived from the dee system alone is not sufficient to provide good regulation. Therefore, an a.c. coupled signal from the oscillator power supply voltage is amplified and fed through a mixer circuit to the ML-6696 grid as shown in fig. 3. Taken alone, this section of the regulator converts the rectifier and regulator into a ripple-free power supply. In addition, we found that fast transients due apparently to the sudden firing of the mercury vapor rectifier tubes were capable of shock exciting the dee system so that the amplitude oscillated between each tube firing with a frequency near ω_{critical}. To eliminate the fast transients, a 3 μF capacitor was installed at the rectifier output as shown in fig. 3. The capacitor and 30 Ω ballast resistor provides sufficient filtering to overcome the difficulties mentioned above.

The regulator system incorporates a number of features which are necessary to make it operable: 1. Before the main power breaker is closed, the ML-6696 grid draws excessive current unless limited by a series resistor (not shown). The resistor is automatically shorted out of the circuit when the main power breaker is closed. 2. In order that the main power breaker may be closed under load without drawing excessive surge current from the rectifier, a resistor (not shown) is placed in series with the 3 μF rectifier filter. It is shorted out automatically after the power is on. 3. At dee voltages below approximate 50 kV the output voltage of the pick-up loop is below the 85 volt regulator level. The Schmitt trigger and toggle circuits shown in fig. 3 hold the regulator inoperative until the dee voltage surpasses ≈ 50 kV. 4. When the cyclotron dees spark to ground, thus momentarily stopping the oscillator, the same trigger and toggle signals the regulator to stop operation. Without this feature the regulator would drive the ML-6696 grid excessively positive and cause the dee voltage to overshoot upon recovery. The response time of the trigger and toggle is very short compared to the normal rise-time of the dee voltage.

Two additional convenience features have been added. A signal from the Schmitt trigger and toggle circuit can be used to turn off experimental detecting equipment from the time a spark occurs until recovery. For experiments requiring pulsed cyclotron output, a periodic disabling signal can be fed to the d.c. amplifier to reduce the dee voltage below threshold.

Meters which read the ML-6696 grid and plate voltage are required at the control desk. The first indicates whether the regulator is in range, and the second ensures that the rating of the tube is not being exceeded. In practice the cyclotron operator adjusts the dee voltage to the desired value by means of the helipot level set control while keeping the regulator in range by manual adjustment of the induction regulator input to the rectifier.

The regulator reduces the dee voltage ripple to $\approx \pm 0.1\%$ in the unloaded condition. Long term stability of the average dee voltage on the regulated dee is better than 0.1%[9]). Effects caused by ion loading are discussed below.

[9]) Since the voltage on only one dee is regulated, this figure presumes that the dee balance is not altered, a presumption which is justified for stable conditions of operation. For a discussion of dee voltage balance, see F. H. Schmidt and M. J. Jakobson, Rev. Sci. Instr. 25 (1954) 136.

4. Cyclotron Operation with the Regulator

The stabilized dee voltage provided by the regulator has introduced several interesting features of cyclotron operation. Some of these were unexpected. In this section we discuss primarily effects on an external target chamber beam.

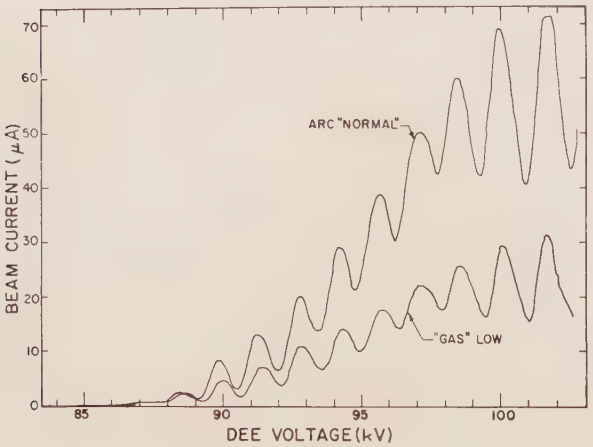

Fig. 4. X–Y recorder plots of the target chamber beam *vs* dee voltage. The upper plot is for a "normal" ion source arc adjustment, the lower for a reduced intensity arc. The position of the peaks is independent of the magnetic field tuning. The separation is $\approx 1.5\%$ in dee voltage and nearly constant. Each successive peak represents one fewer turn in the acceleration cycle. (Compare with fig. 7.)

For the same average external beam operation with the regulator is somewhat more stable than without it. This is not surprising, since the dee voltage required in the regulated case is less than the peak values required for the unregulated operation. In addition, any tendency to overshoot after a spark is suppressed by the regulator.

The external beam to the target chamber is somewhat more concentrated with the regulator. For some bombardments, where a distributed beam is more desirable to avoid target damage, we find it expedient to operate without the regulator.

The external beam exhibits a pronounced structure as the regulated dee voltage is changed. We have studied this structure in some detail by means of an X–Y recorder. In fig. 4 we show two typical results of these studies. The ordinate gives the beam intensity, and the abcissa is proportional to the dee voltage. The change in dee voltage from one maximum to the next is very nearly constant at $\approx 1.5\%$ over the range shown. The positions of the maxima are unchanged by magnetic field tuning. The sharpness of each maximum increases when the angular spread of the external beam is delimited by means of baffles. By the time the beam has reached the remote scattering chamber the peak to valley ratio of a given maximum is a factor of 10 or more.

We interpret this beam structure as due to unit changes in the number of ion turns within the cyclotron. The structure can be related to the average ion phase during the acceleration process in the following manner: The kinetic energy of the ions emerging from the deflector channel is given by

$$T = 4q\, V\, n\, \overline{\cos\phi} \qquad (1)$$

where q = charge of the ions; V = peak dee to ground potential; n = total number of ion turns; and ϕ = ion phase with respect to dee voltage. $\overline{\cos\phi}$ is the average value of this function taken over the entire acceleration cycle. If we differentiate eq. (1) and substitute for $V\, n\, \overline{\cos\phi}$ its value from eq. (1) we obtain

$$\frac{1}{T}\frac{\mathrm{d}T}{\mathrm{d}n} = \frac{1}{V}\frac{\mathrm{d}V}{\mathrm{d}n} + \frac{1}{n} + \frac{1}{\overline{\cos\phi}}\frac{\mathrm{d}\,(\overline{\cos\phi})}{\mathrm{d}n}. \qquad (2)$$

As the dee voltage is increased from one maximum to the one next higher, as shown in fig. 5, n decreases by one, and we can set $\mathrm{d}n = -1$ in eq. (2). Also it is reasonable to assume that the energy is unchanged; this is approximately borne out by observation of the energy analyzed beam in the scattering chamber. Therefore, for a change from one beam maximum to the next eq. (2) becomes

$$\frac{\mathrm{d}V}{V} = \frac{1}{n} - \frac{\mathrm{d}\,(\overline{\cos\phi})}{\overline{\cos\phi}}. \qquad (3)$$

From fig. 5 we have $\mathrm{d}V/V \cong 0.015$. If we assume that the fractional change in $\overline{\cos\phi}$ is small compared with $1/n$, we find that $n \cong 67$. Since an increase in V is most likely accompanied

by an increase in $\overline{\cos\phi}$, this value of n is an upper limit. From eq. (1) we find $\overline{\cos\phi} \geqslant 0.82$. Although this result is very reasonable, it rests upon a difficult and doubtful calibration of the dee voltmeters.

The analysis may be carried further by differentiating a second time and making the assumption that $d^2(\overline{\cos\phi})/dn^2 = 0$. One then concludes that dV/V should depend upon dee voltage. However, our measurements are not sufficiently accurate at this time to detect this dependence.

One final observation on cyclotron operation is of interest. The recorder plots of fig. 4 imply immediately that a higher deflector efficiency and a larger external beam should be obtained with the regulator. For an external alpha beam of ≈ 25 μA, the internal beam as measured on a water cooled probe is ≈ 50 μA, giving a deflector efficiency of 50%. A test at larger beam currents could not be made with the probe available. The comparable deflector efficiency without the regulator is about 30%. Without much effort a new record performance of over 110 μA external alpha beam was established shortly after installation of the regulator. However, the various experimental programs in progress seldom have need for more than 50 to 60 μA maximum.

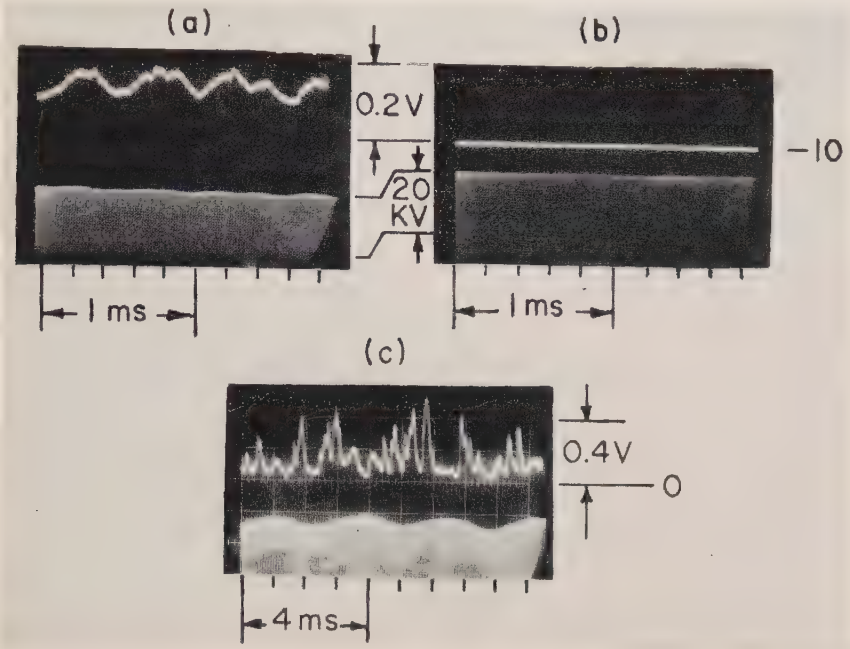

Fig. 5. The upper traces show the α-particle beam modulation in the scattering chamber, the lower the simultaneous dee voltage envelope. (a) Regulator on; (b) Regulator on but ion source arc turned off; (c) Regulator off. Dee to ground voltage in each case $\approx$ 100 kV. Note that even the fine structure of the beam can be associated with fluctuations in dee voltage. The time constant of the beam monitoring photomultiplier circuit was ≈ 60 μsec.

5. "Extracted" Beam Modulation and Collimation

We now return to the orginal motivation for the dee voltage regulator: *viz.*, the beam modulation in the scattering chamber. The method of study was essentially the same as shown in fig. 1. For some observations, in order to study more rapid fluctuations, an emitter-follower circuit was used to drive the cable between the photomultiplier and the oscilloscope. In addition, a newly acquired dual-beam oscilloscope (Tektronix Type 555) permitted simultaneous display of the dee voltage and the beam.

In fig. 5 we show a number of oscillograms of the beam modulation. The lower traces are envelopes of the dee voltage, the upper traces the photomultiplier output proportional to the

beam. Both sweeps were triggered singly at the same instant. The time-constant of the beam detecting circuit was ≈ 60 μsec. For fig. 5b the ion source of the cyclotron was turned off, so that the dee system was unloaded and there was no beam. For fig. 5a the average alpha particle beam into the scattering chamber was ≈ 40 mμA the primary beam from the cyclotron ≈ 20 μA. The duct slits, shown in fig. 1, were opened ≈ 0.05 cm. The beam suffered no further collimation; its physical size at the scattering chamber target was 1.25 cm high by ≈ 2 mm wide, corresponding to an energy spread of $\approx 0.2\%$. The lower trace of fig. 5a indicates a dee voltage modulation of $\approx 1.0\%$ induced by a fluctuating ion source load[10]); the peak to valley ratio of the accompanying beam modulation is about 2.

For purposes of comparison we show in fig. 5c an oscillogram taken with the regulator inoperative. The average beams were the same as for fig. 5a. Note that the oscilloscope sweep speed is altered as well as the vertical gain for the beam trace. A close examination of oscillograms (a) and (c) reveals that fine structure in the beam is matched in time by slight changes in dee voltage.

The oscillograms of fig. 5b and c were taken under conditions of rather severe ion source arc modulation (arc voltage = 450; current 2.5 amps). The same beam to the scattering chamber can be achieved with more modest arc settings. We then observe less beam modulation, but a fine structure still exists.

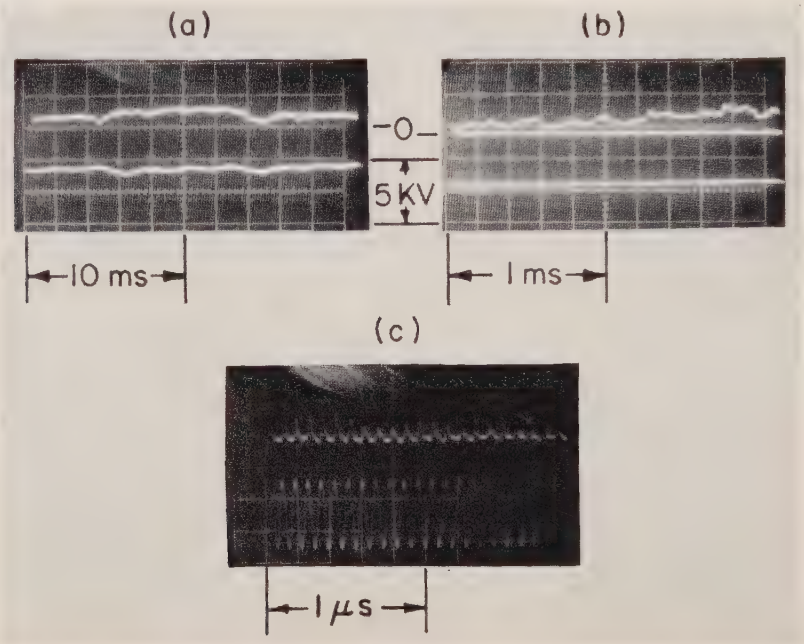

Fig. 6. The upper traces show the α-particle beam modulation in the scattering chamber, the lower the simultaneous dee voltage envelope. For (a) and (b) the time constant of the beam monitoring photomultiplier circuit was ≈ 6 μsec. In (c) we show individual beam pulses registered at the anode of an R.C.A. 7264 14 stage photomultiplier, together with the rf. Note the occasional striking changes in the beam from one pulse to the next.

The oscillograms shown in fig. 6a and b were obtained when the α-beam was collimated by a 6.4 mm high $\times$ 3.2 mm wide slot just before entering the scattering chamber. In addition, a faster output circuit ($\tau \cong 6$ μsec) was used on the beam monitoring photomultiplier. Also, the dee voltage was monitored after rectification; the rapid fluctuations visible in fig. 5b have been partially integrated out. The most rapid beam

[10]) The severity of the induced modulation was much greater before a substantial filter was installed on the arc voltage supply.

variations are random in character. The shortest periods visible are $\approx 20\ \mu$sec. When the final beam is collimated in the manner discussed above, the maximum energy spread is not more than $\approx 0.1\%$. Our oscilloscope studies have

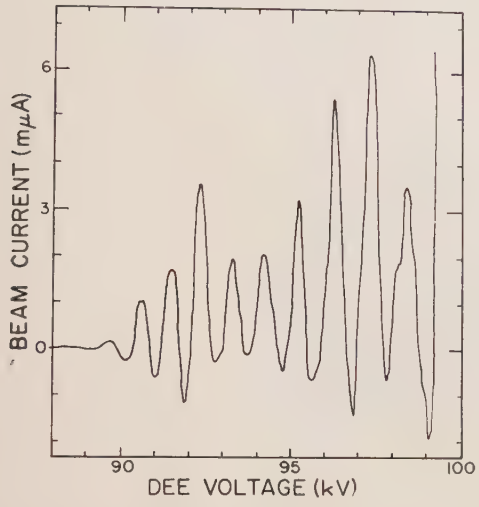

Fig. 7. X–Y recorder plot of scattering chamber beam *vs* dee voltage. The beam was collimated by a 3.2 mm wide by 6.4 mm high slot at the entrance to the scattering chamber. The apparent negative readings are caused by amplifier undershoot. There is no appreciable overshoot. The beam is $\approx$ zero in the valleys.

shown that with poor alignment of the focusing system it is possible to obtain what appear to be usable beams for scattering experiments when monitored only by means of a Faraday cup reading. However, when examined with a phosphor and photomultiplier, the beam may turn out to be badly modulated and present only a small fraction of the time. A situation of this kind can have disastrous effects on an experiment due to "pileup".

As a final step in our study of the beam fluctuations we have examined the individual beam pulses. For this purpose the beam was allowed to impinge as before upon a thin plastic scintillator. A collimating lens was placed near the scintillator inside the scattering chamber to increase the amount of light directed upon the photomultiplier, in this case an R.C.A. 7264. The anode pulses were fed directly into a 125-ohm transmission line. All interconnections were made by means of 125-ohm non-reflecting cable connectors, and the line was terminated in 125 ohms at both ends to reduce reflections well below 1%. Each beam pulse released at least 20 photoelectrons from the photocathode, so that statistical effects are not sufficient to account for the observed variations. Single sweep dual beam oscillograms were made of the beam pulses and the rf in synchronization at sweep speeds up to 100 mμsec/cm. Various methods of triggering were used to insure random sampling of the beam pulses. One of these oscillograms is shown in fig. 6c. For the most part these oscillograms show beam variations consisting of 50 or more rf pulses. However, occasionally a set of pulses vary by a factor of two in height over only 5 to 10 rf cycles, and there are even several instances in which the beam alters intensity by a factor of two from one pulse to the next. Note that fig. 6c exhibits such a case.

The average beam to the Faraday cup of the scattering chamber is a very critical function of the dee voltage setting. Fig. 7 shows an X–Y recorder plot of the beam *vs* dee voltage obtained in the same manner as described in Section 4. Here, the beam was collimated at the entrance to the scattering chamber by a 3.2 mm wide $\times$ 6.4 mm high slot. The appearance of negative readings on the sensitive millimicroammeter is due to amplifier undershoot. Overshoot does not occur. This graph shows very clearly that extreme stability of the dee voltage is required to maintain a constant beam in the scattering chamber.

Lastly, in fig. 8, we exhibit two television monitor photographs of the uncollimated α-particle beam. Fig. 8a was taken with the regulator on, 8b with it off. Otherwise, the cyclotron operating conditions for the two photographs were as identical as possible. The beam of fig. 8b is quite useless for scattering or nuclear reaction studies; that of fig. 8a is adequate for many purposes. It is worth remarking that in addition to the severe beam modulation discussed in Section 2, we found that γ rays originating in any beam collimators near the scattering chamber caused a severe background[11]). On the

[11]) Radiation from the Faraday cup beam catcher is

other hand, uncollimated beams, like the one shown in fig. 8b, gave far too much energy spread and kinematic broadening to be of much use. With the regulator on a beam like fig. 8b can often be simulated by rapidly rocking the dee voltage control knob back and forth over a few percent range.

slits[2]) for the first few turns might serve to reduce the non-useful portion of the ion load and allow a more stable dee voltage. As yet, however, we have not designed such an arrangement of slits which would be compatible with our varied conditions of operation.

Although considerations taking into account

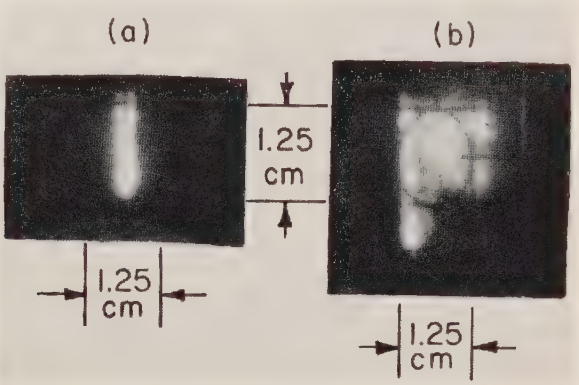

Fig. 8. T.V. photographs of the beam to a view screen in the scattering chamber. (a) Regulator on; (b) Regulator off. Faraday cup beam = 12–15 mμA. Duct slit opening $\simeq$ 0.5 mm. The circle and lines are a "bulls eye" and scaling grid.

6. Discussion

The original motivation for construction of the dee voltage regulator was to eliminate the severe beam modulation. In this objective we have been reasonably successful. Under proper conditions of operation we can now obtain a beam into the scattering chamber which at least is always present, and varies by less than a factor of two over a 60 cps period. Its long term stability, at least as far as effects due to dee voltage is concerned, is very good. A study of oscillograms like the one shown in fig. 6b suggests that the major source of beam modulation is still due to dee voltage amplitude variations[12]). The most likely cause is uneven loading of the dees by fluctuation in ion source output. A set of programming the high "Q" dee system lead one to conclude that dee voltage amplitude variations can cause beam modulations as short as $\approx$ 20 μsec, other sources must be sought to account for the very short periods of 1 μsec and less, as exhibited by fig. 6c. A number of mechanisms have been suggested, but none are supported by evidence beyond speculation. The most likely guess is that the oscillating electric field at the ion source induces random plasma oscillations of a severe nature. Whether these are the primary or secondary cause of beam variations we do not know. It is even possible that ion load fluctuations introduce a frequency modulation which could alter the beam†. It is interesting to note that our method of observing dee voltage amplitude fluctuations would exhibit an amplitude change if the frequency changed.

A stabilized dee voltage has provided a number of unexpected benefits. One notable

greatly diminished by a large paraffin and cadmium shield. (See University of Washington Cyclotron Progress Report for 1960.)

[12]) The problem of observing small variations of the dee voltage is not simple, and we are often not certain that what is seen in an oscilloscope is real, or just due to "cross-talk" induced in the long connecting cables. Conversely, the rf tends to appear in all the places where one does not want it. (See, for example, the trace width of fig. 6b.)

† *Note added in proof*: We have recently searched for frequency modulation and find small frequency shifts ($\sim$ 20 cps) which are insufficient to cause beam modulation.

example is the reduced beam spread as shown in the television photographs of fig. 9. A more subtle benefit is that much less beam strikes the duct slit. This slit, even though the radiation shielding is extensive between it and the analyzing magnet, is a serious source of fast neutrons and hence background gamma radiation.

The regulator has been in nearly constant use for the past six months on a 17 hour per day, 7 day per week schedule with only a few minor troubles. A number of experiments are already in progress which depend vitally upon its functioning properly.

Acknowledgements

We wish to thank R. E. Karns for his excellence in electronic construction and for numerous technical suggestions. Conversations with J. F. Streib aided materially in our understanding of the oscillator system. Many persons helped us during the testing period; in particular we thank J. B. Gerhart, W. A. Kolasinski, and A. J. Lieber. Lastly, we wish to mention T. J. Morgan, who assisted in making the system operational, and to whom we are indebted for many observations of the effects on cyclotron performance.

NUCLEAR INSTRUMENTS AND METHODS **10** (1961) 84–94; NORTH-HOLLAND PUBLISHING CO.

A MAGNETIC PARTICLE SPECTROMETER FOR USE WITH A 12 MeV TANDEM ELECTROSTATIC GENERATOR

A. V. COHEN, J. A. COOKSON and J. L. WANKLING

Atomic Weapons Research Establishment, Aldermaston, Berkshire, England

Received 10 October 1960

A new double-focussing magnetic particle spectrometer, with a solid angle of acceptance of 0.007 steradians is described. The resolving power in energy is 850 for protons of up to 12 MeV; saturation effects lower this figure to 450 for protons of energy 21 MeV. Use of the spectrometer, both for measuring the yields of nuclear reactions, and as a tool for investigating the gamma decay modes of selected nuclear levels, is discussed.

1. Introduction

A magnetic particle spectrometer enables one to examine the charged reaction products associated with one specific resolved level of the residual nucleus, and is particularly useful in determining the gamma-decay modes of nuclear excited states. Such an instrument must not only have a high resolving power, but also a large solid angle of acceptance, and must therefore be "double-focusing", that is to say anastigmatic.

Judd[1]) shows that anastigmatism may be achieved by using a non-uniform magnetic field of suitable characteristics. Snyder *et al.*[2]) describe such a magnet, of solid angle 0.006 steradians, the non-uniform field being obtained by suitably shaping the pole-pieces; protons of energy up to 2 MeV can be focussed with an energy resolution of 500. Unfortunately, the pole-face profile was predicted only approximately by theory, so that it became necessary to demount and remachine the polefaces. Rubin and Sachs[3]) describe a magnet with separately adjustable pole pieces and pole edges, thus enabling both anastigmatism and minimum spherical aberration to be achieved empirically. It has a solid angle of 0.0025 steradian, and energy resolution greater than 1000 for protons of energy up to 2 MeV. Magnets of similar design capable of focussing protons of energy up to about 10 MeV have been constructed and have been noted in the literature[4]).

The Tandem Electrostatic Generator of the Atomic Weapons Research Establishment, Aldermaston, described by Allen *et al.*[5]), produces protons or deuterons of energy greater than 12 MeV. It was therefore felt desirable to construct a double-focussing magnetic particle spectrometer similar in concept to that of Rubin and Sachs, but capable of focussing either protons or deuterons of 12 MeV, with as large a solid angle and resolving power as practicable.

The magnet described here has a solid angle of 0.007 steradian, and a resolving power of about 850 in energy for protons up to 12 MeV. Above that energy, saturation begins to lower the resolution, but even for deuterons of 10.5 MeV, corresponding to protons of 21 MeV energy, the resolving power is about 450 in energy.

2. Theory

Let us adopt cylindrical co-ordinates in which the symbols r, θ, z, refer to the radial, azimuthal and axial co-ordinates respectively. Suppose a non-uniform magnetic field H to exist in a gap between C-shaped pole-pieces, symmetrically

[1]) D. L. Judd, Rev. Sci. Inst. **21** (1950) 213.

[2]) C. W. Snyder, S. Rubin, W. A. Fowler and C. C. Lauritsen, Rev. Sci. Inst. **21** (1950) 852.

[3]) S. Rubin and D. C. Sachs, Rev. Sci. Inst. **26** (1955) 1029.

[4]) W. Whaling and C. W. Li, Phys. Rev. **81** (1951) 150.

[5]) K. W. Allen, F. A. Julian, W. D. Allen, A. E. Pyrah and J. Blears, Nature **184** (1959) 303.

placed about the $z = 0$ plane, and limited by $+\pi/2 > \theta > -\pi/2$, and $r_2 > r > r_1$. The gap is independent of θ but increases from r_1 to r_2; thus the resulting field decreases with increasing r, but is independent of θ apart from edge-effects.

In the plane $z = 0$, $H_r = 0$, and at the central ray radius $r_0 = \frac{1}{2}(r_1 + r_2)$, the value of H_z is defined as H_{z0}. Elsewhere in this plane, H_z may then be written:

$$H_z(r,\theta) = H_{z0}\left[1 - \alpha\left(\frac{r - r_0}{r_0}\right) + \right.$$

$$\left. + \beta\left(\frac{r - r_0}{r_0}\right)^2 + \gamma\left(\frac{r - r_0}{r_0}\right)^3 + \ldots\right]. \quad (1)$$

Judd (who uses a slightly different notation) ignores the fringing field and the terms beyond the first order; the effect of these is examined in a paper by Judd and Bludman[6]). Judd[1]) shows that for any value of α, an object distant d_0 from the entrance pole-edge gives radial and axial foci, distant d_r and d_z respectively from the exit pole-edge, which coincide if $\alpha = \frac{1}{2}$. If $\alpha = \frac{1}{2} + \varepsilon$, the amount of astigmatism is given by:

$$d_r - d_z = 10 r_0 \varepsilon . \quad (2)$$

for the simplest case of $d_r \sim d_z \sim d_0$. The diameter δ_A of least confusion is thus:

$$\delta_A = 10 r_0 \varepsilon \phi_r \phi_z/(\phi_r + \phi_z) \quad (3)$$

where ϕ_r and ϕ_z are the maximum divergence of rays in the radial and axial directions respectively.

The resolving power is determined by δ, the image size in the radial direction, being unaffected by the axial image size. If the counter is placed at the line of radial focussing, δ is determined by the size of the aberration-free image δ_0 and the spherical aberration δ_S. For the case $\alpha = \frac{1}{2}$, $M = 1$, where M is the magnification, the resolving powers R_p and R_E in momentum and energy respectively are:

$$R_E = \tfrac{1}{2} R_p = 2 r_0/\delta . \quad (4)$$

Hedgran *et al.*[7]) discuss spherical aberration for the case of object and image both within the magnetic field. Assuming with Rubin and Sachs that this treatment applies to the present case, then:

$$\delta_S = [\tfrac{2}{3}(8\beta - 1)\phi_r^2 + \tfrac{2}{3}(3 - 8\beta)\phi_z^2] r_0 . \quad (5)$$

Thus no value of β will eliminate spherical aberration. In practice, $\phi_r >> \phi_z$, so that β should be near $\frac{1}{8}$. Putting $\beta = \frac{1}{8} + \sigma$ gives:

$$\delta_S = \tfrac{4}{3}[\phi_z^2 + 4\sigma\phi_r^2] r_0 . \quad (6)$$

In the present magnet, $r_0 = 24''$, $\phi_r = 0.114$ radians, $\phi_z = 0.018$ radians. For R_E greater than 750, eqs. (4) and (6) require $\delta \leqslant 0.064''$ and $\sigma \leqslant 0.03$. Since the counter may not be placed accurately at the radial focus, the image size may be increased by astigmatism. This effect will be of order δ_A. Eq. (3) then implies $\varepsilon \leqslant 0.016$.

The later treatment of Judd and Bludman[6]), which appeared after this magnet was designed, suggests $\alpha = 0.500$, $\beta = 0.227$ and $\gamma = -0.147$ as the best field parameters for our magnet if $M = 1$. The disagreements between the various approximate theories, the difficulty of designing the pole-profiles, and the need to allow for machining tolerances all suggest that it would be best to adjust the field parameters empirically to optimise the focus.

A value of α near $\frac{1}{2}$ may be obtained with conically shaped pole-faces. If z_0 is the half-width of the gap at radius r_0, and u the angle between the pole-face and mid-plane, then to a first approximation:

$$\tan u = \alpha \frac{z_0}{r_0} . \quad (7)$$

With the chosen value $z_0 = 1.25''$, the calculated value of u is 1° 29°.

3. Magnet Construction

3.1. GENERAL

The magnet, which weighs 13 tons, is made throughout of mild steel of carbon content about 0.2% (BSS.EN 3A). This steel was considered adequate for the pole-pieces, and the saturation properties suggest that the decision was reasonable (section 5). The magnet was designed to deflect protons of 20 MeV through 180°. To avoid saturation effects unduly distorting the field profile, H_0 should not exceed 10 k gauss, which

[6]) D. L. Judd and S. A. Bludman, Nucl. Instr. 1 (1957) 46.
[7]) A. Hedgran, K. Siegbahn and N. Svartholm, Proc. Phys. Soc. 63 (1950) 960.

determines r_0 to be 24″. The C-shaped pole faces, machined to the calculated angle $u = 1° 29'$, are made $10\frac{1}{2}$″ wide to give the required solid angle of acceptance, and each is surrounded by two independent pole-edges $\frac{3}{4}$″ wide, bevelled at an angle of 30° to the mid-plane. The pole faces and edges rest in grooves machined in the side-cheeks, and are secured and moved in the axial direction by screws, their positions being measured by micrometers. The magnetic circuit is completed by an inner and outer return.

The gap $2z_0$ can be varied between 2.3″ and 2.7″, thus varying α between 0.534 and 0.463. The pole edges can be moved through $\pm$ 0.5″, giving empirical adjustment of β and γ, while keeping the field symmetrical about the plane $z = 0$.

The stray magnetic fields near the entrance and exit of the main system are relatively low (section 4.3(i)). This minimises interference with photomultiplier detectors, and reduces the effect on particle trajectories. To allow for the latter effect, the magnet is designed to have a tilt of 3° to the vertical, with an adjustment of $\pm$ 3°, and is also adjustable in height.

Screws at the base enable the magnet to be split about the plane z_0, allowing access to the poles and coils. Three radial $1\frac{1}{4}$″ square holes machined in the outer return permit the introduction of a proton resonance head to explore the field in the gap; these holes are normally closed by steel plugs.

The whole assembly stands on a rotatable 3.7″ gun mounting. A schematic section of the magnet is given in fig. 1, and fig. 2 shows a general view.

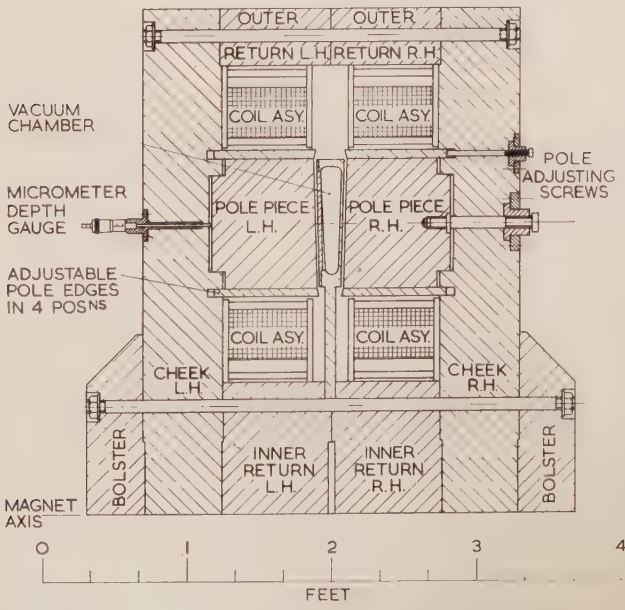

Fig. 1. Upper half of magnet. Schematic section.

3.2. ELECTRICAL

The coils are built as two demountable units, and one is fitted over each pole. Each unit consists of 176 turns of $\frac{3}{8}$″ square aluminium tubing with a central $\frac{1}{4}$″ hole for water cooling. The resistance of the system is about 0.9 ohms, and the inductance 1 henry.

To produce the required field in the gap, currents up to 200 A are required, and these are supplied by a 200V/200A d.c. motor generator. The current is stabilized to about 0.02A over the range 10–200 A and may be varied in steps of 10^{-5} of the maximum value by means of an array of potentiometers. A rough measure of the current is given by a moving-coil meter, and the field is measured accurately by a proton resonance magnetometer (section 3.4).

3.3. VACUUM SYSTEM

The C-shaped magnet box is made of brass, and the stainless steel lid is bolted to it and sealed by gaskets—this design enables one to insert stops as necessary. A cavity in the wall of the box near its exit end provides space for a proton resonance head well inside the field, but clear of the particle orbits.

For angular distribution work, the target chamber has a sliding seal which allows the magnet to be moved relative to the incoming beam direction over a range $-10°$ to $+130°$ without disturbing the vacuum. The target can be rotated, or removed through an air-lock.

The beam, after passing through the target, is stopped in an insulated Faraday cup placed within the target chamber. This produces a high background of gamma rays and neutrons at the highest beam energies. A different system is used for charged-particle-gamma coincidence studies.

in which the magnet is placed at a fixed angle, and the beam stopped in a Faraday cup 6′ beyond the target. This arrangement reduces the background to a satisfactory level.

3.4. MEASUREMENT OF FIELDS

Field measurements are made with a modified proton resonance magnetometer, which enables measurements to be made in the non-uniform field by means of special compensating coils which cancel out the field gradient locally without significantly affecting the field magnitude. This device is described by Vincent *et al.*[8]). Each proton resonance head is about $1\frac{1}{8}''$ cube. A wide field range (2.8–11.4 k gauss) can be covered by three interchangeable heads.

A proton resonance system is inherently capable of an accuracy of perhaps 1 part in 10^5, but this is in the present case reduced by the effects of the compensating coils and the difficulty of correctly locating the three probes in the same position. Tests using the alpha particles from thorium B and interchanging two of the heads suggest that the general reproducibility of results is about 2 parts in 10^4, which corresponds to a movement of 0.3 mm of the probe across the field gradient.

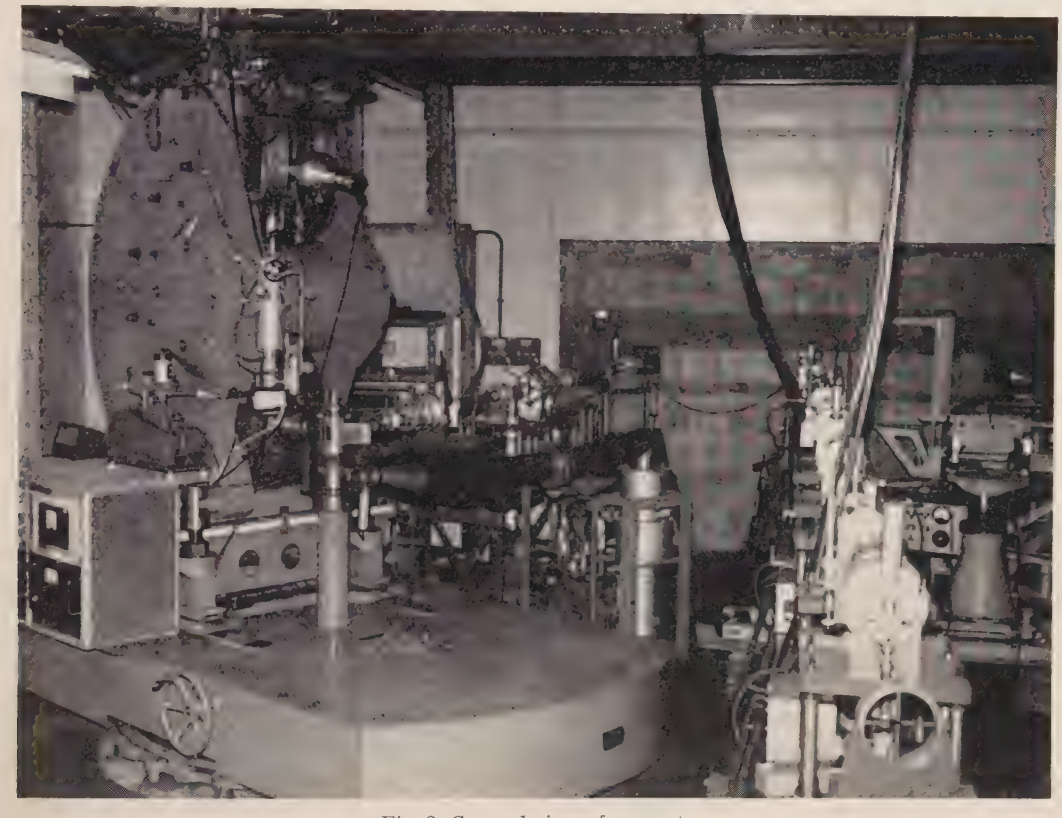

Fig. 2. General view of magnet.

3.5. DETECTOR ASSEMBLY

A slit formed by two cylindrical edges whose separation may be varied between 0 and $\frac{3}{4}''$ from outside the vacuum, is placed at the exit of the magnet and is adjusted by means of a telescopic mounting to coincide with the focus. Immediately behind the slits is placed a caesium iodide crystal, viewed by a 2″ Du Mont 6292 photomultiplier, connected by conventional circuitry to a discriminator and scaler.

[8]) C. H. Vincent, W. G. King and J. B. Rowles, Nucl. Instr. and Meth. **5** (1959) 254.

To examine, with a reasonable counting rate and resolution, the gamma rays from a nuclear level associated with a given group of particles, it is necessary to use a $4\frac{1}{2}''$ sodium iodide crystal. The output from this is gated by the particles focussed in the magnet by means of a fast-slow coincidence circuit[9]), and displayed as a spectrum on a pulse-height analyser.

Protons take a time $202/\sqrt{E}$ ns to travel from target to counter, and the γ-counts must be suitably delayed in order to compensate for this time. Random coincidences are counted simultaneously by a duplicate system using an extra delay. A rotatable arm, coaxial with the magnet turntable, together with suitable supports, enables the crystal to be set in any desired position.

4. Setting-up Procedure

4.1. POSITIONING

The magnet base was set up on levelling screws, and levelled to within 0.005″. The following behaviour was noted as the magnet was rotated through 360°.

1. The distance between the axis of rotation and the vacuum chamber inlet face varied by less than 0.012″.

2. The target chamber support pillar moved by less than 0.006″.

3. The central magnet plane ($z = 0$) passed within 0.030″ of the centre of the target chamber support pillar.

4.2. MAPPING OF FIELD PROFILE

The magnet box was removed, and a proton resonance probe head was introduced through one of the square radial access holes, in order to explore the radial variation of field in the plane $z = 0$.

The pole faces were set so that the value of $2z_0$ was 2.500″, and the pole edges so that the inside of each bevelled edge was flush with the pole face. The observed field profile (fig. 3) can be fitted by: $\alpha = 0.511$, $\beta = \sim 0.32$ for $H_0 = 7160$ gauss. At this position, field profiles were taken for different values of spectrometer current. It was found that α was constant to within ± 0.005 up to $H_0 = 9000$ gauss, corresponding to a proton energy of about 15 MeV, and at higher fields decreased slightly, no doubt due to saturation effects. Field profiles were then taken for various settings of both pole faces and

[9]) R. E. Bell, R. L. Graham and H. E. Petch, Can. J. of Phys. **30** (1952) 35.

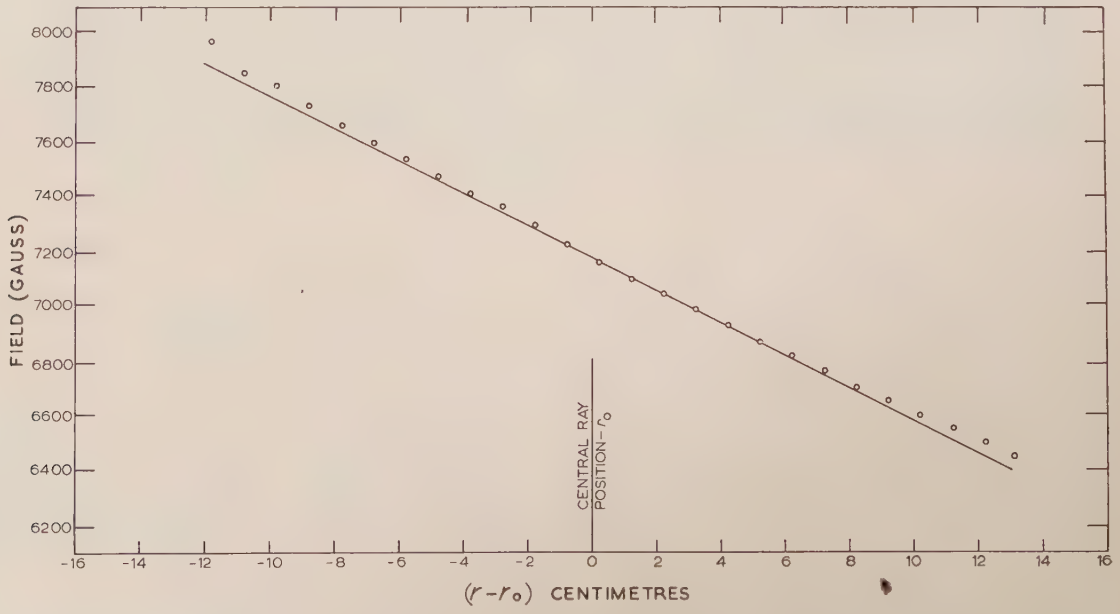

Fig. 3. Field as a function of radial position, $(r - r_0)$. The line shows a linear dependence with $\alpha = 0.51$.

pole edges, and values of α and β corresponding to any likely setting of pole edge and pole face could be estimated.

4.3. FOCUSSING

(i) Location of optic axis

Fig. 4 shows the fringing field, which was explored with a search coil both inside and outside the pole gap, as a function of distance. The expected incoming trajectory of an initially horizontal beam was calculated, and the magnet adjusted both in height and tilt to accept it.

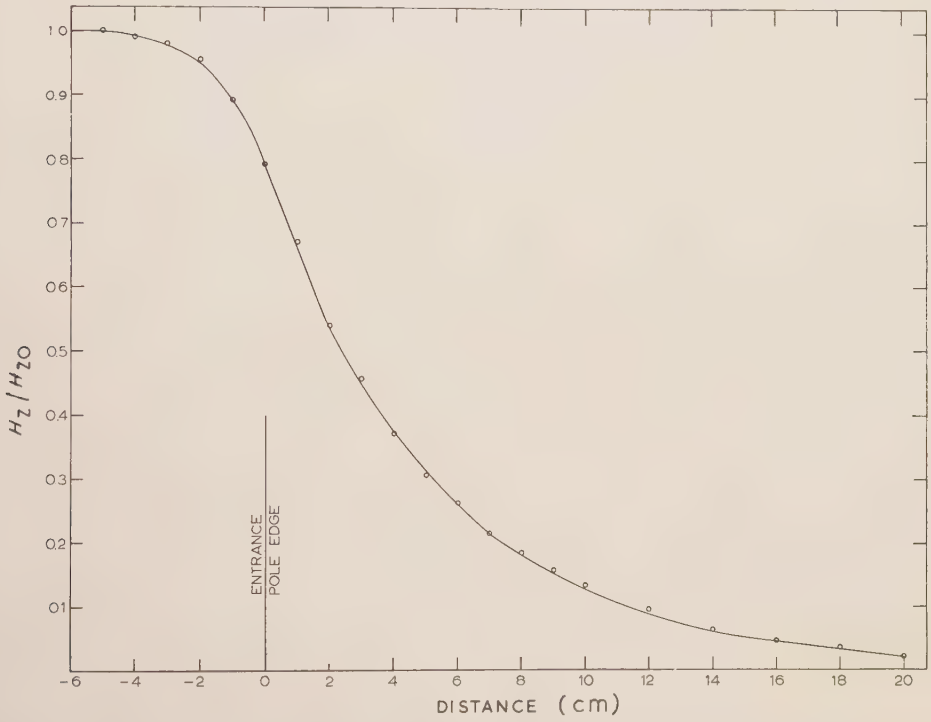

Fig. 4. Fringing field near entrance pole-edge along incoming particle trajectory. $H_{z0} = 960$ gauss.

The central ray $r = r_0$ inside the magnet was then defined by a $\frac{1}{8}''$ hole at the centre of the inlet face, a $\frac{1}{4}''$ hole half-way round the magnet, and a quartz viewer carrying a mark at the centre of the exit face.

The magnet was set in line with a collimated beam of 4.5 MeV protons, and the current varied. It was found impossible to pass the beam on to the viewer; this implied that the initial trajectory was slightly different from that estimated. The magnet was therefore raised by about 0.10″, until the beam passed through the centre of the exit face. In this way, the effective optic axis outside the magnet was found empirically; the effects of slight departures from field uniformity just inside the pole-face were estimated to be small.

(ii) Location of focus

It was found convenient to work at slightly less than unit magnification.

The two stops and the viewer were removed, and another quartz viewer mounted at the expected focal position on a telescopic tube. The beam, collimated to be 0.065″ square, was then "spread" by an a.c. magnet, the centre of which coincided with the axis of rotation of the turntable, and the main magnet field was set to the value used in (i). In this way, the beam could be spread successively in the radial and axial directions so as to fill the aperture of the main magnet as if originating from the centre of the turntable. The radial and axial foci were found; the magnitude and sense of the astigmatism were those associated with $\alpha = 0.505$,

compared with the measured value of $\alpha = 0.511$. The pole faces were withdrawn in small steps until they were 0.026″ from the original setting, when the radial and axial foci were found to coincide. Values of the object and image distances and the magnification are given in section 5.2.

(iii) Minimisation of spherical aberration

The beam-spreading a.c. magnet was used successively in the radial and axial directions, and the size of the image produced from a 0.065″ square beam noted for various positions of the pole edges, until the size, δ, of the image in the radial direction was minimised.

If only $\frac{2}{3}$ of the aperture in the radial direction were filled, δ was still only 0.080″, while when the whole aperture was filled, a "tail" of approximately 0.100″ length in the high-momentum direction developed out of the 0.080″ main image, but this was estimated visually to contain very little of the beam.

Use of formula (4) suggested that the 0.080″ image spot would correspond to a resolving power $R_E = 600$–800, depending on target spot size, and that the sharp peak associated with the spot would have a small "tail" of width 0.002 of the momentum. This has been borne out by experience. It was estimated that by using only $\frac{2}{3}$ of the radial aperture, R_E could be increased to about 1000.

With the pole edges and pole faces in their final positions the following parameters describe the field.

$$\alpha = +0.497 \pm 0.004, \qquad \beta = +0.23 \pm 0.04.$$

Judd and Bludman's theory[6]) predicts parameters of $\alpha = 0.500, \beta = 0.227, \gamma = -0.147$, as the correct values for our system, with symmetrical object and image. Agreement with theory is reasonably satisfactory but we consider that in the circumstances empirically adjustable parameters are necessary.

5. Performance

5.1. RESOLUTION

The resolution of the spectrometer was measured using the 8.786 MeV α particles from Th B. A source, limited in size by a mask 0.1″ in the axial direction and 0.020″ in the radial direction, was placed at the target position, and the detector slit was set at a width of 0.02″.

The resolving power $R_E = E/\Delta E$, and for practical purposes, ΔE was measured as the full width of the peak at half-height. This should lead to values of R_E somewhat higher than those predicted by the theory, but is a useful guide to the performance of the magnet. It was found that $R_E = 850$, which is the ultimate resolving power attainable with the given source size using the full magnet aperture.

In any experiment performed with a nuclear accelerator, several factors reduce the actual resolving power – target thickness, beam energy spread, target spot size, and kinematic recoil effects. As a test of working conditions, the resolution was measured by observing protons of energy up to 12 MeV and deuterons up to 10.5 MeV (equivalent in $H\rho$ to protons of 21 MeV), elastically scattered at 90° by a 100 μg/cm^2 gold target. The observed value of R_E was 750 for protons of energy up to 12 MeV: above this energy the resolving power decreased, and at 21 MeV proton energy equivalent, R_E was 450. The shapes of the groups for 10 MeV protons and 10.5 MeV deuterons are shown in figs. 5a and 5b respectively.

Both peaks have a "tail" in the high-momentum direction, extending to $\Delta p/p = +0.0026$, which is associated with the "tail" observed visually. At the highest energies, relatively more of the particles go into the "tail".

The value of $R_E = 750$, up to 12 MeV, represents the accumulated effects of the factors mentioned above on the ultimate value of 850, while the reduction to 450 at 21 MeV is due mainly to the effects of field profile distortions caused by saturation: this effect becomes noticeable near the same field values as do other saturative effects (section 5.3). The resolution even at the highest energies will be adequate for most experiments, and may be improved if necessary by stopping down the radial aperture.

Even at low energies, the resolving power will be lower than 750 if targets of light atomic

weight are used; the kinematic effects then predominate over all others. This effect is illustrated in fig. 5c, which shows the inelastic scattering at 20° of 6 MeV protons from the 2.976 MeV–2.999 MeV doublet in Al^{27}.

The separation $E/\Delta E$ is 130, and the value obtained for R_E is 400 even at full aperture. This value agrees with calculations of the kinematic effect.

dicted magnification of the system was 0.922, and the predicted solid angle was 7.7×10^{-3} steradians.

The solid angle was measured directly. A thorium B source was placed at the target holder and the counting rate due to 8.786 MeV alpha particles (using the full aperture of the magnet) compared with that obtained with a smaller solid angle defined by a suitably positioned aperture.

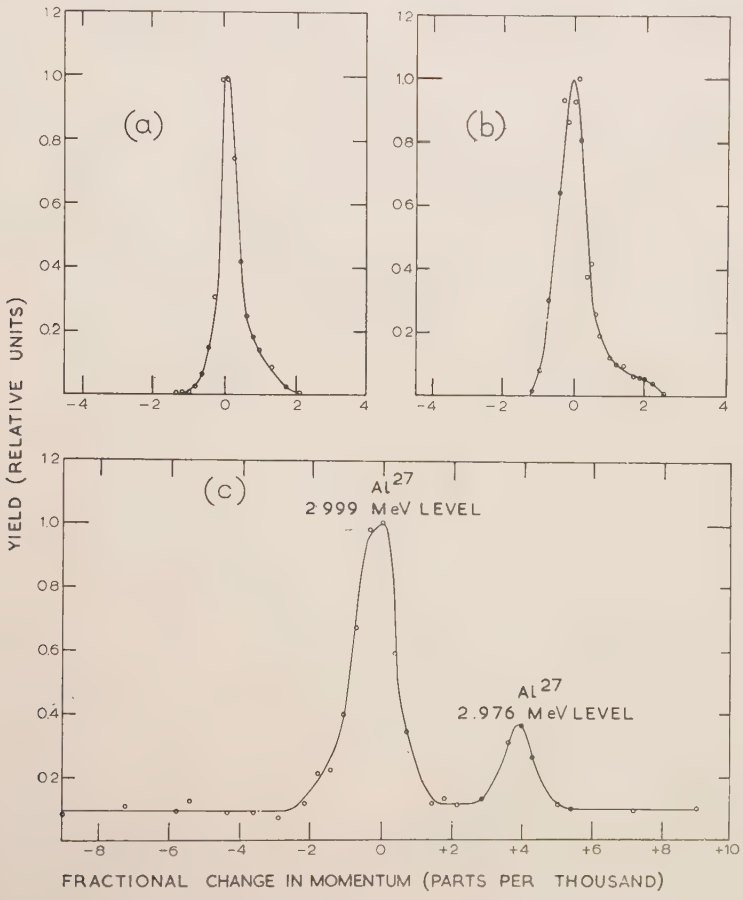

Fig. 5. Resolution of magnet. Target spot size 0.030″, and detector slit width 0.050″. (a) 10 MeV protons elastically scattered at 90° by 100 μg/cm² gold target. $R_E = 750$; (b) 10.5 MeV deuterons similarly scattered. $R_E = 450$; (c) 6 MeV protons inelastically scattered at 20° by 50 μg/cm² aluminium target. $R_E = 400$.

5.2. MAGNIFICATION, BENDING ANGLE, AND SOLID ANGLE OF ACCEPTANCE

The bending angle of the magnet established by the setting-up procedure agrees with the value of 188° estimated from the fringing fields. The object and image distances are 20.75″ and 13.9″ respectively. With these values, the predicted magnification of the system was 0.922, and the predicted solid angle was 7.7×10^{-3} steradians.

The solid angle was measured directly. A thorium B source was placed at the target holder and the counting rate due to 8.786 MeV alpha particles (using the full aperture of the magnet) compared with that obtained with a smaller solid angle defined by a suitably positioned aperture.

The solid angle was thus measured to be $7.0 \pm 0.3 \times 10^{-3}$ steradians.

5.3. EFFECTS OF SATURATION ON ENERGY MEASUREMENTS

To measure accurately the energy of a group of particles focussed in the spectrometer, it is

necessary to know the relation between $H\rho$ and the measured proton resonance frequency ν_s. This will not be strictly linear if saturation effects distort the field profile, since ν_s is measured in a position of relatively low field.

A linear relationship should hold at low energies and was tested by using the three alpha groups from thorium B (6.050 MeV, 6.090 MeV and 8.786 MeV). The three values of $H\rho/\nu_s$ agreed within 0.15%, the expected accuracy of the measurement.

well-defined in position. The first effect is estimated to be much less than the corresponding effect in the spectrometer, and the second to be about 1 part in 10^3. Within these limitations, the ratio ν'_s/ν_0 should be independent of energy until the spectrometer begins to saturate.

This ratio, reduced to unity for low energy deuterons, is plotted in fig. 6 as a function of energy. The proton ratios are systematically 0.1% higher than those of deuterons of the same $H\rho$, and it is believed that this is due to the

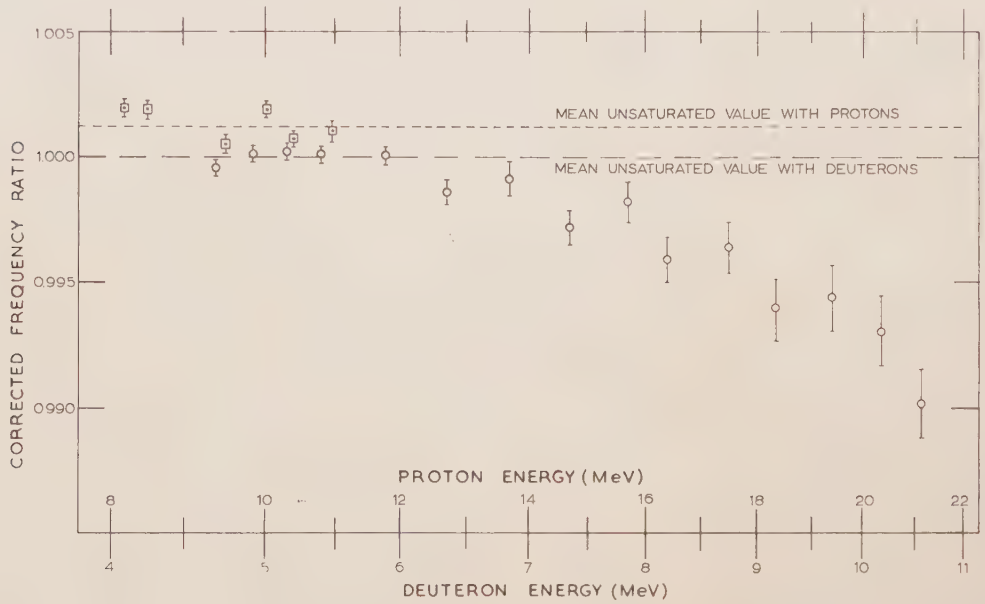

Fig. 6. Test of saturation in magnet. Ordinates are normalized values of ν'_s/ν_0. Circles and squares represent points obtained with deuterons and protons respectively.

To investigate the matter further, protons and deuterons of energy up to 10.5 MeV were elastically scattered by gold foils and observed with the magnet at 90° to the incoming beam direction, the value of ν_s being noted at each energy and corrected to a value ν'_s to allow for recoil from the scattering gold nucleus. The proton resonance frequency ν_0 of the uniform magnetic field that deflects the vertical Tandem Generator beam into the horizontal plane, was also recorded at each energy, and must be accurately proportional to $H\rho$, provided that the effects of saturation upon the fringing fields of the deflecting magnet are negligible, and that the beam is

slightly different positions of proton and deuteron beams in the Tandem Generator. Apart from this, the ratio is substantially constant within $\pm$ 0.1% for proton equivalent energies up to 12 MeV: above this it decreases significantly, being 1.0% $\pm$ 0.2% low at a proton equivalent energy of 21 MeV.

Energy calibrations with the magnet are therefore reliable to $\pm$ 0.2% up to $E_p = 12$ MeV, and $\pm$ 0.4% up to $E_p = 21$ MeV. It is not considered necessary at present to improve the quality of the calibration, since the magnet is not intended primarily to determine the energies of nuclear levels.

6. Scope of the Spectrometer

The spectrometer can be used to examine spectra, angular distributions and excitation functions of nuclear reaction products. It is not primarily intended for this purpose, since in most cases the desired results can be obtained more quickly and more reliably with a magnetic spectrograph. The spectrometer has however been used for some work of this type. In particular, very weak groups of particles can be detected even when close to strong elastic arises. Particles traversing different trajectories take different times to reach the detector slit. This "time-spread" is $\pm$ 10.2% of the mean time of flight[10]; that is $\pm 20.5/\sqrt{E}$ ns for E MeV protons. The resolving time is consequently limited at present to 35 ns for proton energies of $\sim$ 2 MeV.

Fig. 7 shows the coincidence rate for the reaction C^{12} (p,p'γ)C^{12} as a function of delay for an incident proton energy of 9.44 MeV. The figure shows also a theoretically derived curve. The

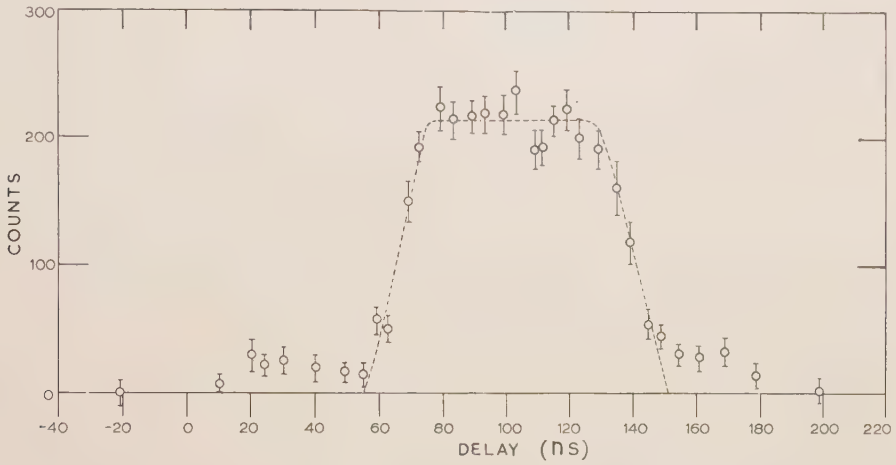

Fig. 7. C^{12}(p,p'γ). Delay curve of gamma rays above 0.5 MeV energy in coincidence with protons exciting the 4.43 MeV level. Incident proton energy — 9.44 MeV. Resolving time 35 ns.

groups. An example of this (to be reported more fully elsewhere) is the inelastic scatter at 130° of 12 MeV protons by gold, which excited the 550 keV level and 275 keV doublet. The peaks due to protons thus scattered were readily detected since the background was only about 2×10^{-4} of the elastic peak.

The magnet is used most advantageously as a "gate" to study the gamma-spectra in coincidence with a given level (section 3.5). Provided that the γ-counting rate, including background, is limited to $\sim 10^5$/sec, coincidence spectra may readily be obtained. The apparatus is adequate for the experiments at present being undertaken, but to examine levels produced less prolifically, one must work at higher background gamma counting rates and suitably modify the electronic circuitry.

Even when this is done, a further limitation difference between this and the experimental points is ascribed to instrumental and background effects.

The large time-spread is determined by the radius of the magnet and the need to make $\phi_r >> \phi_z$ to minimize fringing effects. It should be possible to compensate for the time-spread by using a suitable counter assembly.

7. Conclusions

The spectrometer described here has achieved the purpose for which it was originally designed. It will focus protons of energy up to 12 MeV with a solid angle of acceptance of 0.007 steradians and a resolving power of 850 in energy; at higher energies the resolving power is less.

Its principal use is as a gate to study the gamma decay schemes of the excited states of residual nuclei.

[10] B. E. F. Macefield, Private Communication.

Acknowledgements

We would like to thank Dr. K. W. Allen for initially suggesting the value of this type of spectrometer, and for much advice and encouragement during the course of its construction and installation.

Thanks are also due to the engineers responsible for the detailed design, Mr. A. J. Marriott, Mr. T. Dyke and Mr. R. Hucklesby, and to Mr. A. J. Cole for much technical assistance.

NUCLEAR INSTRUMENTS AND METHODS 10 (1961) 95–107; NORTH-HOLLAND PUBLISHING CO.

EXPERIMENTS WITH ELECTRODELESS GENERATION AND ACCELERATION OF PLASMA RINGS

L. HÖGBERG and K. VOGEL

Institute of Physics, University of Uppsala, Sweden

Received 1 October 1960

The design and performance of an electrodeless plasma gun is described. The driving circuit consists of a capacitor feeding a single primary turn, placed behind the flat end wall of a Pyrex tube. Max. primary current is 65 kA with a risetime of 0.35 μs. The discharges have been studied by means of magnetic pick-up loops, a Kerrcell camera, and by spectroscopical measurements. Plasma rings of comparatively high purity and with velocities up to 5 cm/μs have been produced. By means of a longitudinal magnetic field, strength up to 1200 gauss, the burst of plasma has been contracted to the center of the tube.

1. Introduction

The various and growing applications of magnetically driven plasma guns span at present from high temperature spray-coating to the propulsion of space vehicles. In basic plasma physics research such guns, i.e. mechanisms for the creation and acceleration to high directional velocities ($> 10^6$ cm/s) of a plasma, are of interest in connection with a number of experiments, e.g. injection into various types of magnetic bottles[1,2]), and generally for studies of the interaction between moving plasmas and magnetic fields. The extensive use of the same type of mechanisms for the generation of strong shock waves should also be mentioned[3]).

Most frequently variations of the rail type[4]) or coaxial[5,6]) geometry have been used, where the plasma forms a movable conductor between two fixed electrodes. In electrodeless geometries[7,8]), on the other hand, the acceleration depends on the interaction between external fields and induced currents in the plasma.

Apart from the problem of high energy conversion efficiency, the purity of the plasma delivered by the gun is of critical importance, especially in thermonuclear research[1,9]). As recently reported[6]), contaminations from the electrodes in a coaxial gun may be absent under certain circumstances. Nevertheless the extremely high purity demands strongly favour an electrodeless geometry. Moreover a properly chosen shape of the primary and a proper programming of the primary current open a possibility of ohmically heating the plasma prior to the main acceleration. The electrical problems, e.g. the coupling between the plasma and the primary, may, however, be somewhat more cumbersome in an electrodeless geometry. Some considerations of theoretically attainable efficiencies for a simplified case are given in sect. 2 of this paper.

The work at Uppsala on an electrodeless plasma gun was initiated in the end of 1958, based on a concept by K. Siegbahn to create a plasma ring in the familiar toroidal geometry

[1]) R. F. Post, Proc. Second UN Int. Conf. Geneva 1958, Vol. 32, p. 245.

[2]) J. Tuck, Proc. IVth Int. Conf. on Ionization Phenomena in Gases, Uppsala 1959, Vol. II p. 926.

[3]) A. C. Kolb, Proc. IVth Int. Conf. on Ionization Phenomena in Gases, Uppsala 1959, Vol. II p. 1021.

[4]) W. H. Bostick, Proc. Second UN Int. Conf., Geneva 1958, Vol. 32 p. 427.

[5]) H. Alfvén, L. Lindberg and P. Mitlid, J. Nucl. Energy Part C **1** (1960) 116.

[6]) J. Marshall, Phys. Fluids **3** (1960) 134.

[7]) J. Marshall, Proc. Second UN Int. Conf. Geneva 1958, Vol. 31 p. 341.

[8]) I. S. Shpigel, J. Exptl. Theoret. Phys. (U.S.S.R.) **36** (1959) 411 (Transl. JETP **36** (1959) 285).

[9]) R. F. Post, Int. Summer Course in Plasma Physics, Risö, Denmark, 1960 (to be published).

and then shoot it away from its primary. Some preliminary results have been reported earlier[10,11]). Although a "split toroid" primary[11]) has been tested, the present investigation comprises the performance of a gun with the simpler primary geometry of a flat turn.

2. Theory

Notations:

m total mass of plasma ring

L_1 inductance of primary (assumed constant)

L_2 inductance of plasma ring secondary

$M = g\sqrt{L_1 L_2}$ mutual inductance between primary and plasma ring

$g = g(r,z)$ coupling factor ($g \leq 1$)

Subscript zero indicates initial values, i.e. at the moment of closing of the primary.

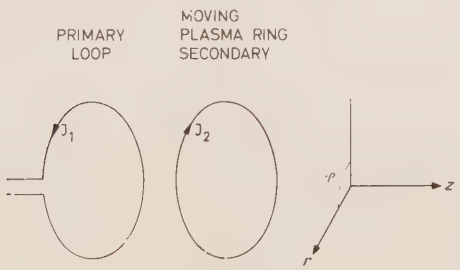

Fig. 1. Idealized picture of the electromechanical system.

General theoretical principles for the motion of plasma loops in axially symmetric fields have been given elsewhere [12,13]). If dissipative terms (friction, resistive losses, etc.† are ignored in a very idealized case, the motion of the plasma ring secondary (cf. fig. 1) can be described by an equation of the form[13])

$$m\frac{\partial \mathbf{v}}{\partial t} = -\nabla U\,, \tag{1}$$

U being a magnetic energy function, including both primary and secondary circuits.

A characteristic time T during which the main part of the acceleration takes place is given by

$$T \sim l\sqrt{\frac{m}{U_{\max}}}\,, \tag{2}$$

† Some consideration to breakdown behaviour may, however, be included in specifying the initial conditions.

where $U_{\max}$ is of the order of $|MI_1I_2|_{\max}$ and l is a characteristic length describing the decrease of M, i.e. $(M_l - M_0)/M_0 \ll 1$. To achieve high acceleration efficiency I_1 and I_2 should reach their maxima in a time about equal to or shorter than T. For the dimensions and pressures used in these experiments T will be of the order of some μs compared with a primary current rise time of 0.35 μs.

To estimate the maximum efficiency obtainable we consider a simple "crowbar" case. We assume that no additional external fields (e.g. a d.c. B_z-field) are present, and that the secondary is a perfect conductor already at $t = 0$. I_1 is raised to its max. value, $I_{1\max}$, in a time $t_1 \ll T$, whereupon the primary is short-circuited at $t = t_1$. For $t > t_1$ eq. (1) assumes the form

$$m\frac{\partial \mathbf{v}}{\partial t} = L_1 I_1{}^2_{\max}(1 - g_1{}^2)\,\nabla\left(\frac{1}{1 - g^2}\right) \tag{3}$$

the maximum kinetic energy being

$$(\tfrac{1}{2}mv^2)_{\max} = \tfrac{1}{2}L_1 I_1{}^2_{\max}(1 - g_1{}^2)\,g_1{}^2 \tag{4}$$

whereas the total magnetic energy W_{magn} in the system at $t = t_1$ is

$$W_{\text{magn}} = \tfrac{1}{2}L_1 I_1{}^2_{\max}(1 - g_1{}^2)\,. \tag{5}$$

Substituting some appropriate effective value for $I_{1\max}$ these results have some bearing also on cases where I_1 varies sinusoidally with a frequency $\gg 1/T$.

Maximum theoretical efficiency for the acceleration process is thus $g_1{}^2$ which could be made close to 1. For such values of g_1, however, stray inductances in the feeding circuit (e.g. capacitors) may be dominant during the time of transfer, $0 < t < t_1$, of energy into the proper acceleration circuit. This must be taken into account determining the maximum overall

[10]) L. Högberg, K. Siegbahn, K. Bockasten, Conference of the Swedish National Committee for Physics, Stockholm June 1959 (abstract in Arkiv för Fysik **16** (1960) 500).

[11]) L. Högberg, K. Siegbahn and K. Bockasten, Proc. IVth Int. Conf. on Ionization Phenomena in Gases, Uppsala 1959, Vol. II p. 1156.

[12]) A. I. Morozov, J. Exptl. Theoret. Phys. (U.S.S.R.) **32** (1957) 305 (Transl. JETP **5** (1957) 215).

[13]) L. M. Kovrizhnykh, J. Exptl. Theoret. Phys. (U.S.S.R.) **36** (1959) 1834 (Transl. JETP **36** (1959) 1308).

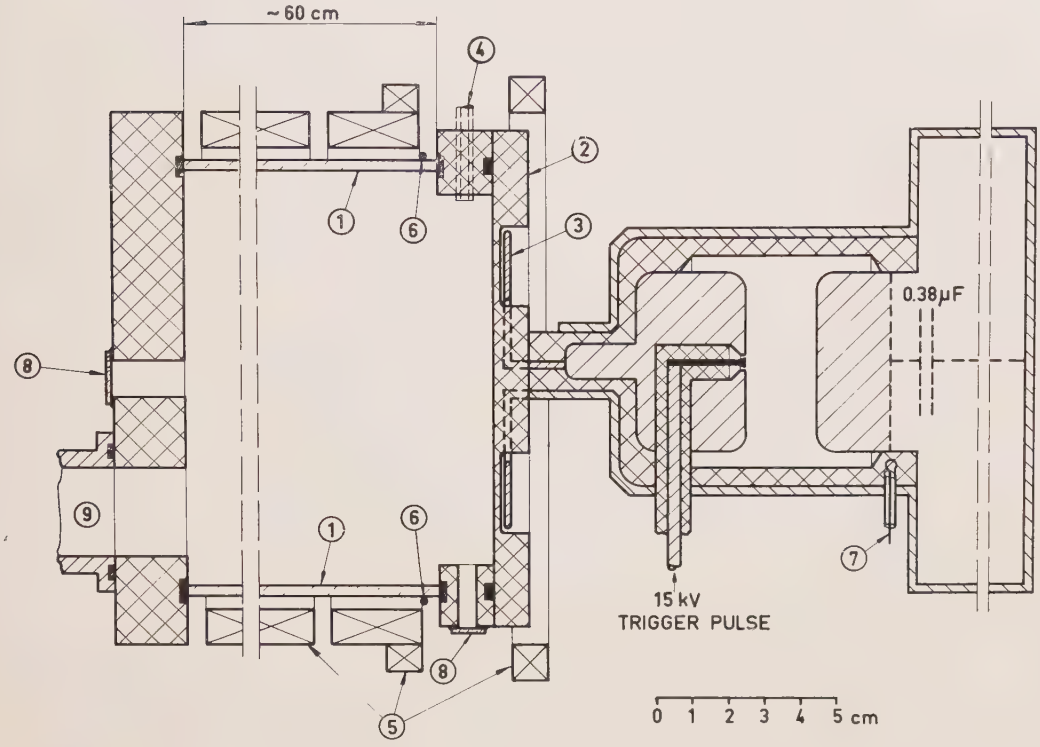

Fig. 2a. Schematic drawing.

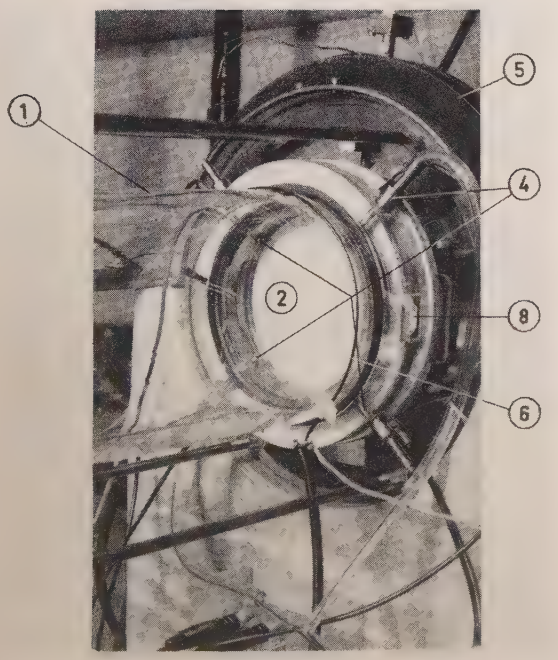

Fig. 2b. Primary end of the discharge tube.

Fig. 2. The apparatus.

(1) Pyrex tube
(2) Porcelain disc
(3) Flat, single turn copper primary
(4) Combined gas inlet and glow discharge preionization electrode
(5) Coils for B_z field
(6) Loop for measurement of $d\phi/dt$ from gas current
(7) Loop for measurement of dI/dt from primary current
(8) Quartz observation windows
(9) Pump outlet.

efficiency of the system and corresponding optimum values of g_1.

These considerations have served as a basis of design of the apparatus. As described in the following, however, the discharge phenomena in the present stage are too complex to permit, for example, experimental determinations of the efficiency as compared with the simple calculations above.

possible (< 3 mm) to improve the coupling factor g (see section 2). Compared with the earlier arrangement[11]) with a groove on the inside of the porcelain disc in which the discharge started, the completely plane inner surface of the wall now used gives a cleaner plasma.

The electrical characteristics of the primary circuit used in this investigation are given in table 1.

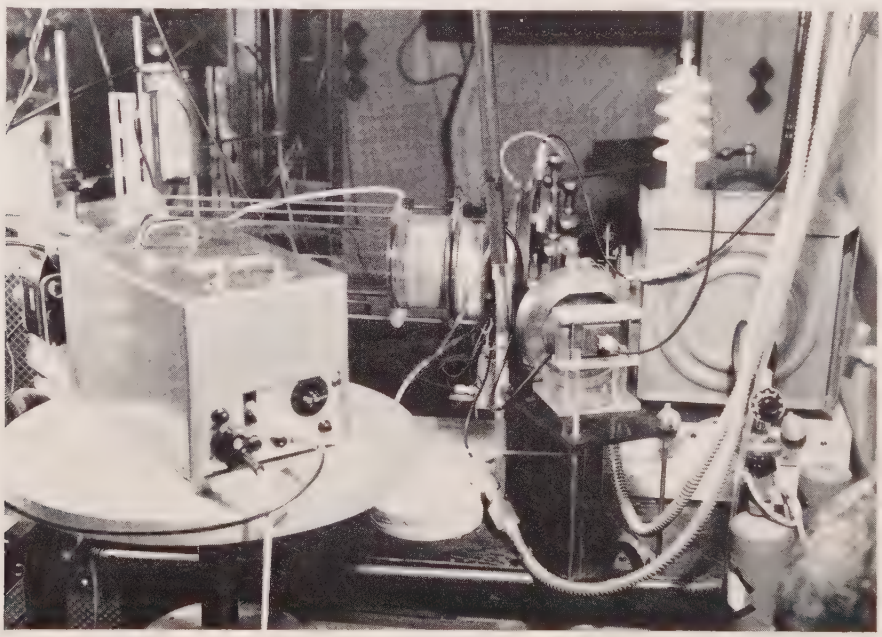

Fig. 3. General view of setup. From right to left: Capacitor with gas inlet system in front, spark gap with auxiliary trigger equipment, discharge tube with solenoid windings partly removed to provide view for Kerrcell camera at near left.

3. Apparatus

The principal features of the apparatus will be briefly outlined (cf. figs. 2 and 3), as it has been somewhat changed with the description earlier given[11]). The main discharge vessel is a 120 mm i.d. Pyrex tube about 600 mm long. It is evacuated to a base pressure of about 10^{-5} mm Hg. One end wall consists of a porcelain disc which has a ringshaped groove on the outside in which the primary is located, a single flat copper turn, 70 mm broad and with a main diameter of 65 mm. This shape gives a strong radial component of the magnetic field near the primary, i.e. the z-component of ∇g and thus also of the accelerating force will be large. The porcelain wall in front of the primary has been made as thin as

TABLE 1
Electrical characteristics of the primary circuit

Capacitor†	0.38 μF
Inductance: total	140 nH
spark gap + condenser	70 nH
Max. primary current (at 40 kV capacitor voltage)	65 kA
Rise time of primary current	0.35 μs

† ASEA, type CTU.

A glow discharge (see fig. 2b) preionizes the gas to ensure breakdown in the first or, at lower pressures, at least in the beginning of the third quarterperiod of the primary current.

A solenoid surrounding the discharge tube

gives a longitudinal magnetic field with strengths up to 5000 gauss. It is fed from a small condenser bank. The rise time of the B_z-field is 1.4 ms, and the main discharge is triggered at the moment of field maximum in the solenoid. Compensating windings indicated in fig. 2 keep the field constant within 5% up to the position of the primary.

4.1. METHODS

Magnetic pickup loops are placed around the Pyrex tube and in the primary circuit (cf. fig. 2). Usually two such loops, one of each kind, were balanced against each other by means of a differential amplifier to exclude the signals from the primary current, and the $d\phi/dt$ caused by the gas current alone could be studied on an oscilloscope. Preliminary tests have been made with a probe consisting of a small Rogovski belt (large diam. 20 mm, small diam. 2 mm) introduced into the discharge.

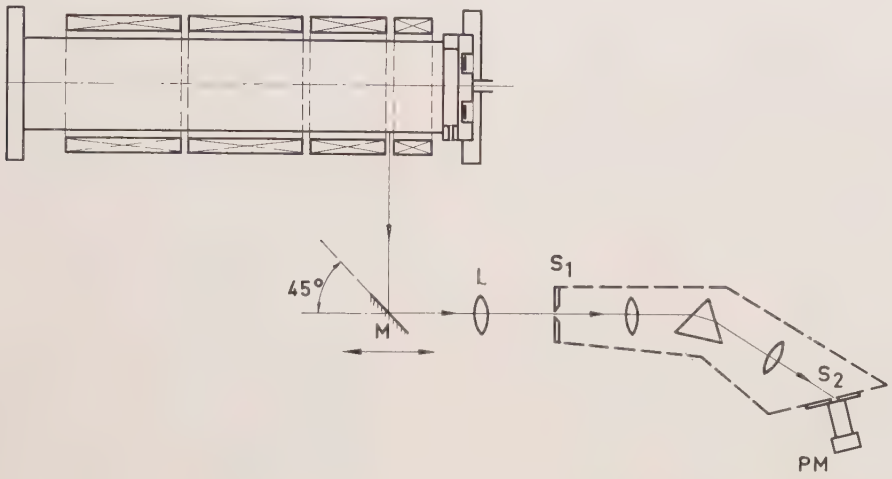

Fig. 4. Arrangement for recording intensity of spectral lines as function of time and position (z) along the discharge tube. M movable mirror, L lens, S_1 entrance slit of spectrograph, S_2 exit slit of spectrograph, PM photomultiplier.

4. Measurements

The following notations for the discharge parameters are used:

- V voltage on the capacitor in the primary circuit
- B_z strength of the longitudinal magnetic field
- p gas pressure in the discharge tube
- z distance along the tube with $z = 0$ at inner surface of porcelain disc in front of the primary
- t time with $t = 0$ at the moment of breakdown of the spark gap in the primary circuit.

V has been varied between 20 and 40 kV, B_z between 0 and 1200 gauss. During experiments gas is kept continuously streaming through the tube. Deuterium has been used in most cases with p mainly in the range 75 to 400 μ.

Pictures of the discharge have been taken with a Kerrcell camera, exposure time 0.1 μs. Information on the general structure of the discharge was also obtained from stigmatic spectrograms taken with a Hilger Medium Quartz Spectrograph. The intensity of the light from the discharge at different wavelengths as a function of time and distance along the tube was recorded with the arrangement shown in fig. 4, using the Medium spectrograph or a Hilger E 1 spectrograph. The velocity of the plasma has mainly been determined from these measurements. Doppler shift measurements with the setup earlier described[11]) have occasionally been made as a check on the ion velocities.

4.2. RESULTS

A representative record of a discharge is shown in fig. 5. The reproducibility from shot to shot is very good except at some combinations of the discharge parameters involving low values of V and p together with a strong B_z-field.

At the presence of a B_z-field the plasma contracts towards the center of the tube, and rather irregular but still reproducible shapes are observed (fig. 8).

The electrical characteristics are consistent with the general picture of the discharge given

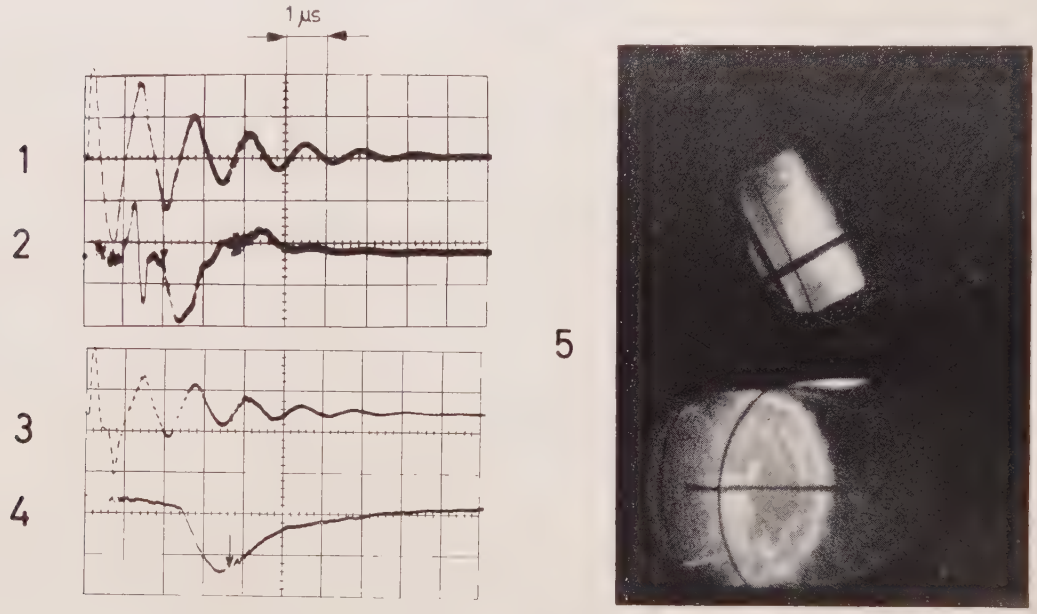

Fig. 5. Typical record of a discharge. $V = 40$ kV, $B_z = 0$, $p = 400$ μ; 1. primary dI/dt; 2. signal from Rogovski belt; 3. $d\phi/dt$ from gas current measured by loop around Pyrex tube (6 in fig. 2); 4. intensity of continuum radiation, $\lambda = 3640$ Å, at $z = 5.6$ cm; 5. Kerrcell photo. Upper image obtained through mirror. Moment of exposure registered at arrow in trace 4. The arrow in trace 2 at 2 μs indicates the moment when the light front entered the Rogovski belt.

A discharge at $B_z = 0$ proceeds typically as follows: Gas breakdown occurs in the beginning of the first or—at lower pressures—third quarterperiod of the primary current. A plasma ring is formed and starts travelling down the tube reaching a velocity of some cm/μs. The interaction with the neutral gas decelerates the ring which gradually disintegrates. Typical ringshapes are shown in the Kerrcell pictures in figs. 6 and 7. Each picture comes from a series, taken in different discharges but with the same value of t for the moment of exposure. The reproducibility within such a series—even of the finer details—is remarkably good. The variation in ring-shapes between different values of V and p can probably be ascribed to differences in the breakdown mechanism.

above. It is believed that surface currents in residual gas and knocked-out impurities at the walls of the discharge tube near the primary are responsible for a main part of the secondary $d\phi/dt$ recorded during the later periods of the primary current (trace 3, fig. 5). Some evidence for this is given by the Kerrcell pictures. The data from the Rogovski probe—although to be considered as very rough and preliminary—strongly indicates that the main light front is associated with a moving ringshaped current (cf. trace 2 in fig. 5). The short pulse preceding the arrow may be associated with a weak but fast-moving light front observed in the photomultiplier measurements travelling ahead of the main plasma ring (see below).

The discharge spectra (cf. figs. 9 and 10) are

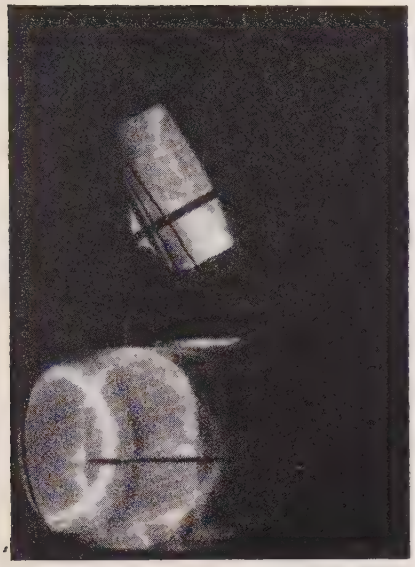

$t = 2.5\ \mu s$

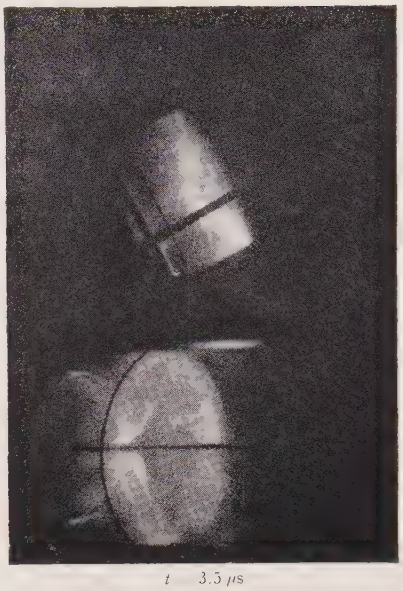

$t = 3.5\ \mu s$

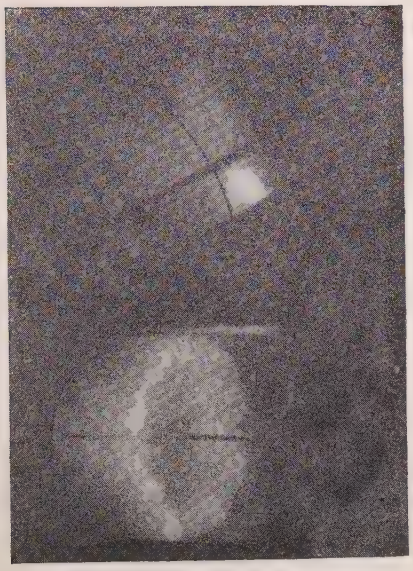

$t = 6.3\ \mu s$

$t = 8.0\ \mu s$

Fig. 6. Proceeding of discharge shown in series of Kerrcell pictures. $V = 40$ kV, $B_z = 0$, $p = 200\ \mu$.

dominated by the Balmer series with carbon as the main impurity. O IV and C IV are the highest ionization stages observed. As the same number of shots have been used at $V = 20$ kV and $V = 40$ kV there is a considerably greater effective exposure of the spectroscopic plate in the latter case due to the increased light intensity from the discharge at the higher voltage. The effect is particularly pronounced for the impurity lines, the stronger members of the Balmer series already being overexposed in both cases. Organic materials in parts of the vacuum system, especially near the primary end wall, are believed to be responsible for the carbon impurities.

There is a pronounced concentration in the intensity of the lines, especially those from higher ionization stages, to a ring-shaped region

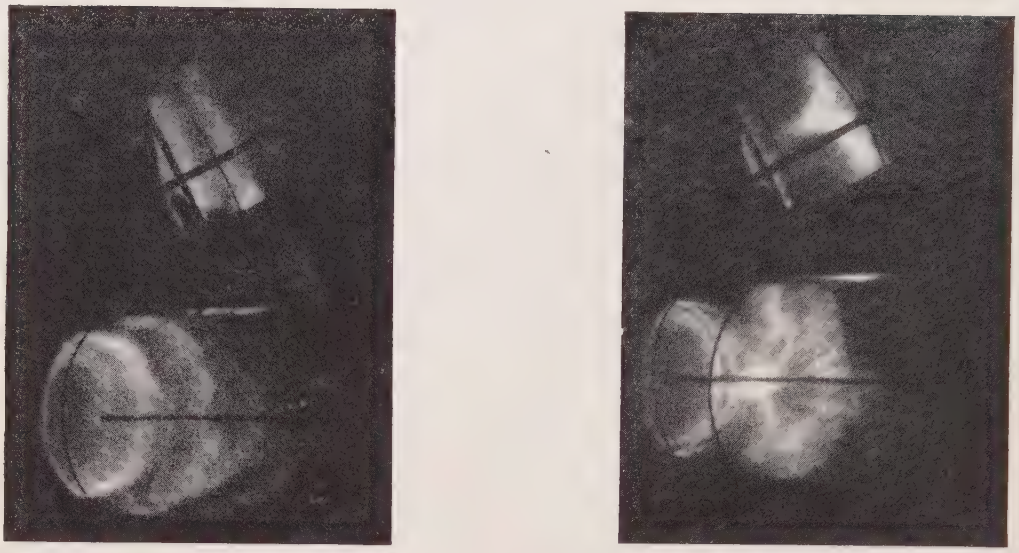

t = 2.3 μs t = 3.7 μs

a. $V = 40$ kV, $B_z = 0$, $p = 75$ μ;

t = 3.2 μs t = 6.2 μs

b. $V = 40$ kV, $B_z = 0$, $p = 400$ μ;

Fig. 7. Kerrcell pictures of some typical ring shapes for different values of V and p.

when $B_z = 0$ (cf. fig. 10). The contraction of the discharge to the central part of the tube under the influence of the B_z field is also demonstrated in the spectrograms. A strong continuum radiation then appears at the center of the tube, indicating a high electron density. A similar but weaker continuum is emitted by the imploding "beaks" of the plasma funnels produced at certain values of the parameters (cf. fig. 7a, $t = 3.7$ μs).

At wavelengths shorter than about 2500 Å the Medium spectrograph has sufficient dispersion to

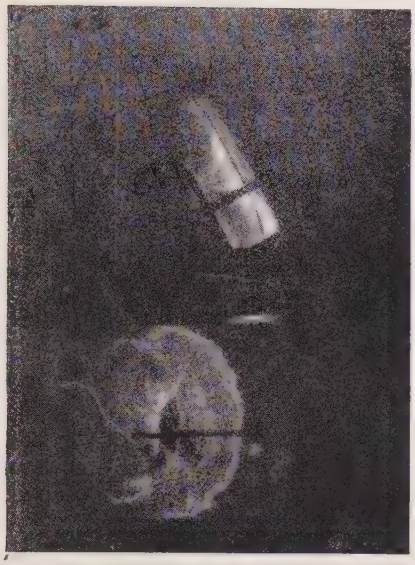

$t = 2.8\ \mu s$

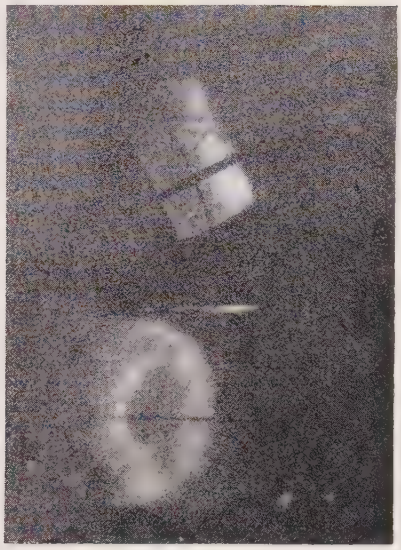

$t = 6.1\ \mu s$

Fig. 7. Kerrcell pictures of some typical ring shapes for different values of V and p.
c. $V = 28$ kV, $B_z = 0$, $p = 400\ \mu$.

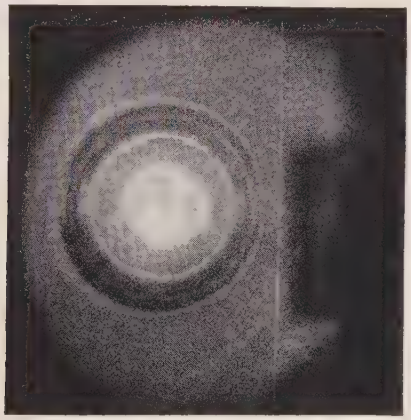

Fig. 8. Kerrcell picture taken end on of a discharge in a longitudinal magnetic field.
$V = 40$ kV, $B_z = 1200$ gauss, $p = 200\ \mu$, $t = 3.9\ \mu s$.

display a Doppler shift between spectra taken end on and from the side. The shifts agree with the results from the other methods of velocity measurements. In fig. 11, taken from an earlier series, the displacement of the intensity maximum corresponds to an axial velocity of 2–3 cm/μs. These measurements also show that actually a large percentage of the ions are accelerated.

The best accuracy in the velocity measurements is obtained with the setup of fig. 4. The time at which one half of maximum intensity is reached has been taken as a measure of the arrival of the main part of the plasma. (This method has been found to give the best defined determinations.) In this way the motion of the plasma ring (z-position as a function of time) can be plotted (fig. 12).

Fig. 12a demonstrates the agreement between measurements at different wavelengths, the

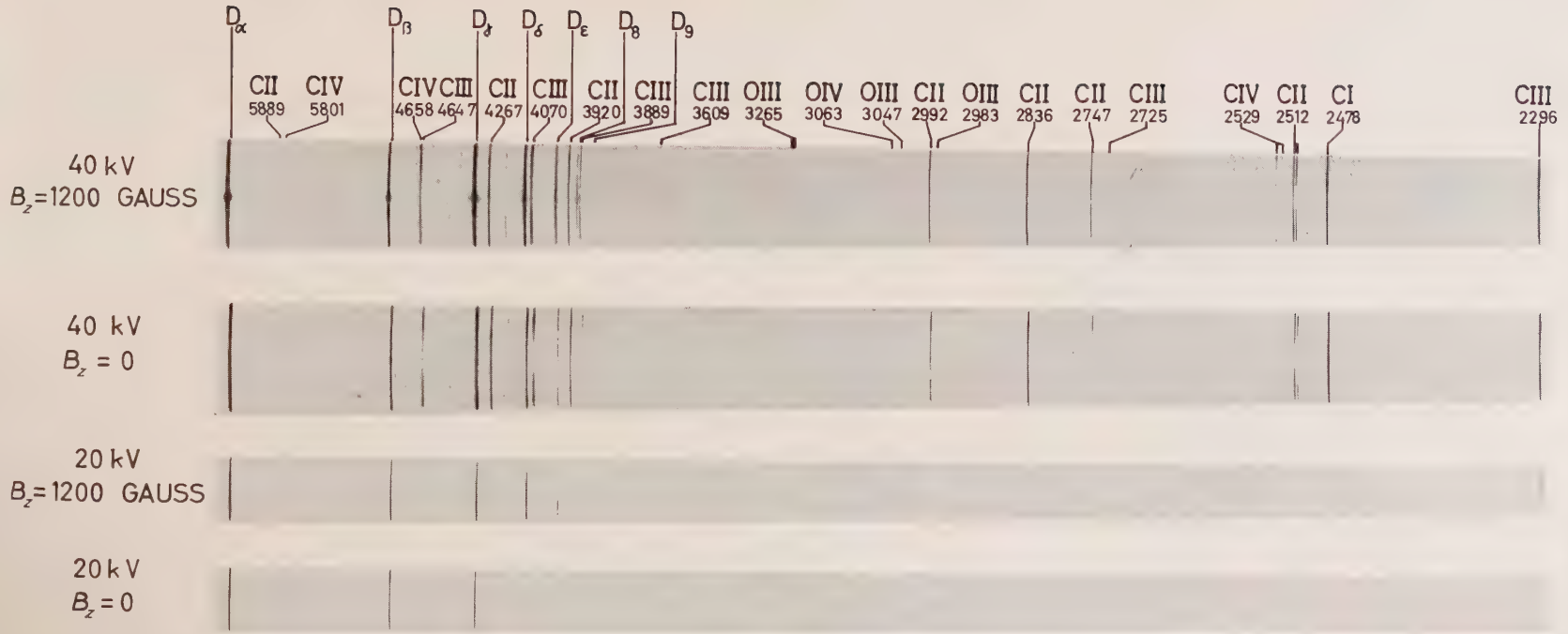

Fig. 9. Stigmatic spectrograms taken through the window in the end wall opposite the primary (cf. fig. 2a). The discharge is imaged along a whole diameter at 40 kV, along the upper half of the same diameter at 20 kV (cf. fig. 10). Exposure: 50 shots.

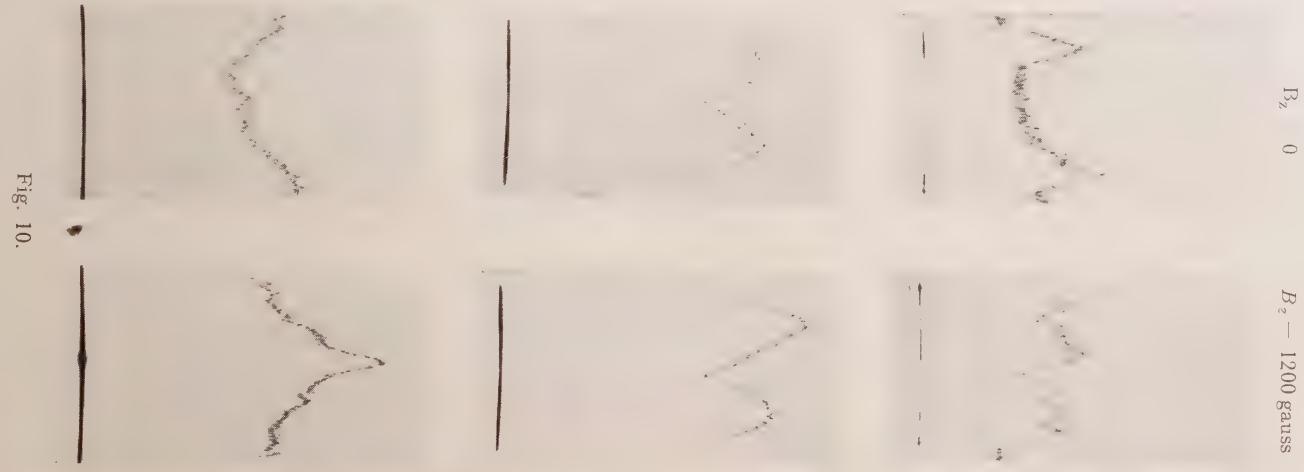

Fig. 10.

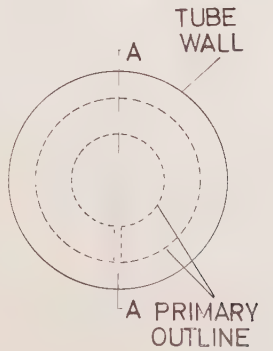

Fig. 10.

Microphotometer traces for three lines of the stigmatic spectra of fig. 9. Primary end wall outlined as seen by spectrograph with A–A indicating the diameter imaged.

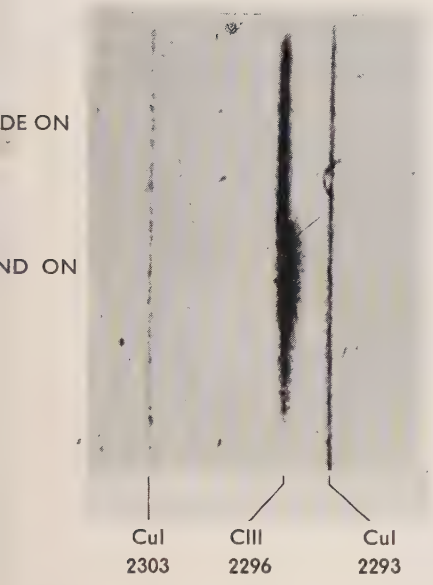

g. 11. Doppler shift of the C III λ 2296 line between pectra taken end on and from the side. The Cu spectrum as been superimposed afterwards on the plate for calibraon purposes. The displacement of the intensity corsponds to a radial velocity of 2–3 cm/μs. $V = 20$ kV, $B_z = 0$, $p = 37\ \mu$.

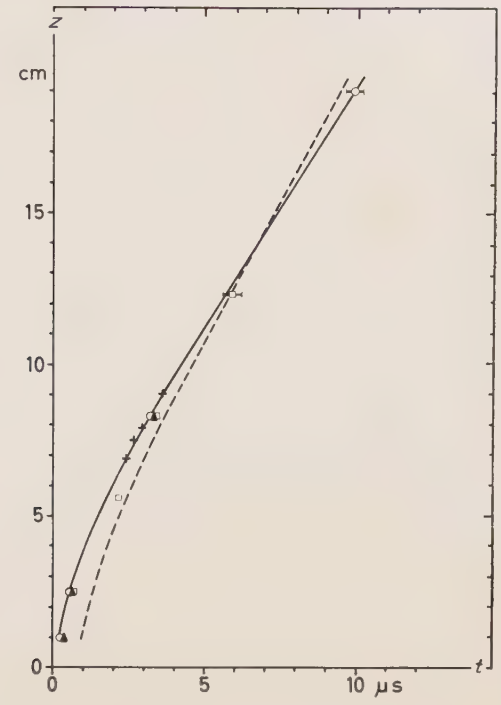

Fig. 12a.

Fig. 12a. Solid line: $V = 40$ kV, $B_z = 0$, $p = 200\ \mu$. Data obtained by photomultiplier records of D_β (○), C III λ 4667 (▲), continuum radiation at λ 3640 (□) and by Kerrcell photos (+). Broken line: $V = 40$ kV, $B_z = 1200$ gauss, $p = 200\ \mu$†. (The discrete points pertaining to this case are not plotted for clarity.)

† Gas breakdown in third quaterperiod of primary current.

Fig. 12b. Motion of plasma front at three different voltages $V = 20, 28, 40$ kV, $B_z = 0$, $p = 200\ \mu$.

Fig. 12c. Motion of plasma front at three different pressures. $V = 40$ kV, $B_z = 0$, $p = 75$†, 200, 400 μ. Broken line: fast light front at $p = 75\ \mu$ (cf. fig. 13).

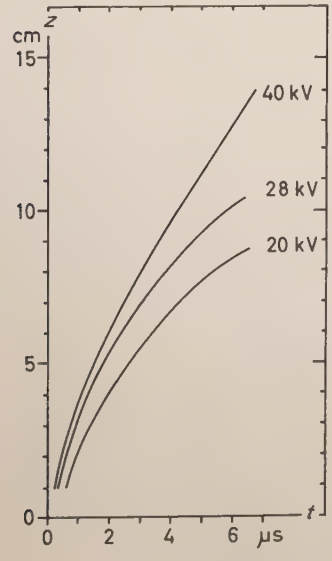

Fig. 12b.

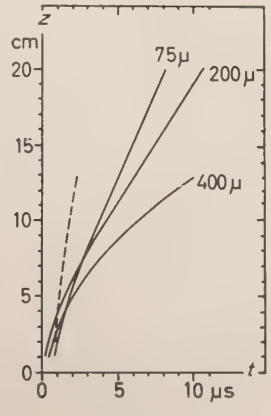

Fig, 12c.

Fig. 12. Motion of plasma front: z-position as function of time.

points being plotted with the maximum deviation from the mean value of several shots. For comparison points obtained from Kerrcell photos are also given. The determination errors in these points are, however, considerably

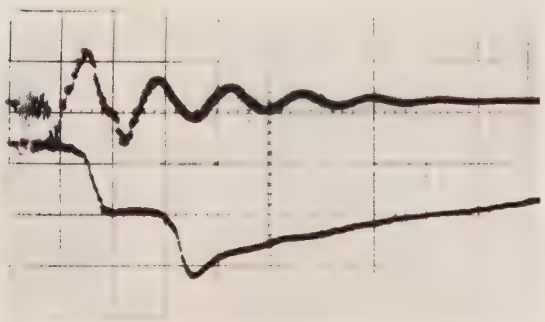

Fig. 13. Recorded intensity of D_β at $z = 8.3$ cm showing fast but weaker light front preceding main plasma ring. $V = 40$ kV, $B_z = 0$, $p = 75\ \mu$, sweep 1 cm/μs.

greater (not shown in the diagram). As can be seen, the light from C III and from the continuum always arrives some tenths of a microsecond later than the light from $D\beta$. As is also demonstrated in fig. 12a, the presence of a B_z-field of 1200 gauss results in a slightly in-

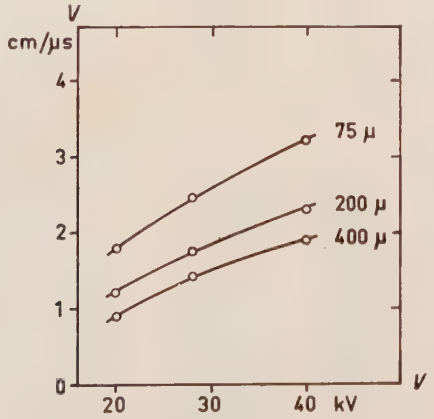

Fig. 14. Average velocities between $z = 3$ cm and $z = 8$ cm as a function of voltage V and pressure p.

creased plasma velocity. The effect is typical also for other values of V and p, and is observed at lower B_z-fields (600 gauss) too. The influence of capacitor voltage V at constant pressure p is shown in fig. 12b. The decelerating effect of the neutral gas at higher pressures in the discharge tube is demonstrated in fig. 12c.

A comparatively weak light front is usually observed moving ahead of the main plasma ring, and with a considerably greater velocity (8–12 cm/μs). It is probably due to some sort of a shock wave phenomenon. The effect is especially pronounced for $p = 75\ \mu$ (cf. fig. 13). For this pressure the fast front is indicated by the broken line in fig. 12c.

The velocity measurements are summarized in fig. 14 which gives the mean velocity between $z = 3$ cm and $z = 8$ cm as a function of V and p. The velocity has also been averaged over the different values of B_z. The velocity at $z = 3$ cm is, however, some factor of two higher than this mean velocity, as at this stage the neutral gas has had no appreciable decelerating effect.

5. Discussion of Results

The actual discharge phenomena in this plasma gun involve a number of secondary effects which will inhibit any quantitative comparison with the simplified theoretical considerations of sect. 2. Particularly there is the complicated interaction between the moving plasma and the neutral gas in front of it. (This will be avoided in the future by using a pulsed gas inlet[7,14,15].)

Among the qualitative results there is especially the encouraging fact that impurities from the porcelain wall at which the discharge starts, seem to be prevented, probably by the very rapid rise of the accelerating field driving the plasma away from the wall in a very short time.

Summing up the present investigation it may be concluded that, with a slightly improved apparatus of this type it should be possible to generate plasma rings of high purity and with velocities of the order of 10 cm/μs.

Acknowledgements

Our most sincere thanks are due to Prof. K. Siegbahn who originally initiated this work, and whose stimulating interest in it has been invaluable.

[14] I. S. Shpigel, Instr. and Meas. Eng. (U.S.S.R.)1 (1959) 115.

[15] B. Gorowitz, K. Moses and P. Gloersen, Rev. Sic. Instr. 31 (1960) 146.

The fruitful discussions and cooperation with ıe other members of the Uppsala plasma ıysics group are gratefully acknowledged, specially the assistance of Dr. K. Bockasten and ıs spectroscopical team.

We also want to express our gratitude to lessrs. Litsenius and Zalenski, The Research rstitute for National Defense, Stockholm, kindly supplying the Kerrcell camera, and to Mr. G. Larsson for skilled workmanship in the construction of the apparatus.

This work has been sponsored in part by the Air Research and Development Command, United States Air Force, through its European Office, and by the Swedish Board for Atomic Research.

NUCLEAR INSTRUMENTS AND METHODS **10** (1961) 108–112; NORTH-HOLLAND PUBLISHING CO.

DIE BILDUNGSGESCHWINDIGKEIT VON NEBELSPUREN IN DER NEBELKAMMER

LUDWIG MEYER

Kernphysikalisches Institut der Deutschen Akademie der Wissenschaften zu Berlin

Eingegangen am 14. Oktober 1960

The development of cloud-chamber tracks of ionizing particles is investigated in several gases with various densities of ionization. It is shown that the intensity of light scattered from these tracks, which is proportional to the droplet cross sections, increases linearly with time only in a small initial time interval of some 10^{-2} seconds, whereas the further growth proceeds substantially slower, Calculations and measurements concerning this process are given for α-particles as well as for slow and fast electrons in argon, air and hydrogen.

1. Einleitung

Nach dem Durchgang eines ionisierenden Teilchens und nach dem Einsetzen der kritischen Übersättigung bilden sich in der Nebelkammer Tröpfchen, welche zunächst submikroskopisch sind, dann zu sichtbarer Größe anwachsen und schließlich Durchmesser von einigen hundertstel Millimetern erreichen, wobei sie zu Boden sinken. Die Geschwindigkeit, mit der sich

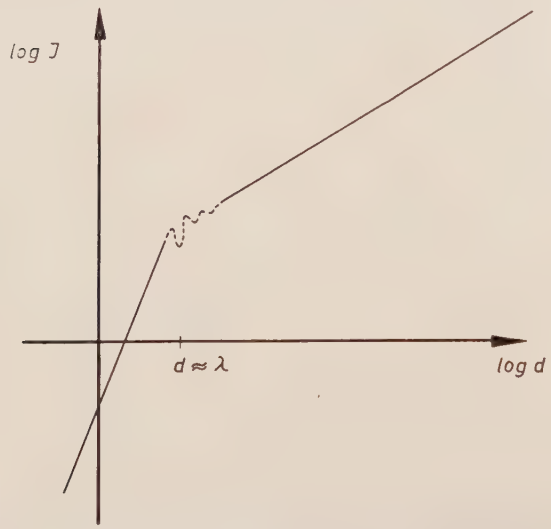

Fig. 1. Abhängigkeit der Intensität I des Streulichts vom Durchmesser d der Tröpfchen.

dieser Vorgang abspielt, ist für einige praktische Fragen von Bedeutung, z.B. für die Messung der Ionisationsdichte von Nebelspuren aus der Schwärzung des fotografischen Bildes oder überhaupt für die Bestimmung des günstigsten Moments für die fotografischen Aufnahme. Für diese Fragen ist die an den Nebeltröpfchen gestreute Lichtintensität maßgebend, welche mit dem Tropfendurchmesser d in der in Abb. 1 dargestellten Weise in Zusammenhang steht. Für Tropfendurchmesser kleiner als die Wellenlänge des Lichtes wächst die Lichtintensität mit d^6 an (Raleigh-Streuung). In der Gegend der Lichtwellenlänge λ gibt es einige durch Beugungserscheinungen hervorgerufene Maxima und Minima, deren genaue Lage noch vom Winkel zwischen Beleuchtungs- und Beobachtungsrichtung abhängt und im einzelnen nicht näher bekannt ist (vgl. z.B. Van de Hulst[1])). Für Tropfendurchmesser größer als die Lichtwellenlänge erfolgt dann der Anstieg der Intensität des Streulichts proportional zu d^2 (Reflexion und Brechung). Im großen und ganzen kann man also sagen, daß die Tröpfchen sichtbar werden, wenn ihr Durchmesser die Lichtwellenlänge erreicht, und daß von da an die Intensität des Streulichts mit dem Tropfenquerschnitt ansteigt.

Berechnungen und Versuche verschiedener Autoren[2,3,4]) haben nun ergeben, daß bei einem

[1]) H. C. van de Hulst, Optics of Spherical Particles (Amsterdam, 1946).

[2]) W. E. Hazen, Rev. Sci. Instr. **13** (1942) 325.

[3]) E. O. Barrett und L. S. Germain, Rev. Sci. Instr. **18** (1947) 84.

[4]) E. Bagge, F. Becker und G. Bekow, Zeitschr. f. angew. Phys. **3** (1951) 201.

inzelnen Tröpfchen in einem übersättigten Gasaum der Querschnitt linear mit der Zeit anvächst. Hieraus erklärt sich die verbreitete nnahme, daß auch bei einer Nebelspur die an en Nebeltröpfchen gestreute Lichtmenge proortional zur Zeit ansteigt. Eine einfache Überegung zeigt jedoch, daß dies nur in einem sehr egrenzten Zeitraum so sein kann, nämlich olange, bis die Tropfen den Dampf in ihrer unittelbaren Umgebung aufgebraucht haben und ich darauf gegenseitig die herandiffundierende Dampfmenge streitig machen. Von diesem ugenblick an kann man eine geradlinige Nebelpur als einen langgestreckten Zylinder betrachen, an den Flüssigkeit aus dem umgebenden Dampfraum zylindersymmetrisch herandiffuniert, um sich dann in irgendeiner Weise auf die inzelnen Tröpfchen aufzuteilen.

2. Berechnungen zur Spurenbildung

Um einen Anhaltspunkt über das dann zu rwartende weitere Anwachsen der Nebel-tröpfhen zu gewinnen, wurde die Dampfmenge bechnet, welche an einen unendlich langgetreckten Zylinder vom Radius r_0 herandiffuniert, an dessen Oberfläche die Dampfdichte ρ len Wert ρ_0 der Sättigungsdampfdichte bei der emperatur T_0 besitzt, welche sich aus dem leichgewicht zwischen der freiwerdenden Konensationswärme und der Wärmeableitung an as umgebende Medium ergibt. In dem Zylinderoordinatensystem um die Achse dieser idealierten Nebelspur gelten dann folgende Diffuions- bzw. Wärmeleitungsgleichungen:

$$D\left(\frac{\partial^2\rho}{\partial r^2}+\frac{1}{r}\frac{\partial\rho}{\partial r}\right)=\frac{\partial\rho}{\partial t} \tag{1}$$

zw.

$$a\left(\frac{\partial^2 T}{\partial r^2}+\frac{1}{r}\frac{\partial T}{\partial r}\right)=\frac{\partial T}{\partial t}\,. \tag{2}$$

it den Randbedingungen

$$\rho(r_0,t)=\rho_0 \quad \text{bzw.} \quad T(r_0,t)=T_0$$

nd den Anfangsbedingungen

$$(r,0)=\rho_2 \text{ für } r>r_0 \quad \text{bzw.} \quad T(r,0)=T_2 \text{ für } r>r_0\,.$$

Dabei bedeuten D den Diffusionskoeffizienten es Dampfes im Füllgas der Nebelkammer und a die Temperaturleitfähigkeit des Gas-Dampf-Gemisches. Lösungen der Gleichung (1) lassen sich in der Gestalt angeben:

$$\rho=\mathrm{e}^{-K^2\frac{D}{r_0^2}t}\left(c_1 I_0\left(K\frac{r}{r_0}\right)+c_2 N_0\left(K\frac{r}{r_0}\right)\right).$$

Dabei sind I_0 und N_0 die Zylinderfunktionen erster bzw. zweiter Art vom Index Null und c_1, c_2 und K Konstante. Die Lösung des Randwertproblems läßt sich daher aufstellen in der Form:

$$\rho=\sum_{\nu=1}^{\infty}\left(c_\nu I_0\left(K_\nu\frac{r}{r_0}\right)+c'_\nu N_0\left(K_\nu\frac{r}{r_0}\right)\right)\mathrm{e}^{-K_\nu^2\frac{D}{r_0^2}t}\,, \tag{3}$$

wobei die K_ν durch die Randbedingungen bestimmt sind, während sich die Koeffizienten c_ν und c'_ν auf Grund der Orthogonalitätseigenschaften der Zylinderfunktionen aus den Anfangsbedingungen berechnen lassen. Für die Dampfmenge, welche den Zylinder erreicht, ist nun die Ableitung $\partial\rho/\partial r$ bei $r=r_0$ maßgebend. Hierfür erhält man aus (3) die Beziehung:

$$\left(\frac{\partial\rho}{\partial r}\right)_{r=r_0}=4\frac{\rho_2-\rho_0}{r_0}\sum_{\nu=1}^{\infty}C_\nu\,\mathrm{e}^{-K_\nu^2\frac{D}{r_0^2}t} \tag{4}$$

wobei die Koeffizienten C_ν nur von den Eigenwerten K_ν des Problems abhängen. Die numerische Berechnung dieser Koeffizienten ergab nun, daß die Beziehung (4) in einem großen Intervall $(10\leqslant D/r_0^2\,t\leqslant 10^3)$† sehr gut angenähert werden kann durch die Funktion

$$\left(\frac{\partial\rho}{\partial r}\right)_{r=r_0}\approx\tfrac{3}{4}\frac{\rho_2-\rho_0}{r_0}\left(\frac{D}{r_0^2}t\right)^{-\frac{1}{6}}. \tag{5}$$

Diese Funktion verhält sich auch für $t\to 0$ und $t\to\infty$ ebenso wie man es von der Ableitung $(\partial\rho/\partial r)$ der Problemstellung nach erwarten muß (nämlich $\partial\rho/\partial r\to\infty$ bzw. $\partial\rho/\partial r\to 0$). Aus (5) ergibt sich damit für den Dampfstrom $\mathrm{d}M/\mathrm{d}t$, der die Nebelspur, d.h. den Zylinder vom Radius r_0, pro Einheit der Spurenlänge erreicht:

$$\frac{\mathrm{d}M}{\mathrm{d}t}=2\pi r_0 D\left(\frac{\partial\rho}{\partial r}\right)_{r0}=\tfrac{3}{2}\pi D(\rho_2-\rho_0)\left(\frac{D}{r_0^2}t\right)^{-\frac{1}{6}} \tag{6}$$

† Dies entspricht dem für unsere Untersuchung interessanten Zeitintervall $10^{-2}\,\mathrm{sec}<t<1\,\mathrm{sec}$, wenn man $r_0\approx 10^{-2}\,\mathrm{cm}$ annimmt und berücksichtigt, dass die Diffusionskoeffizienten für gebräuchliche Gase und Dämpfe die Größenordnung $0.1\ \mathrm{cm^2/s}$ besitzen.

und hieraus erhält man schließlich

$$M = \tfrac{9}{5}\pi\, r_0^{\frac{1}{3}}\,(\rho_2 - \rho_0)\,(Dt)^{\frac{5}{6}}\,. \qquad (7)$$

In dieser Gleichung ist noch die Dampfdichte $\rho_0 = \rho_s\,(T_0)$ als Sättigungsdampfdichte bei der Temperatur T_0 an der Zylinderoberfläche zu bestimmen. Diese Temperatur wiederum ergibt sich aus dem Gleichgewicht zwischen der durch Kondensation freiwerdenden Wärmemenge $s\,\mathrm{d}M/\mathrm{d}t$ (s = Kondensationswärme des benutzten Dampfes) und der durch Wärmeleitung an die Umgebung abgeführten Wärmemenge $2\pi\, r_0\,\lambda\ (-\partial T/\partial r)$ (λ = Wärmeleitfähigkeit des Kammergases). Das hierbei auftretende Temperaturgefälle $\partial T/\partial r$ wiederum erhält man durch Behandlung des Problems (2) analog zu (5) als

$$\left(\frac{\partial T}{\partial r}\right)_{r=r_0} = \frac{3}{4}\,\frac{T_2 - T_0}{r_0}\left(\frac{a}{r_0^2}\,t\right)^{-\frac{1}{6}}$$

und damit kann die Temperatur T_0 bestimmt werden aus der Gleichung

$$s\,D^{\frac{5}{6}}\,(\rho_2 - \rho_s\,(T_0)) = \lambda\,(T_0 - T_2)\,a^{-\frac{1}{6}}, \qquad (8)$$

in welcher sich die Zeitabhängigkeit herausgehoben hat. Aus dieser Gleichung errechnet man z.B. für Alkoholdampf in gebräuchlichen Gasen (Ar, Luft, H_2 um 1 at) bei einer Ausgangstemperatur von 20°C Werte von T_0, welche um 10°C herum liegen (T_2 liegt dann bei ca. 4°C), d.h. ähnliche Temperaturen, wie sie sich für Einzeltröpfchen errechnen lassen (vgl. J. G. Wilson[5])).

Die durch Gleichung (7) gegebene Flüssigkeitsmenge verteilt sich nun auf die einzelnen Nebeltröpfchen der Spur. Die an den Tröpfchen gestreute Lichtmenge I ist aber, wie oben schon erläutert, dem Tropfenquerschnitt proportional so daß man aus (7) für I erhält:

$$I \sim r_0^{\frac{2}{3}}\,(\rho_2 - \rho_0)^{\frac{2}{3}}\,(Dt)^{\frac{5}{9}}\,. \qquad (9)$$

Ganz grob kann man also sagen, daß die an einer Nebelspur gestreute Lichtinensität annäherend mit der Quadratwurzel aus der Zeit anwachsen sollte, nachdem in einem mehr oder weniger kurzen Anfangszeitraum der Anstieg linear mit der Zeit erfolgte. Wann dieser Übergang stattfindet, wird von der Breite der Nebelspur (r_0), von der Zahl N der Nebeltröpfchen pro cm Spurlänge und von der Diffusionsgeschwindigkeit des Dampfes abhängen. Als Anhalt für diesen Zeitpunkt kann man die Zeit 1* zugrunde legen, in der die Einzeltropfen bei ungehindertem Wachstum, die in dem Zylinder vom Radius r_0 verfügbare Dampfmenge verbrauchen würden. Die auf einem Einzeltropfen kondensierende Flüssigkeitsmenge m läßt sich (vgl. z.B. J. G. Wilson[5])) wiedergeben durch

$$m = \tfrac{4}{3}\pi\,\rho_f\left(2D\,\frac{\rho_2 - \rho_0}{\rho_f}\,t\right)^{\frac{3}{2}}.$$

Dabei bedeutet ρ_f die Dichte der Flüssigkeit im flüssigen Zustand. Ist N die Zahl der Nebeltröpfchen pro cm Spurlänge, so steht im Durchschnitt jedem Tröpfchen innerhalb der Nebelspur die Flüssigkeitsmenge $\pi r_0^2(\rho_2 - \rho_0)/N$ zur Verfügung. Durch Gleichsetzen dieser beiden Beträge erhält man für den gesuchten Zeitpunkt des Übergangs:

$$t^* = \frac{1}{2D}\left(\frac{3r_0^2}{4N}\right)^{\frac{2}{3}}\left(\frac{\rho_f}{\rho_2 - \rho_0}\right)^{\frac{1}{3}}. \qquad (10)$$

Dieser Zeitpunkt hängt also im wesentlichen von der Spurbreite, dem Diffusionskoeffizienten, der Tröpfchenzahl und in geringem Maße von dem Dampfdichtegefälle ab.

Zum Vergleich mit den in Abschnitt 3. beschriebenen Messungen wurden nach dieser Formel die Übergangszeiten t^* für die dort untersuchten Fälle berechnet und in Tabl. 1 zusammengestellt.

Der Rechnung wurden dabei folgende Diffusionskoeffizienten für Äthylalkohol bei 1.3 at Gesamtdruck zurgrunde gelegt:

$$D_{Ar} = 0.055\ \mathrm{cm^2/s}\,; \qquad D_{Luft} = 0.083\ \mathrm{cm^2/s}\,;$$
$$D_{H_2} = 0.315\ \mathrm{cm^2/s}\,.$$

Als Anfangstemperatur wurde 20°C und als mittlere Temperatur der Tröpfchen 10°C angenommen, so daß

$\rho_0 = 0.64 \times 10^{-4}\ \mathrm{g/cm^3}$ und $\rho_2 = 0.97 \times 10^{-4}\ \mathrm{g/cm^3}$

für Luft und Wasserstoff und $\rho_2 = 1.02 \times 10^{-4}$ g/cm³ für Argon (infolge des geringeren Expansionsverhältnisses) gesetzt werden kann.

[5]) J. G. Wilson, The Principles of Cloud Chamber Technique (Cambridge, 1951).

Tabelle 1
Zeiten t^* für Alkoholdampf in verschiedenen Gasen bei 1.3 at Gesamtdruck

Art der Spur / Gasart	α-Teilchen von Po^{210} ($r_0 = 0.06$ cm)	Elektronen ca. 30 keV ($r_0 = 0.04$ cm)	Elektronen ca. 1 MeV ($r_0 = 0.03$ cm)
Argon	3.0 ms ($N \approx 6 \times 10^4$/cm)	45 ms ($N \approx 500$/cm)	140 ms ($N \approx 50$/cm)
Luft	2.5 ms ($N \approx 5 \times 10^4$/cm)	36 ms ($N \approx 400$/cm)	120 ms ($N \approx 40$/cm)
Wasserstoff	1.9 ms ($N \approx 10^4$/cm)	28 ms ($N \approx 80$/cm)	90 ms ($N \approx 10$/cm)

. Messungen

Die an den Nebelspuren gestreute Lichtintenität wurde mit Hilfe eines Fotovervielfachers Typ VPG 69, Fa. Maurer) gemessen, dessen Fotostrom durch einen Schleifenoszillografen nter Zwischenschaltung eines Gleichstromverstärkers registriert wurde. Zur Beleuchtung liente eine Quecksilberdampf-Höchstdruckampe HBO 107, welche infolge ihrer kleinen

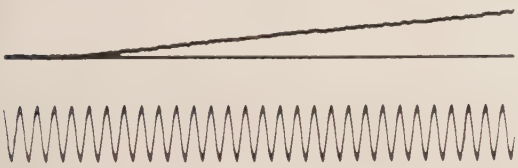

Fig. 2. Intensität des Streulichts von verteiltem Hintergrundnebel (Einzeltröpfchen).

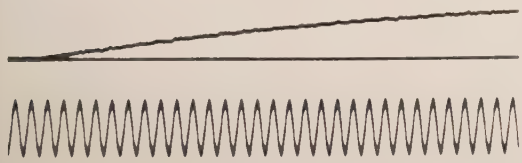

Fig. 3. Intensität des Streulichts von der Spur eines schnellen Elektrons (ca. 50 Tröpfchen/cm).

Leuchtfläche ein sehr scharf begrenztes Lichtbündel lieferte, dessen blauer und violetter Anteil mit Hilfe eines Schottfilters (GG 9) beseitigt wurde. Ein Gesichtsfeld von ca. 1 cm^2 in der Nebelkammer wurde mit einer lichtstarken Optik auf die Katode des Vervielfachers abgebildet. Die Linearität der ganzen Anordnung wurde mit einem Probekörper im Gesichtsfeld überprüft, dessen Beleuchtungsstärke unter Benutzung des Abstandsquadratgezetzes verändert wurde.

Die Steuerung der Nebelkammer (Blacket-Typ, 15 cm ϕ, mit Überrekompression) erfolgte automatisch in einem Zyklus von 40 sec. Der Oszillograph wurde nach der Uhr kurz vor den Expansionen von Hand ausgelöst. Zur Registrierung wurde ein Papiervorschub von ca. 0.2 m/sec benutzt.

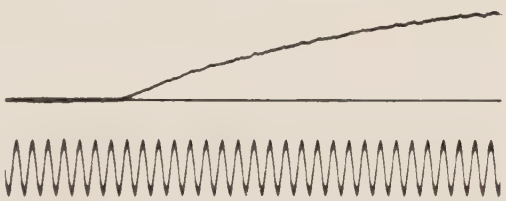

Fig. 4. Intensität des Streulichts von der Spur eines langsamen Elektrons (ca. 500 Tröpfchen/cm).

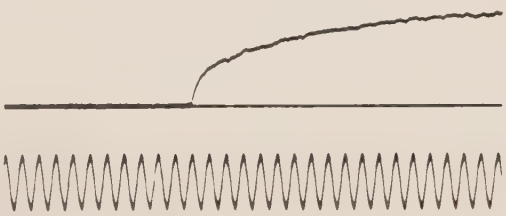

Fig. 5. Intensität des Struelichts von der Spur eines α-Teilchens (ca. 6×10^4 Tröpfchen/cm).

Um einen Überblick über das Spurenwachstum bei allen vorkommenden Ionisationsdichten zu erhalten, wurden Messungen mit α-Teilchen und mit langsamen und schnellen Elektronen durchgeführt. Die α-Teilchen stammten von einem sehr

schwachen Polonium-Präparat, das dicht vor dem Gesichtsfeld des Vervielfachers angebracht war. Gleichzeitig mit der Registrierung wurden die Spuren visuell beobachtet, so daß verbreiterte Spuren, welche von Teilchen stammen, die kurz vor der Expansion das Kammergas durchquerten, ausgeschieden werden konnten. Für die Messungen an langsamen Elektronen wurde ein Röntgenstrahlimpuls von ca. 1 ms Dauer bei ca. 35 kV Röhrenspannung benutzt. Die Strahlung wurde durch Aluminium (2 g/cm^2) gefiltert, so daß man für die entstehenden Fotoelektronen Energien um 30 keV annehmen kann (das entsprach auch den beobachteten Reichweiten). Die schnellen Elektronen wurden mit einem Co^{60}-Präparat durch Fotoeffekt erzeugt und besaßen Energien um 1 MeV.

Die Abb. 2–5 zeigen als Beispiel Oszillogramme, welche mit Argon bei einem Fülldruck von 1.3 at aufgenommen wurden. Zur Zeitmarkierung ist eine 50 Hz-Schwingung gleichzeitig registriert.

Man erkennt auf Abb. 2 den linearen Anstieg der Lichtintensität bei Einzeltropfen (verteilter Hintergrundnebel bei etwas überhöhtem Expansionsverhältnis), während die Teilchenspuren (Abb. 3–5) qualitativ den nach den Überlegungen in Abschnitt I zu erwartenden Verlauf zeigen. Der Übergang vom linearen Anstieg der Lichtintensität zu dem nach Gl. (9) zu erwartenden erfolgt allerdings bei Elektronenspuren sehr allmählich. Nur bei α-Teilchen ist der Zeitpunkt diese Übergangs schärfer ausgeprägt.

Außer Argon wurden noch Luft und Wasserstoff als Füllgase untersucht (1.3 at Gasdruck). Die Oszillogramme zeigen einen ganz ähnlichen Verlauf, nur daß der Anstieg besonders bei Wasserstoff schneller erfolgt. Die Zeiten t^* für den Übergang vom linearen zum langsameren Verlauf, die sich allerdings nur sehr grob abschätzen lassen, entsprechen relativ zueinander etwa den in Tab. 1 errechneten Werten, doch würde man die absoluten Werte auf Grund der Oszillogramme insgesamt um etwa 50% höher schätzen.

NUCLEAR INSTRUMENTS AND METHODS **10** (1961) 113–120; NORTH-HOLLAND PUBLISHING CO.

DEFLECTION COIL FOR AN EXTERNAL ACCELERATOR BEAM†

R. BENAROYA and W. J. RAMLER

Argonne National Laboratory, Argonne, Illinois

Received 6 September 1960

A compound vertical and horizontal deflection coil using a motor-stator type iron core and a winding with a sinusoidal turns distribution makes a useful tool for precisely positioning, and sweeping the external beam of an accelerator. The design, method of construction, performance and characteristics of this coil are discussed.

1. Introduction

Precisely positioning an external, focused, accelerator beam onto a target is a requirement for efficient experimental set up and operation. Beam positioning can be achieved by either remotely changing the spatial position of the target or by a means of beam deflection. In general, magnetic or electrostatic beam deflection techniques are preferred because of simplicity.

In reviewing the external beam requirements of the Argonne 60-inch cyclotron, it was determined that the use of a motor-stator type deflection coil with two independent sinusoidally distributed windings spaced 90 mechanical degrees apart was superior to other methods. Such a coil provides a uniform magnetic field capable of precise positioning of the beam in any of the four quadrants.

An electrostatic deflection system was not given serious consideration because of the high voltage requirements and inherent sparking. This sparking is dependent upon vacuum and system contaminants and for a broad experimental program these requirements are too critical for reliable operation.

The use of C-type magnets result in units especially unattractive to use in the cramped sections of a multiport beam tube system. Such a method involves two individual units for the required four quadrant deflection.

† Based on work performed under the auspices of the U.S. Atomic Energy Commission.

Since the stator-type coil consists of only one unit, it provides the following advantages: only one set of mechanical adjustments is required for alignment, only one magnetic field volume is present for deflection, and over-all mechanical compactness allows close coupling to the focusing system. In the following sections, a general design and a particular ANL cyclotron motor-state type coil is presented.

2. Theory and Design

"If any surface is built up of plane loops of wire carrying the same current, arranged parallel to each other and spaced so that the number of loops per unit length along the normal to the planes of the loops is constant, the magnetic field inside this surface will be uniform if the surface is of the second degree"[1]). If in a motor-stator type coil the number of turns per degree at the circumference of the circular cross section is made proportional to the sine of the vertical angle, when a vertical field is intended, then the winding distribution will be of the above type[2,3]). Such a distribution of turns is referred to as a sine distribution.

The following design was predicated by the need for a unit that would uniformly deflect a beam regardless of particle position with respect to the axis of the coil, and therefore has

[1]) E. Mascart and J. Joubert, Leçons sur l'Electricité et le Magnétisme, Vol. I (Masson, Paris, 1896) p. 545, par. 357.

[2]) Deflection Coils, Ch. 8, Vol. 22, MIT Radiation Lab Series (McGraw-Hill Book Co., New York, 1948).

[3]) K. Schlesinger, Electronics **22** (1949) 102; etc.

TABLE 1

Horizontal and vertical magnetic field values, gauss/NI, computed for different points inside a motor-stator type winding with a sinusoidal distribution and a 5°, 10°, 15°, and 30° separation between slots. The winding is assumed to be of infinite length, concentrated at a radius of 1.125 inches such as would be the case if an iron core was used with slots whose tips extend to this radius. Refer to fig. 4, see slot geometry. The starting angle for a slot is $\Delta\theta/2$, $\Delta\theta$ being the angle between slots.

Y distance from center (In.)		0		0.16		0.31		0.47		0.63		0.79		0.95	
X distance from center (In.)	$\Delta\theta$ in degrees	H_H	H_V	H_H	H_V	H_H	H_V	H_H	H_V	H_H	H_V	H_H	H_V	H_H	H_V
0	5	0.0000	2.5197	0.0000	2.5197	0.0000	2.5197	0.0000	2.5197	0.0000	2.5197	0.0000	2.5197	0.0000	2.5197
	10	0.0000	1.2598	0.0000	1.2598	0.0000	1.2598	0.0000	1.2598	0.0000	1.2598	0.0000	1.2598	0.0000	1.2608
	15	0.0000	0.8399	0.0000	0.8399	0.0000	0.8399	0.0000	0.8399	0.0000	0.8399	0.0000	0.8401	0.0000	0.8451
	30	0.0175	0.4853	0.0085	0.4889	0.0015	0.4899	0.0114	0.4881	0.0199	0.4846	0.0264	0.4838	0.0309	0.4906
0.16	5	0.0000	2.5197	0.0000	2.5197	0.0000	2.5197	0.0000	2.5197	0.0000	2.5197	0.0000	2.5197	0.0000	2.5197
	10	0.0000	1.2598	0.0000	1.2598	0.0000	1.2598	0.0000	1.2598	0.0000	1.2598	0.0000	1.2598	0.0020	1.2604
	15	0.0000	0.8399	0.0000	0.8399	0.0000	0.8399	0.0000	0.8399	0.0000	0.8399	0.0002	0.8397	0.0013	0.8303
	30	0.0234	0.4945	0.0115	0.5001	0.0021	0.5017	0.0154	0.4987	0.0254	0.4914	0.0258	0.4833	0.0123	0.4971
0.31	5	0.0000	2.5197	0.0000	2.5197	0.0000	2.5197	0.0000	2.5197	0.0000	2.5197	0.0000	2.5197	0.0001	2.5194
	10	0.0000	1.2598	0.0000	1.2598	0.0000	1.2598	0.0000	1.2598	0.0000	1.2598	0.0000	1.2599	0.0070	1.2502
	15	0.0000	0.8399	0.0000	0.8399	0.0000	0.8399	0.0000	0.8399	0.0000	0.8399	0.0028	0.8300	0.0054	0.8738
	30	0.0326	0.5052	0.0166	0.5156	0.0030	0.5184	0.0221	0.5137	0.0391	0.5010	0.0468	0.4721	0.0045	0.4062
0.47	5	0.0000	2.5197	0.0000	2.5197	0.0000	2.5197	0.0000	2.5197	0.0000	2.5197	0.0000	2.5197		
	10	0.0000	1.2598	0.0000	1.2598	0.0000	1.2598	0.0000	1.2598	0.0000	1.2598	0.0016	1.2603		
	15	0.0000	0.8399	0.0000	0.8399	0.0000	0.8399	0.0000	0.8399	0.0003	0.8400	0.0085	0.8415		
	30	0.0480	0.5210	0.0257	0.5383	0.0049	0.5431	0.0313	0.5347	0.0565	0.5258	0.1064	0.4934		
0.63	5	0.0000	2.5197	0.0000	2.5197	0.0000	2.5197	0.0000	2.5197	0.0000	2.5197				
	10	0.0000	1.2598	0.0000	1.2598	0.0000	1.2598	0.0000	1.2598	0.0005	1.2601				
	15	0.0000	0.8399	0.0000	0.8399	0.0000	0.8399	0.0003	0.8401	0.0049	0.8368				
	30	0.0755	0.5367	0.0461	0.5752	0.0135	0.5852	0.0497	0.5512	0.0363	0.5546				
0.79	5	0.0000	2.5197	0.0000	2.5197	0.0000	2.5197	0.0000	2.5197						
	10	0.0000	1.2598	0.0000	1.2598	0.0001	1.2597	0.0001	1.2580						
	15	0.0000	0.8394	0.0007	0.8401	0.0017	0.8416	0.0035	0.8266						
	30	0.1270	0.5331	0.0113	0.6462	0.0302	0.6933	0.1460	0.5409						
0.95	5	0.0000	2.5197	0.0000	2.5196	0.0006	2.5203								
	10	0.0000	1.2541	0.0046	1.2520	0.0327	1.2520								
	15	0.0000	0.8095	0.0254	0.8735	0.0826	0.7896								
	30	0.2111	0.4114	0.4178	0.7158	0.2164	1.1566								

attempted, as closely as is practical, to produce a coil with a sinusoidal distribution of turns. In order to determine an allowable sinusoidal

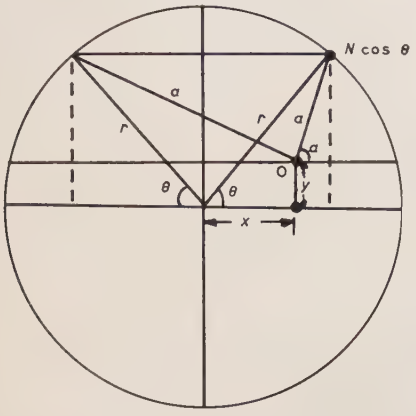

Fig. 1.

winding approximation, and associated homogeneity of field, numerical integrations were performed for five, ten, fifteen and thirty degree stator slot intervals for a number of spatial points inside a 2.25 inch diameter coil aperture.

$$H_V = 0.4\,NI \int_0^{2\pi} \frac{(r\cos\theta - X)\cos\theta\,d\theta}{a^2}$$

$$H_H = 0.4\,NI \int_0^{2\pi} \frac{(r\sin\theta - Y)\sin\theta\,d\theta}{a^2}$$

$$a^2 = (r\sin\theta - Y)^2 + (r\cos\theta - X)^2 .$$

The numerical integration results are summarized in table 1. From these data one concludes that for a 10 degree slot interval, the magnetic field within a radius of about 0.8 inch is uniform to at least 0.1% for a coil of infinite length. In a practical case, this field uniformity holds true only for the center of the coil and deteriorates at the ends. The addition of an iron core with 10 degree winding slots does not appreciably affect the magnetic field contour as given by the table 1 data but does help to minimize end effects. The use of a cylindrical iron core with winding slots increases the deflection efficiency by decreasing the magnetic reluctance and brings the effective radius of the turns to the edge of the slots.

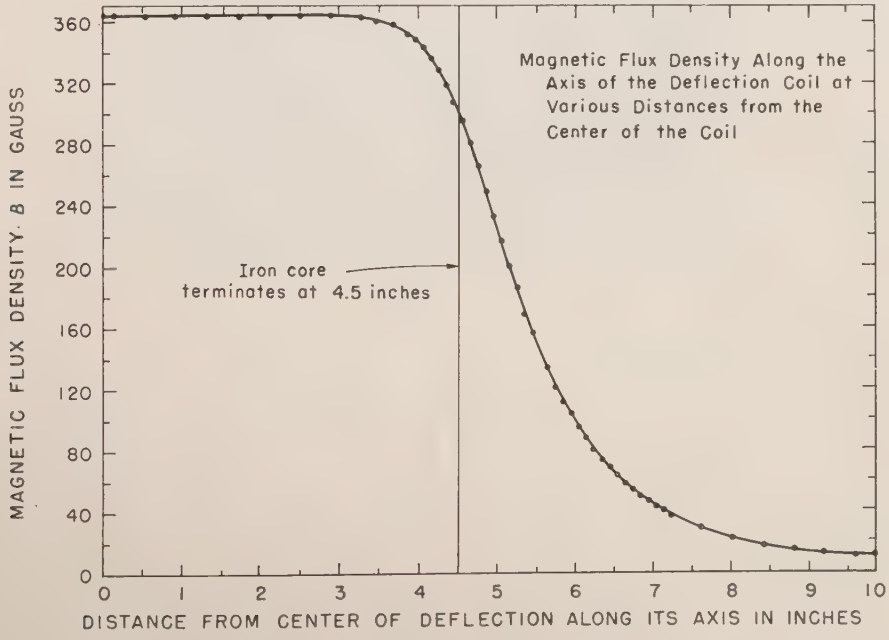
Magnetic Flux Density Along the Axis of the Deflection Coil at Various Distances from the Center of the Coil
Iron core terminates at 4.5 inches
MAGNETIC FLUX DENSITY, B IN GAUSS
360
320
280
240
200
160
120
80
40
0
0 1 2 3 4 5 6 7 8 9 10
DISTANCE FROM CENTER OF DEFLECTION ALONG ITS AXIS IN INCHES

Fig. 2. Field plot, through center axis, along coil length. $I = 1.45$ A.

Referring to fig. 1, the expressions used to obtain the magnetic field, both vertical and horizontal, at any point 0 inside the coil, are as follows:

The deflector coil was designed to deflect the external 21.6 MeV deuteron beam of the ANL cyclotron a distance of one inch from the normal trajectory, at a point 60 inches from the center

of the coil. Since 4 quadrant deflection is required, the unit was designed with two independent windings spaced 90 mechanical degrees apart.

The coil parameters, magnetic field B_c and effective length L_c, are related to the particle deflection distance d, BR of projectile and the distance l from coil center to point of deflection as follows:

$$B_c L_c \cong \mathrm{BR}\,\frac{d}{l}.$$

the required NI is 450, where N is the maximum amplitude of the sinusoidal winding distribution and I is the current in amperes. To apply this to the 9 inch iron core coil, a multiplying factor must be used which will correct for the iron (K_1) and finite coil length (K_2). Adding an iron core, decreases the magnetic reluctance by two, hence $K_1 = \frac{1}{2}$. To correct for the finite coil length effect, the factor $K_2 = 1/\sin\gamma$ is applied to the center field, where γ is the angle between the line joining the edge of the iron at the end of the core

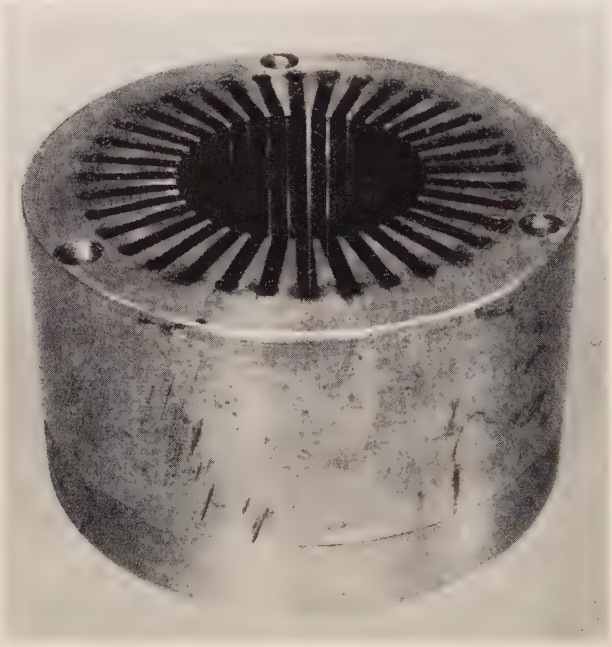

Fig. 3. A 3-inch core section.

For the given requirements, $B_c L_c = 6.33$ kg inches. The value of L_c is 11.2 inches as determined from the experimental data of magnetic field vs. coil length, fig. 2 and beam trajectory deflections. The mechanical length of 9 inches was chosen for convenience of machining. The magnitude of excitation current required was readily available from existing power supplies. For an L_c equal to 11.2 inches, the required coil field (B_c) is 570 gauss.

To determine the NI required to establish this field, the data of table 1 can be used. For a 10 degree slot interval and an infinitely long air coil, the center magnetic field is 1.26 gauss/NI and and the center point in the coil, and the perpendicular to the core from this point. For a 9 inch long core and a slot tip radius of 1.125 inches, K_2, = 1.03. The design value of ampere turns is then 450 K_1K_2 or 232.

For the required NI, 144 turns was set as a maximum number of turns for any given slot, and was established by load characteristics of available power supplies, wire size and mechanical geometry of the core.

Since two identical coils, horizontal and vertical deflection, are mounted in the same core and oriented 90 mechanical degrees to each other, the total number of turns in any one slot

is $n = N \sin\theta + N \cos\theta$. The maximum turns/slot, 144, occurs at θ equal to 45 degrees. The corresponding value of N is 102. For an N equal to 102, an excitation current of 2.28 amperes established the required 232 ampere turns.

The windings were isolated from the core and each other by the use of 0.002 inch thick mylar insulation. Each coil was made up of four prewound sections, for example, AA′, BB′, CC′, and DD′, in fig. 4, constitutes one section. Con-

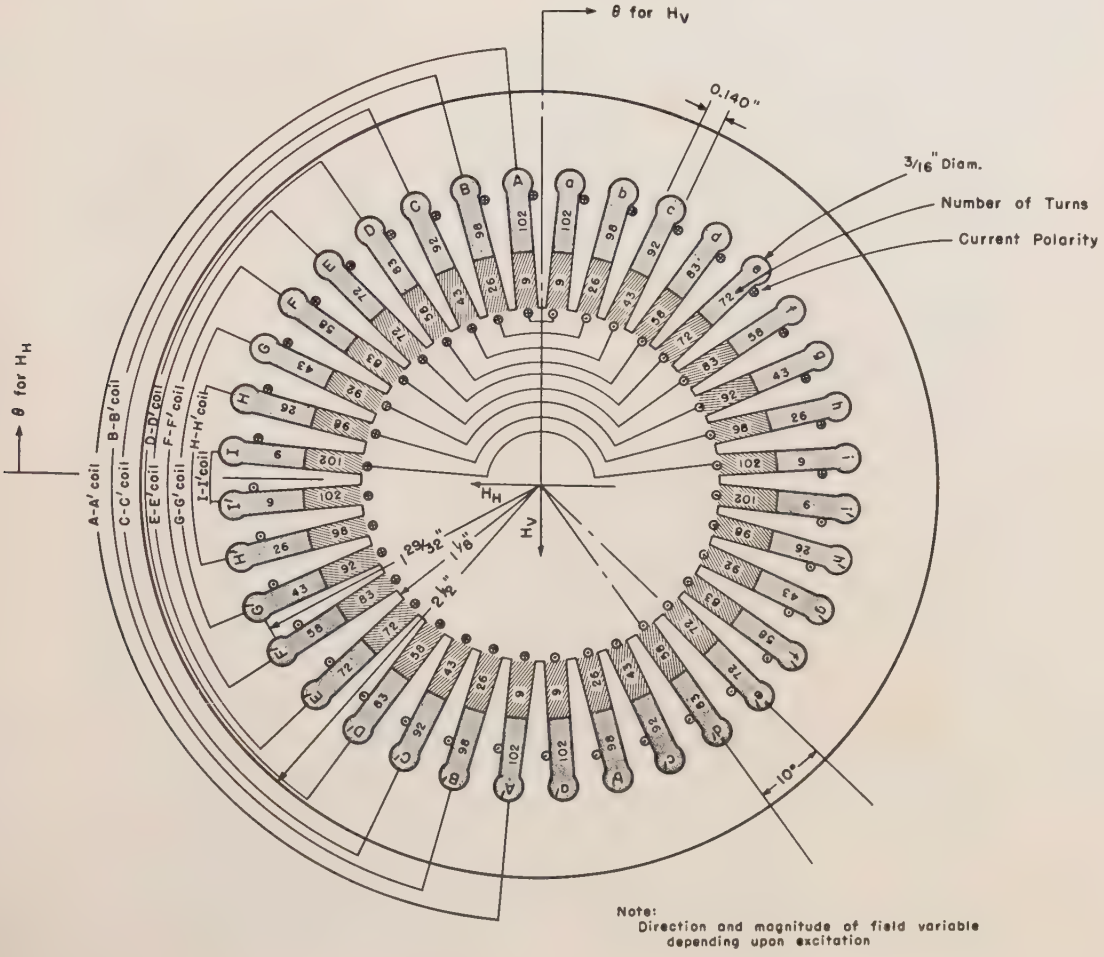

Fig. 4. Cross section of core, and winding schedule.

3. Construction

The construction of the 9 inch core, Type MB 1113 steel, was facilitated by machining the unit in 3 equal sections, fig. 3. The completed core was obtained by the doweling of these sections. Refer to fig. 4 for the cross-sectional dimensions of the core and winding slots. The external surface of the core was grooved to facilitate the soft soldering of several turns of $\frac{1}{4}$ inch copper tubing and provide good thermal contact for water cooling.

ductor size was 23 Awg, with a 0.0019 inch minimum layer of epoxy insulation, AIEE class B rating. Upon insertion of the coil sections in their respective core slots, they were externally connected to form a series winding. This procedure was followed for each of the required deflection coils.

To hold these coils in their slots a cylinder of bakelite, O.D. 2.25 inches and I.D. 2.0 inches, was snugly fitted into the core aperture. Inside of this cylinder, the brass beam tube was placed

and then the entire assembly was impregnated with silicone varnish and baked, fig. 5.

With the exception of the core and casing, this entire unit is now constructed commercially for ANL at a very reasonable cost, fig. 6.

couple was inserted is inefficiently cooled, and coil temperature in slots is relatively low, the maximum operating current is limited by the temperature of the external winding. In future designs, if the external cooling is increased, the

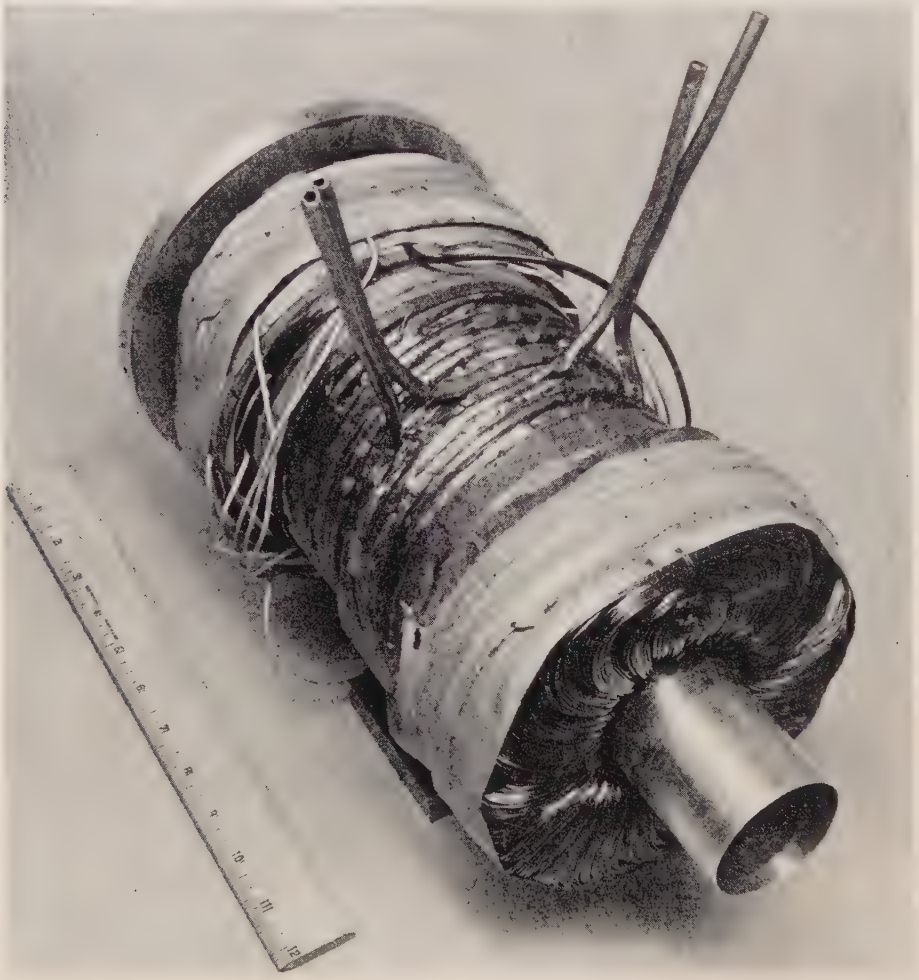

Fig. 5. A view of the coil after impregnation.

4. Test Results and Use

Table 2 shows the electrical characteristics of the coil. For a horizontal or vertical deflection of 1 inch at a distance of 60 inches, the required power input to a coil is about 200 watts.

A thermocouple, inserted during winding, at a region in the coil believed to be least affected by water cooling, registered a steady temperature of 130°C with 2.8 amperes in both coils. Since the external section of the coils where the thermo-

maximum current and designed deflection range of the unit can be extended.

Magnetic field test data obtained for both the horizontal and vertical deflection coils were within 1% of the calculated values. The uniformity of the field in any cross section within $\pm$ 3 inches from center was better than 0.1%. These measurements were made with a Rawson type 720 rotating coil gaussmeter. The unit was mounted on a support stand capable of all three

axial motions as well as a circular sweep, and modified for the purpose of accurate rectangular field plotting. The 3 foot long probe was mechanically reinforced in order to eliminate drooping. This reinforcing limited the scan of the field to a radius of $\frac{47}{64}$ inches.

the magnet, indicates that distortion effects are negligible throughout the coil. Beams subjected to deflection with this coil are free of noticeable distortion effects.

Fig. 7 represents the magnetization curve of the core and no saturation is observed within the

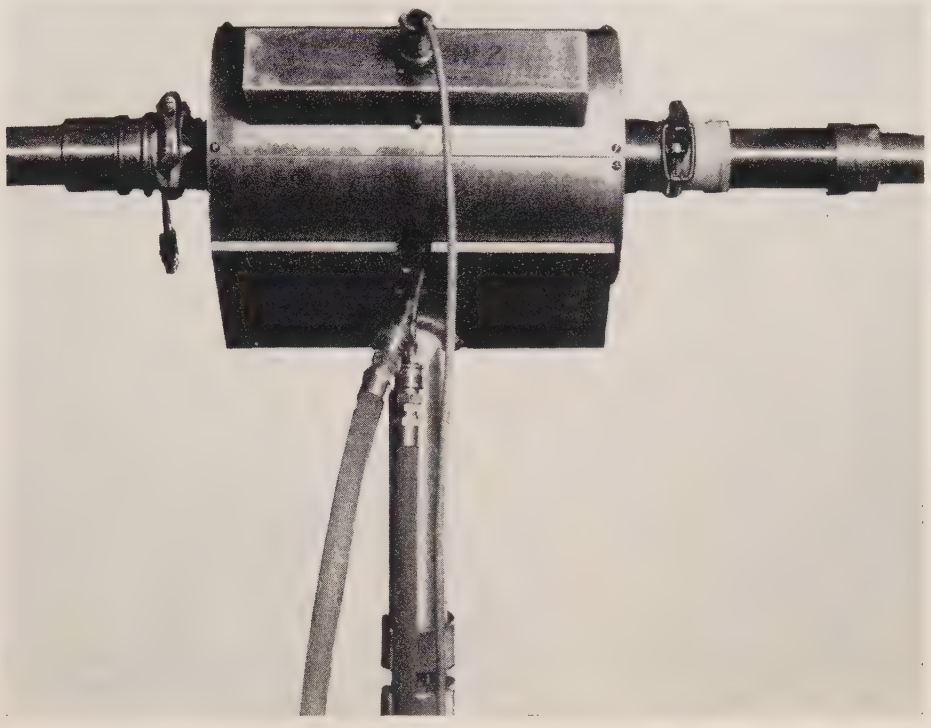

Fig. 6. Completely assembled unit placed in the external focusing system. Casing extends 11.5 inches and is $7\frac{1}{8}$ inches in diameter.

TABLE 2
Test results on the horizontal deflection coil †

Resistance at 20°C (in ohms)	74
Average coil temperature when both horizontal and vertical coils have a current flow of 2.3 amperes	68°C
Inductance (in henries)	0.150
Impedance at 60 cycles (average coil temperature of 50°C (in ohms))	235

† The vertical deflection coil has an approximately identical test data.

An analysis of field integrations along trajectory lines parallel to the coil axis beyond the $\pm$ 3 inch axial coil length, where the field starts dropping off, all the way past the fringing field of current range (3.2 amps–limit of test power supply) applied to the coil.

The uses of the compound deflection coil has become quite diversified. In addition to precise beam positioning, such as the centering of a 2 mm diameter beam on a 1 $\times$ 2 mm aperture, the units have been used for beam sweeping, shuttering and Faraday cup systems.

To obtain a uniform target irradiation, a 60 cps sweep voltage was superimposed on the D.C. current to the coils resulting in irradiations with nonuniformity in particle number better than 2%. The unit has also been used as a shutter when the time requirements were greater than milliseconds.

Since these coils are constructed with an electrically isolated beam tube and can be quickly moved, aligned, and connected to the main tube by quick connect vacuum couplings, they are also used as Faraday cup systems.

systems, and could be readily used with a slit and electronic control system to position stabilize an external beam. Beams subjected to deflection with these units are free of noticeable aberrations.

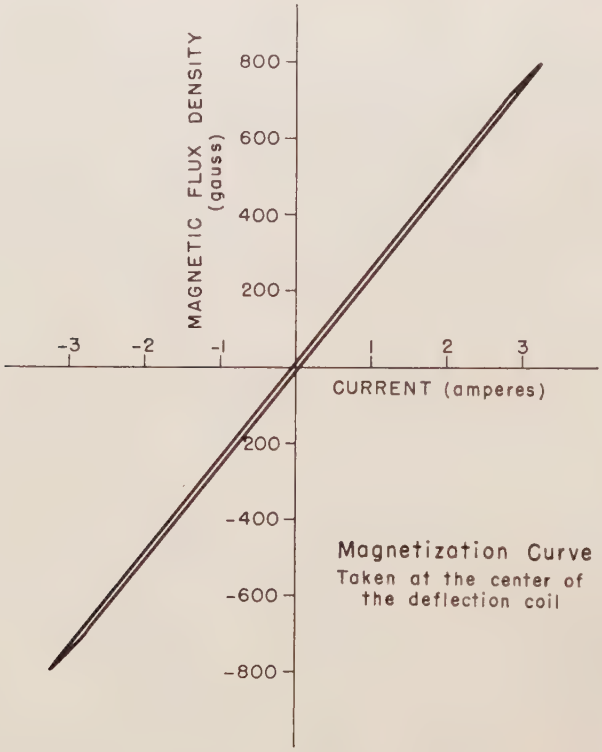

Fig. 7. Magnetization curve.

5. Conclusions

The external focusing system of the Argonne 60-inch cyclotron presently employs four deflector coils of the motor-stator type. These coils have satisfactorily performed a very necessary task of precise beam alignment for use with the 60-inch scattering chamber, energy degradation system and general targetry associated with isotope production, radiation chemistry, and solid state physics. In addition to beam positioning, the coil serves as a convenient means of providing beam sweep, shuttering, Faraday cup proportional to the charge (Q^{+1}) and inversely

Since the deflection of this unit is directly proportional to both the nucleon number (N^{-1}) and the square root of the energy/nucleon $(E/N)^{-\frac{1}{2}}$, the described design should in general prove quite useful for the external beam systems of heavy ion accelerators, high multiple charge states, and the AVF machines now under construction.

Acknowledgements

The authors wish to acknowledge the important contributions of G. W. Parker to the mechanical design of the system.

NUCLEAR INSTRUMENTS AND METHODS **10** (1961) 121–124; NORTH-HOLLAND PUBLISHING CO.

INVESTIGATIONS ABOUT THE CRITICAL RADIUS OF THE BF_3 COUNTERS

J. CSIKAI, E. MOLNÁR and B. SCHLENK

Atomki, Debrecen, Hungary

Received 19 October 1960

In disagreement with results obtained by the authors A. Milojević, M. Kurepa and S. Ribnikar[5]), we have not found any critical radius in the investigated BF_3 proportional counter. Alpha-particles were introduced parallel with the anode into the mica end-window counter filled with BF_3-gas of Hgmm 150, and the radial change of the number of impulses was thus studied. In the counter filled with BF_3-gas Hgmm 150 and 300, the integral amplitude distribution was investigated in the function of electronic amplification at various distances of the source from the anode. The result obtained by Milojević and collaborators may be due to the impurity of the gas used.

In the past years, a number of investigations have been carried out with regard to the properties of the BF_3 proportional counter[1–5]). A considerable number of these examinations deals with the effect exerted by the contamination of BF_3-gas upon the functional properties of the counter. These investigations unequivocally reveal that the properties of the counter are considerably influenced by the quite negligible electronegative contamination present in the gas.

A. Milojević, M. Kurepa and S. Ribnikar[5]) gave account of an interesting new property, the so-called critical radius of the BF_3-counters. They introduced alpha-particles into an end-window counter filled with BF_3-gas, in parallel with the anode, and studied the number of the observed impulses in the function of the

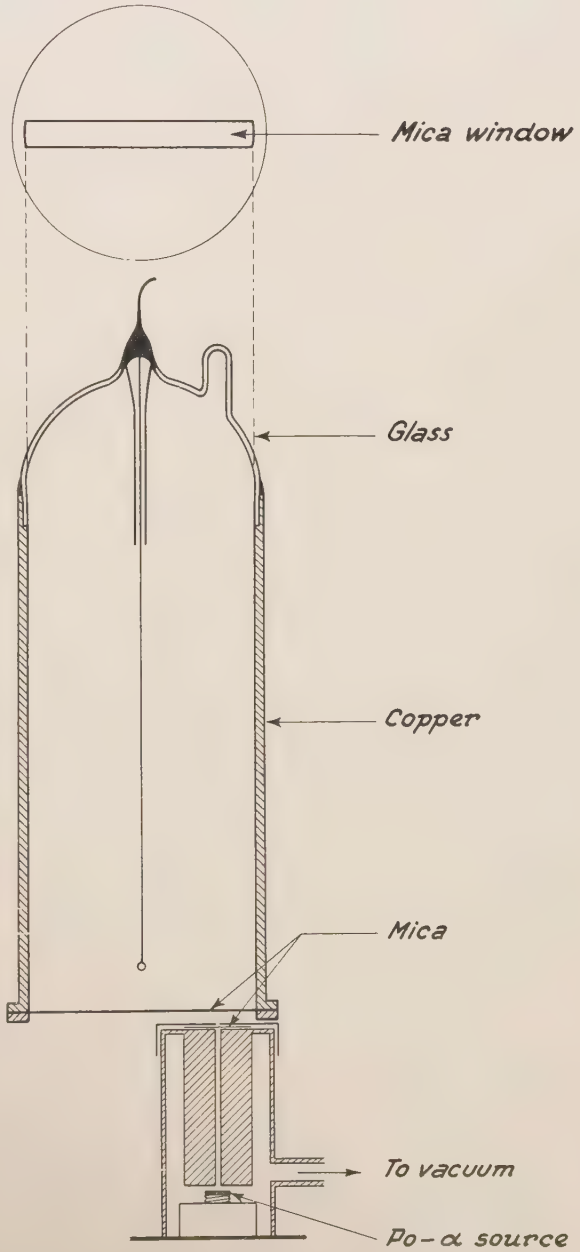

Fig. 1. Geometrical arrangement of the counter and source.

[1]) J. Davila Aponte and S. A. Korff, Rev. Sci. Instr. **31** (1960) 532.

[2]) R. B. Mendell and S. A. Korff, Rev. Sci. Instr. **30** (1959) 442.

[3]) H. F. Brinckmann and D. Gerber, Kernenergie **3** (1960) 309.

[4]) J. Csikai and M. Buczkó, Nucl. Instr. and Meth. **8** (1960) 73.

[5]) A. Milojević, M. Kurepa and S. Ribnikar, Proceedings of the Second International Conference Geneva **14** (1958) 325 P/493.

distance from the anode. They found the number of impulses to decrease to null beyond a certain distance. They termed this distance "critical radius" and asserted its value to be 4–8 mm according to their measurements, in a pressure-interval of Hgmm 380–100. This result would mean that the sensitive volume of the BF_3 counter in parallel with the anode by an angular spread of 2.3°. The end-window of the counter was a mica foil of 2 mg/cm² thickness, its cathode was a brass tube 25 mm in diameter, its anode was tungsten 0.1 mm in diameter and the length of its sensitive volume: 45 mm. The thickness of the mica windows and that of the air-space

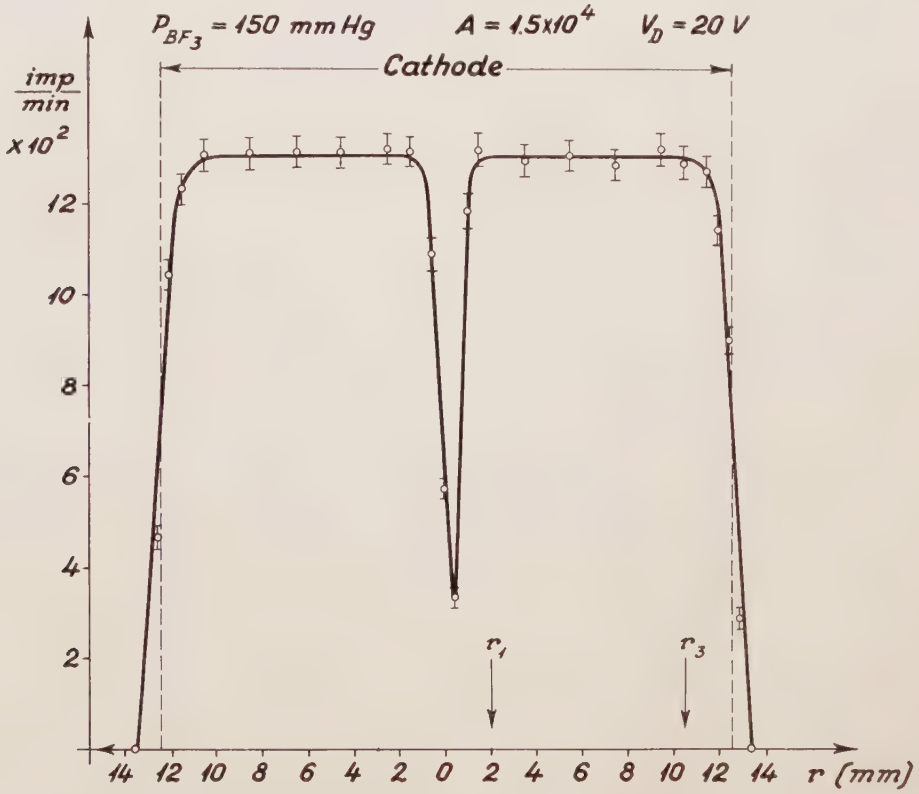

Fig. 2. Change of the number of impulses in the function of the distance between anode and source.

proportional counter is determined by the critical radius which is independent of geometric dimensions.

It could be supposed that electronegative contamination might have an important influence exerting the above-mentioned effect. For this reason, the measurement was repeated with gas produced in a different way[6]—through the thermal decomposition of $CaF_2(BF_3)_2$. For the investigation, a Po^{210}-source of about 1 mc was used which was placed in an evacuated collimator from which alpha-particles got into the between them were chosen so that the residual energy of the alpha-particles should approximately agree with the total kinetic energy of the $B^{10}(n,\alpha)Li^7$ reaction products.

First of all, the radial change of the number of impulses was examined in the case of BF_3-gas pressure of Hgmm 150 (electronic amplification being 1.5×10^4, rise-time: 0.2 μsec, clipping time: 5 μsec) in such a manner that the discriminator bias was at about half of the maximal impulse amplitude. As it can be seen in fig. 2, the counter is equally sensitive in its entire volume, and there is no critical radius. The abrupt decrease of the number of impulses in the axis of

[6]) M. Buczkó and J. Csikai, ATOMKI Közlemények 1 (1960) 29.

the counter is caused by the absorption of the glass bead at the end of the wire.

Subsequently, the integral amplitude distribution was investigated at BF_3-gas pressures of Hgmm 150 and 300, at various electronic amplifications; with alpha-particle-beams of 2, 7 and 10.5 mm—at anode distance. For each electronic amplification the high voltage of the counter was chosen so that the average amplitude of the amplitude distribution measured at the

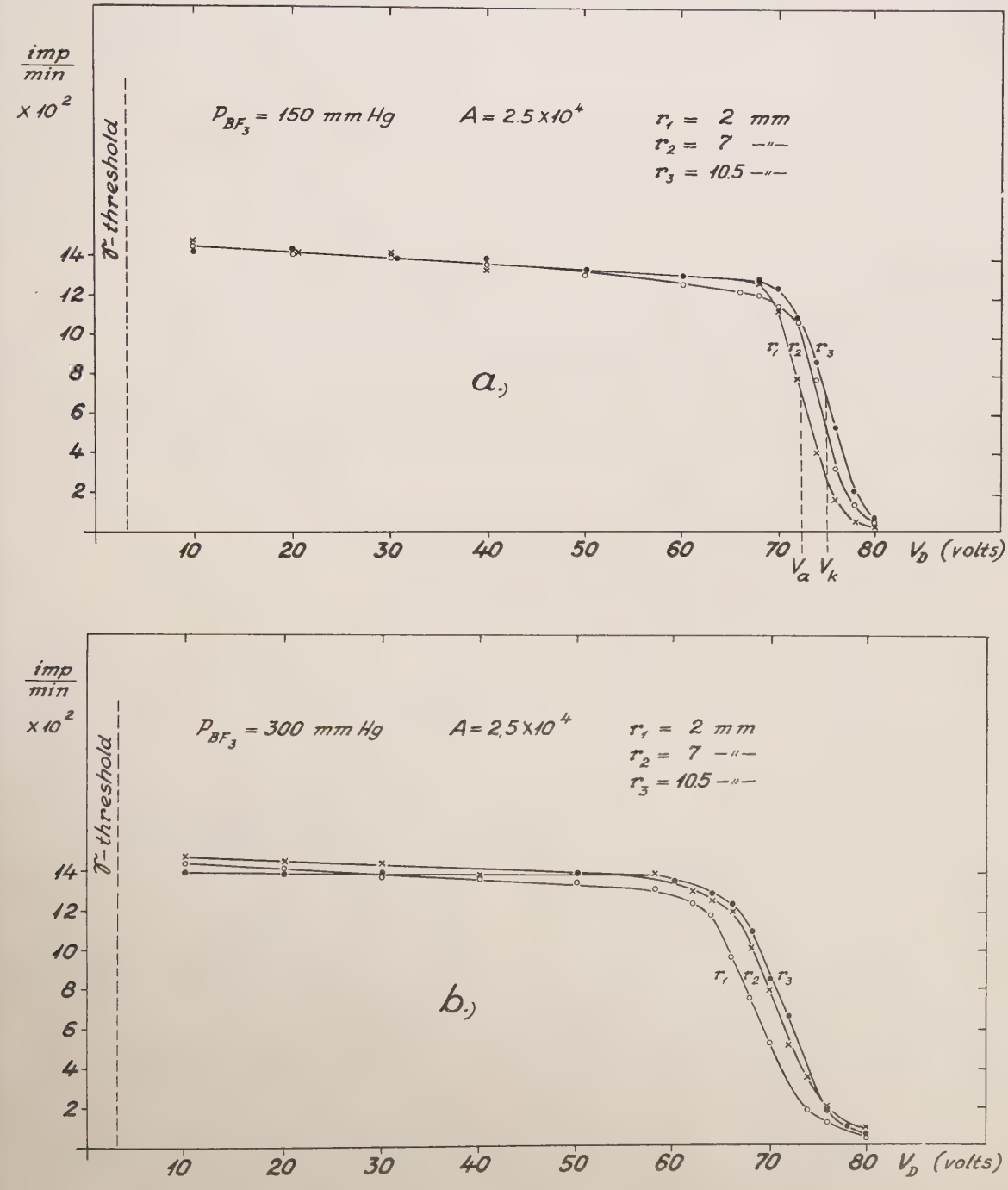

Fig. 3a and b. Integral amplitude distribution at various distances between anode and source.

cathode should be approximately at the same discriminator voltage. As fig. 3a and b show, the integral amplitude distribution corresponds to the mono-energetic Po-alpha rays, and it depends, only to a slight degree, on the site of primary ionization at a 2.5×10^4 times electronic amplification. Departure from the above characteristic of integral amplitude distributions occurs at extremely high amplification values only.

impulses arriving from the anode ($V_k/V_a > 1$). By a further increase of amplification, the position becomes reversed ($V_k/V_a < 1$). This latter portion of the curve may be explained by the occurrence of recombination. The fact that in some electronic amplification ranges $V_k/V_a > 1$, may be accounted for by the inhomogeneity of the electric field in the counter. First of all, the glass bead at the end of the wire as well as the

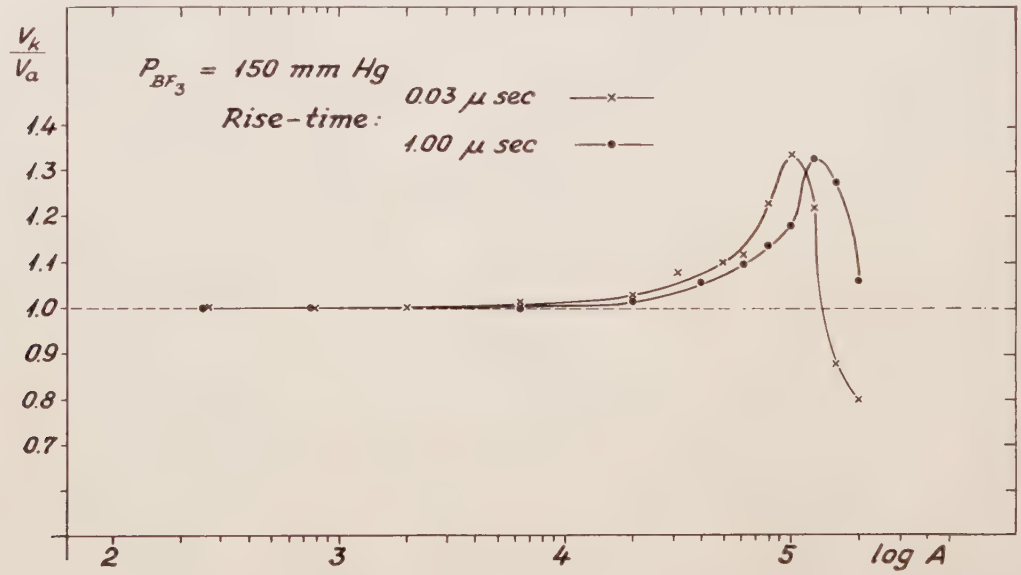

Fig. 4. Ratio of average amplitudes measured at the cathode and anode in the function of the logarithm of electronic amplification.

The alpha-particles were introduced into the counter at 2–2 mm distance from the anode and cathode respectively (see r_1, r_3 points in fig. 2), and the ratio of the average amplitudes (V_a, V_k) measured at these points were studied in the function of electronic amplification. The observations were made at 0.03 and 1 μsec rise-time values respectively. As it can be seen in fig. 4, in the wide amplification range, the $V_k/V_a \approx 1$, which means that here the magnitude of amplitudes is independent of the distance measured from the anode. At a high electronic amplification, however, the amplitude of the impulses coming in from the cathode is larger than of the mica window are responsible for the inhomogeneity of the field.

Finally, it must be noted that Brinckmann's[7]) investigations carried out by other methods independent of ours do not confirm the existence of the critical radius either.

The effect observed by Milojević and collaborators may have been due to the electron affin contamination of the BF_3-gas.

The authors are greatly indebted to prof. A. Szalay, director of this Institute, for facilitating the execution of their task.

[7]) H. F. Brinckmann, Kernenergie **3** (1960) December (to be published).

NUCLEAR INSTRUMENTS AND METHODS **10** (1961) 125–128; NORTH-HOLLAND PUBLISHING CO.

A COLD CATHODE ION SOURCE FOR A SYNCHROCYCLOTRON

ÅKE SVANHEDEN

The Gustaf Werner Institute for Nuclear Chemistry, University of Uppsala, Sweden

Received 24 October 1960

Ion sources of the cold cathode type have been installed in the Uppsala synchrocyclotron. Two ion sources with Uranium cathodes were placed symmetrically above and below the median plane of the pole gap, and both can be operated simultaneously. The arc working voltage is in the region of 700 volts with a hydrogen gas working pressure of around 5 mTorr (5×10^{-3} mm Hg). The beam intensity is slightly increased with this new type of ion source, and the working stability is very good.

1. Introduction

The demand for long continuous experiments in the beam of the cyclotron made it necessary to build a more reliable ion source than the hot filament type. A cold cathode ion source was developed which reduces the service time for the cyclotron since replacement of filaments in the old hot cathode source is eliminated.

The principle of an ion source of the Penning discharge type has been well described in the literature.

2. Construction

Following the idea of Keller[1]), a cold cathode ion source was constructed with uranium cathodes. Uranium was used because of its low work function and its high reflection coefficient for oscillating electrons which give a rather low arc voltage, as found by Flinta and Pauli[2]). The slight pre-ionization due to the radioactivity of uranium might also be of advantage in igniting the arc.

A design similar to that described by Keller[1]) was tried first. Experiments were performed with and without an outer annular extracting electrode. No advantages were found when the potential of this electrode was varied from + 1000 to — 1000 volts. A final version was tried and is shown in fig. 1.

[1]) R. Keller, Comportement d'une source d'ions du type Penning dans le synchrocyclotron du Carnegie Institute of Technology. CERN/SC 139.

The distance between the cathodes was 3.5 cm, the inside diameter of the annular copper anode was 1 cm, and the outlet hole in the cathode was 0.5 cm in diameter. Hydrogen gas was fed into the ion source through a narrow copper tube.

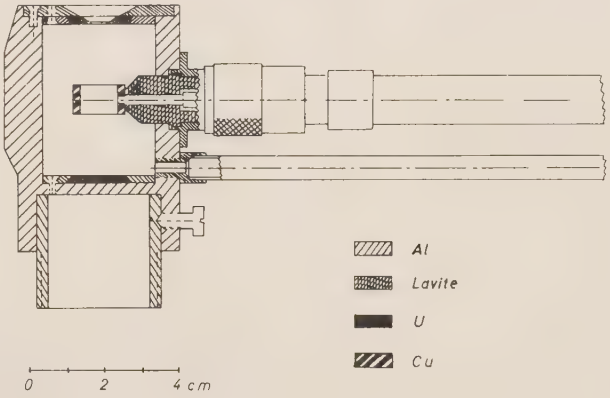

Fig. 1. Drawing of the ion source.

The high tension pulse was fed to the anode via a Teflon-insulated coaxial line screened by a copper tube. Fig. 2 shows a photograph of the ion source. Two such ion sources were installed in the cyclotron symmetrically above and below the median plane of the pole gap. The distance between the outlet holes of the cathodes was 10 cm, and each source was recessed 1 cm below the Dee-electrode. The gas tubes and the coaxial lines were placed inside of the dummy dees in order to make available more space for experiments in the internal circulating beam. The ion sources were cooled indirectly by conduction to

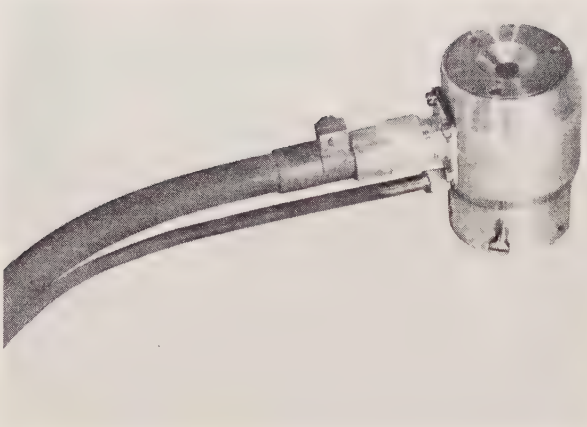

Fig. 2. A photograph of the ion source.

the water cooled, grounded high frequency line to which they were attached.

When the position of the ion source giving minimum energy spread of the internal circulating beam has been found experimentally, the source then can be permanently fixed in that position. In the present case this has been found to be at the geometrical centre of the pole tips. Here the strength of the magnetic field is about 21000 gauss.

The escape of gas from the ion source should be chosen to not exceed the maximum capacity of the vacuum pumps of the cyclotron tank. In this case a hydrogen gas supply (G) of 5×10^{-6} gram/sec could be accepted. One finds from a formula[3]) for the gas quantity streaming through a hole in a thin wall,

$$G = Fp\left(\tfrac{3}{4}\varkappa\frac{M}{RT}\right)^{\frac{1}{2}}\text{gram/sec}, \qquad (1)$$

where F is the outlet area, p is the gas pressure in the ion source (assumed to be much greater than the pressure in the cyclotron tank), $\varkappa$ is the ratio C_p/C_v (specific heat at constant pressure/constant volume). M is the molecular weight, R is the gas constant, and T is the absolute temperature of the gas. Evaluating eq. (1), one gets a hydrogen pressure, $p = 5 \times 10^{-3}$ Torr (or 5 mTorr), when the diameter of the outlet hole is 0.5 cm and G is put at 5×10^{-6} gram/sec.

The intercathode distance (s) was calculated from the equations[2])

$$\frac{1}{\lambda} = \frac{2}{s}\left(\frac{m_e}{M}\right)^{\frac{1}{2}} \qquad (2)$$

and

$$p = \frac{1}{\lambda}f(V), \qquad (3)$$

where λ is the mean free path for an oscillating electron to produce an ionizing collision, m_e and M are the masses of the electron and positive ion, resp., and p is the gas pressure. The function $f(V)$ could be put equal to 0.4 Torr·cm (see ref.[2])). Combining (2) and (3) gives then an intercathode distance, $s = 3.5$ cm.

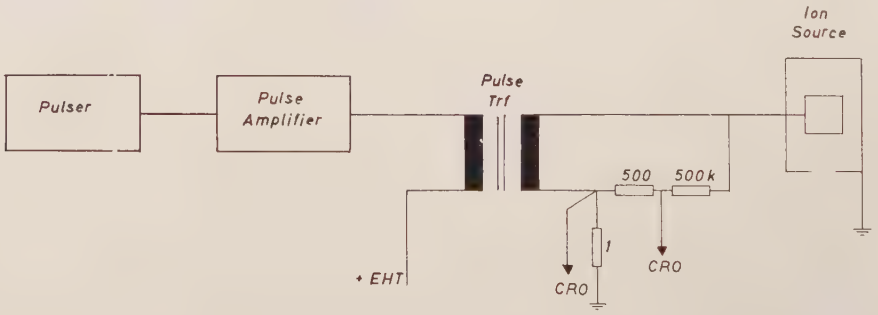

Fig. 3. Block scheme of the pulsing equipment.

3. Measurements and Results

The ion source was operated by means of a pulser, a pulse amplifier, and a pulse transformer as seen from the block scheme in fig. 3. The voltage and current of the pulse were measured by studying oscilloscope displays of the voltages

[2]) J. Flinta and R. Pauli, Pulsed High-Intensity Ion Source, Nucl. Instr. 2 (1958) 219.

[3]) K. Diels and R. Jaeckel, Leybold Vakuum-Taschenbuch (Springer-Verlag, Berlin, 1958).

over a bleeder resistor connected across the ion source terminals and over a resistance put in series with the ion source, resp. The length of the almost rectangular-shaped pulses to the ion

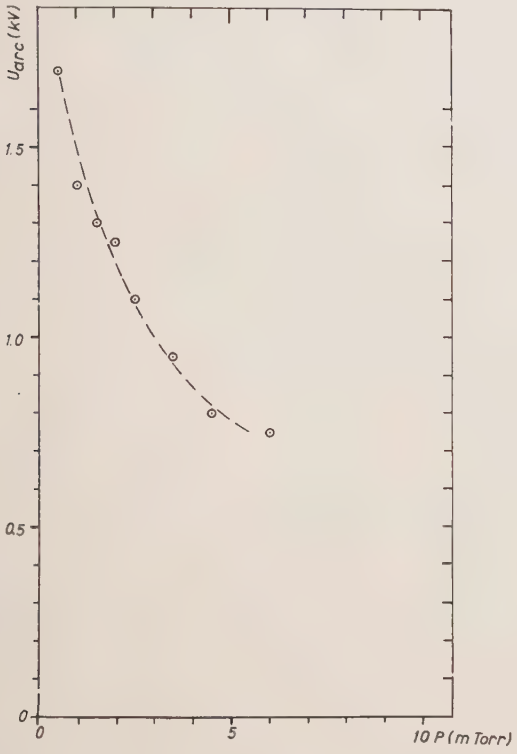

Fig. 4. The arc voltage (U_{arc}) as function of hydrogen gas pressure (p, mTorr) in the ion source.

Experiments were performed to determine the optimum operating conditions with regard to the pressure of hydrogen gas and the amplitude of the pulse voltage. One set of measurements gave the arc voltage (U_{arc}) as a function of hydrogen gas pressure (p) in the ion source as seen in fig. 4. The gas pressure in the ion source was then calculated from eq. (1) knowing the pumping speed measured as a function of the tank pressure for the vacuum pumps of the cyclotron.

In another set of measurements the time for building up a stable arc, here called "ignition time", was observed as a function of the (spike) voltage on the anode of the ion source. Fig. 5 shows an oscillogram of a typical voltage pulse, 50 μsec long, across the ion source. It is seen how the voltage after the "spike" drops down to the arc voltage. When the pulse was expanded on the oscilloscope screen, it was possible to measure the time needed for building up the stable arc. This ignition time depends on the gas pressure in the ion source and on the pulse voltage applied between the anode and cathode. Fig. 6 shows a typical curve of the ignition time (t_i) versus the spike voltage (U_{sp}) on the anode. (The curve corresponds to a hydrogen gas pressure of 5 mTorr.) Under normal working conditions the ignition time was about 3 μsec.

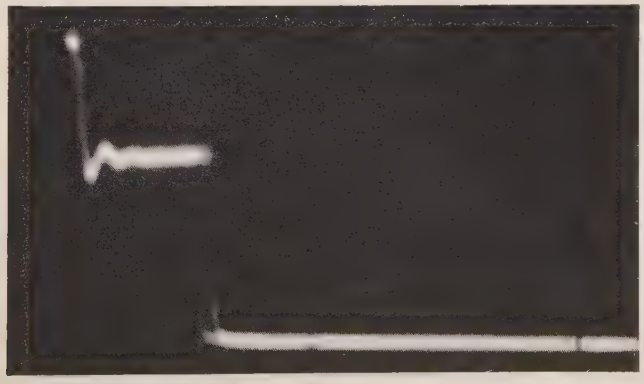

Fig. 5. A typical voltage pulse (50 μsec long) across the ion source.

source could be varied but was normally 50 μsec. (The repetition rate was about 300 pulses per sec and the acceptance time for catching ions was around 30 μsec.)

Fig. 7 shows two curves of the external and internal beam intensities as functions of the spike voltage (U_{sp}). (In this case the hydrogen gas pressure was 3.5 mTorr.) The internal beam

intensity (I_{pi}) (in arbitrary units) still rises at a spike voltage of 2.5 kilovolts, but the external beam intensity (I_{pe}) (also in arbitrary units) is seen to be "saturated". This effect was probably due to the fact that the energy spread of the internal circulating beam increases with the arc current in the ion source (as found in earlier measurements). As the external beam is extracted according to the strongly nonlinear regenerative method[4]), which is very selective as regards the particle energy, probably the beam intensity in the appropriate part of the internal energy spectrum reaches an optimum value, and therefore the external beam does not continue to increase.

The reason for installing two ion sources was mainly to have a spare ready for operation if one fails. However, both ion sources can be used simultaneously which may be of advantage considering the effect of space charge in the arc. Sometimes a slightly higher beam intensity has been observed with both ion sources working simultaneously. In those cases, however, both ion sources were connected to only one pulse power amplifier. A second pulse power amplifier is planned.

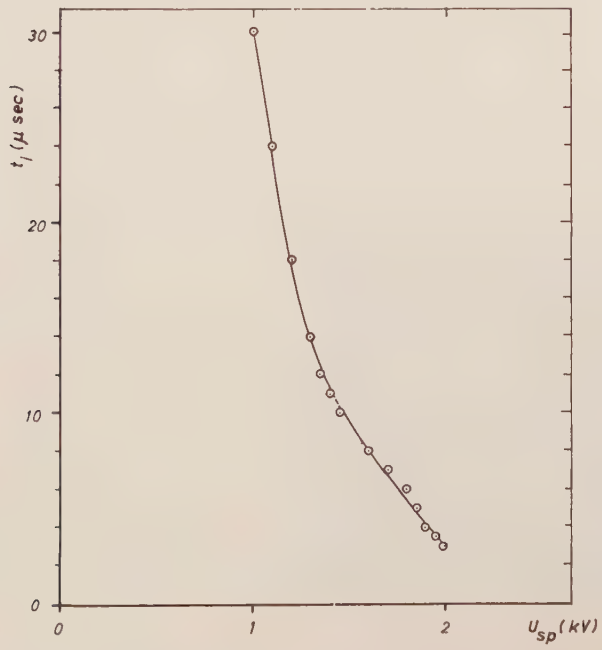

Fig. 6. The ignition time (t_i) versus the spike voltage (U_{sp}) taken with $p = 5$ mTorr.

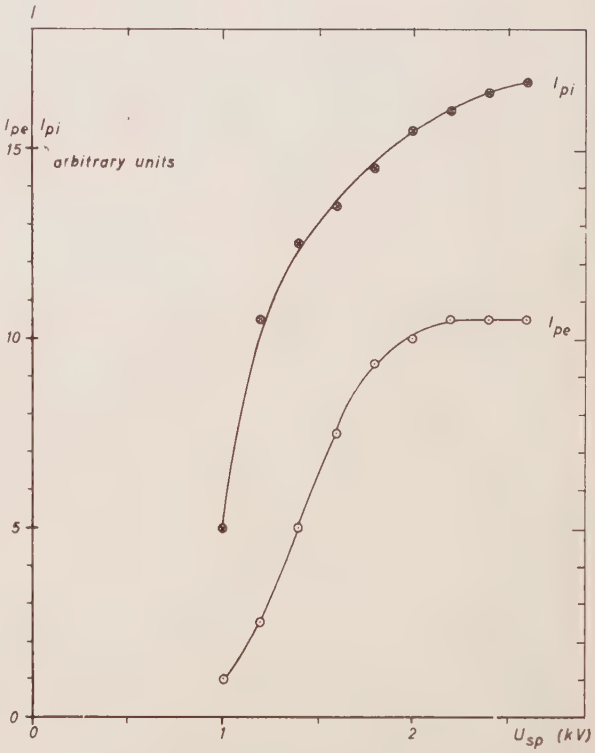

Fig. 7. The internal circulating beam (I_{pi}) and the external beam (I_{pe}) as functions of the spike voltage (U_{sp}) on the ion source at $p = 3.5$ mTorr.

The ion sources have now been in use for about a year, and as they have served very well it may be concluded that an ion source of the described cold cathode type is well suited for a synchrocyclotron.

Acknowledgements

The author is indepted to Professor The Svedberg for his stimulating interest. He also wishes to thank K. W. Ståhl, B. Hemryd and the cyclotron crew for assistance during the course of construction and experiments.

[4]) K. J. LeCouteur and S. Lipton, Non-Linear Regenerative Extraction of Synchrocyclotron Beams, Phil. Mag., Ser. 7, **46** (1955) p. 1265.

NUCLEAR INSTRUMENTS AND METHODS **10** (1961) 129–144; NORTH-HOLLAND PUBLISHING CO.

A DOUBLE-FOCUSING MAGNETIC SPECTROMETER FOR STUDIES OF ENERGY LOSSES IN MATTER OF ELECTRONS FROM A 5 MeV BETATRON

TORBJÖRN WESTERMARK

Division of Physical Chemistry, The Royal Institute of Technology, Stockholm 70, Sweden

Received 10 September 1960

A discussion is given of the best choice of energy region and electron source for an energy loss study program with emphasis on chemical valence effects on stopping power. The particular role played by multiple scattering and bremsstrahlung is stressed and a few MeV selected as the appropriate energy region. A 5 MeV betatron designed and constructed by Wernholm and Smårs is used as electron source. A double-focusing 90° sector type magnetic spectrometer is described and its focusing properties studied. The electrostatic technique for measuring line-widths is used.

1. Introduction

The study of the absorption of beta particles in matter is of considerable importance because, for example, questions related to it very often occur in experimental work with radioactive substances and in radiation chemistry. Moreover, many useful applications are based on the absorption properties, e.g. thickness and concentration measurements in industry and in the laboratory (see for instance[1])).

From a more fundamental point of view, the continuous energy distribution (which is true in most cases) and the presence in many cases of electromagnetic radiations make it preferable or even self-evident to turn from beta radiation of this type to the use of mono-energetic electron sources. Studies of the elementary processes occurring in the interaction of fast electrons (including beta rays) with matter, e.g. energy loss, scattering and the production of bremsstrahlung, are examples of such cases. In this laboratory, a desire to explain an abnormal behaviour in the absorption of beta rays in certain chemical compounds[1,2]) led to a study of the absorption of beta radiation in matter, but later a betatron was placed at our disposal rendering possible the study of the energy loss of nearly mono-energetic electrons in some light elements and compounds. In this paper — after a closer examination of the selection for this purpose of a mono-energetic electron source — a description of the energy measuring device, a double focusing magnetic spectrometer of 90° sector type, will be given. In subsequent papers, the methods used for energy loss measurements will be described and compared with those published by other workers[6,12–15,18,19,40,17]).

2. Choice of Conditions for Electron Energy Loss Studies, Energy Region and Electron Source

2.1. PRINCIPLES OF ENERGY LOSS STUDIES

As is well-known, a collimated beam of fast, charged mono-energetic particles (electrons in the present case) will suffer, when passing a layer of matter, an energy loss and at the same time a straggling in this energy loss (figs. 1 and 2). The energy loss is due to inelastic collisions with the atoms in the absorber which lead to ionization and excitation (for recent reviews, see[3,4,5,6,7,9])

[1]) T. Westermark, Some applications of beta radiation, Transactions Instruments and Measurements Conference, Stockholm 1949, p. 308–314.

[2]) T. Westermark, Phys. Rev. **93** (1954) 400; ibid **93**, (1954) 835.

[3]) H. A. Bethe, J. Ashkin, Passage of radiations through matter, in Experimental Nuclear Physics Vol. I, Ed. by E. Segré (John Wiley, New York, 1953) p. 166.

[4]) S. K. Allison, S. D. Warshaw, Rev. Mod. Phys. **25** (1953) 779.

[5]) W. Paul, H. Steinwedel, Interactions of electrons with matter, in Beta- and Gamma-ray Spectroscopy Ed. K. Siegbahn (North-Holland Publishing Company, Amsterdam 1955) Ch. I.

(and other reviews quoted in these references). The energy loss spectrum (fig. 2) follows an asymmetric distribution described theoretically by Landau[8]) and others. In addition, the production of electromagnetic radiation (external bremsstrahlung) adds to the energy loss.

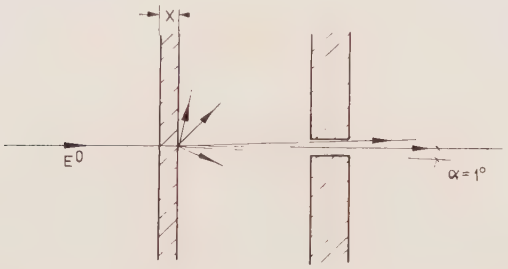

Fig. 1. The passage of a fast charged particle through a layer of matter. The initial energy is E_0. Some particles penetrate the layer without any appreciable angular scattering. The diagram shows the case of 1° limitation, a case adopted in the work described in the paper. Particles scattered through larger angles than this are not detected.

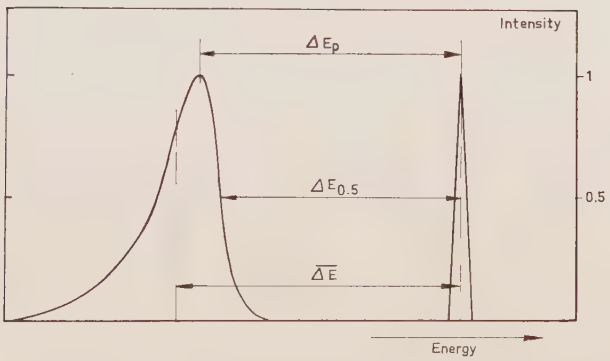

Fig. 2. The energy loss of a fast charged particle when passing a thin layer of matter (schematically). The symbols for the most common ways of characterizing the energy loss are explained. ΔE_p is the most probable energy loss, ΔE the average energy loss. $\Delta E_{0.5}$ is counted from the steep high energy side of the energy loss spectrum at half peak height. The energy loss spectrum is normalized to the same peak height as the primary line.

The scattering of the electrons by atomic nuclei and to some smaller extent by atomic electrons leads to various experimental complications. For example, fig. 3 shows how a longer path than the geometrical may be imagined. This phenomenon makes it necessary to limit the electron beam to narrow angles, of course not only on the entrance side but also on the exit side of the absorber. Moreover, the thickness of the absorbers has to be limited (see below).

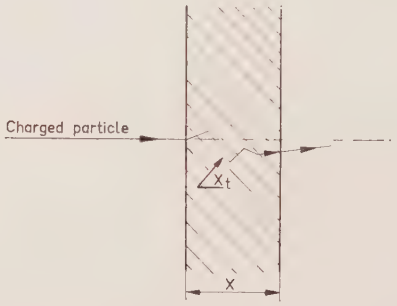

Fig. 3. Sketch of the tortuous path of a fast electron when passing through matter. The path increase factor ("Umwegfaktor") is the average over the actual path lengths as caused by multiple scattering divided by the geometric path.

The experimental problem is to measure the mean energy loss ($\Delta\bar{E}$), the most probable energy loss (ΔE_p) and other properties describing the process (cf. fig. 2) all referred to a material absorber with certain properties and to a known kinetic energy. The half-width of the energy loss spectrum or straggling parameter (Γ) is also of interest.

2.2. CHOICE OF ENERGY REGION

The present problem of energy loss in matter studied mainly from a chemical point of view makes it very necessary to include liquids in the studies. This point makes it impossible generally to go down to the low electron energy regions (about 0–100 keV) where characteristic energy losses of the order of 10 eV have been observed (see ref.[10]) for a recent review). One obvious reason is that windows cannot in general be avoided for holding the liquid in the appropriate position. Our investigations will instead be devoted to larger energy losses constituted by a great many elementary processes forming together a statistical distribution or an energy loss spectrum.

[6]) R. D. Birkhoff, Handbuch der Physik Vol. **34** (Springer Verlag, Berlin, 1958) p. 53.

[7]) R. M. Sternheimer, Phys. Rev. **88** (1952) 851.

[8]) L. Landau, J. Phys. U.S.S.R. **8** (1944) 201.

[9]) E. Uehling, Ann. Rev. Nucl. Science, Vol. **4** (1954) 315.

[10]) C. J. Powell, J. B. Swan, Origin of the characteristic energy losses in aluminium, Phys. Rev. **115** (1959) 869. This paper apparently gives a virtually complete reference list to earlier work (see also the same authors, ibid **116** (1959) 81.

The two further points governing the choice of electron energy region are *scattering* and *bremsstrahlung*.

The multiple scattering leads to a longer path (X_t) in the absorber than the geometrically expected one (X) and an "Umwegfactor" can be defined as follows:

$$q = \frac{X_t}{X}. \qquad (1)$$

This factor has been calculated by means of the so-called small-angle approximation by Yang[11]).

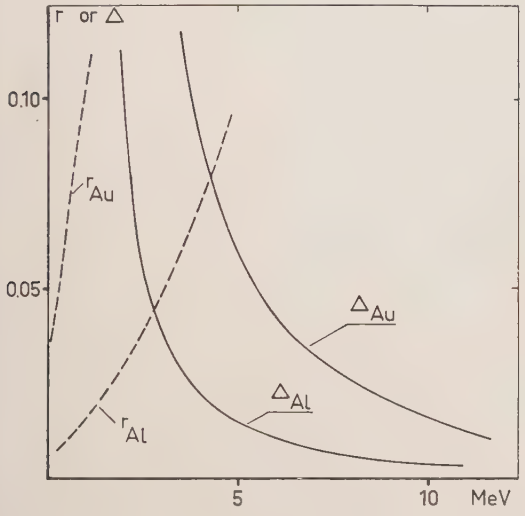

Fig. 4. The path increase factor q (actually $q-1$ in fig.) as a function of electron energy for aluminium and gold for 300 mg/cm² absorber thickness (calculated according to Yang[11]). The diagram also gives energy loss due to bremsstrahlung divided by ionization loss (cf. text) (Denoted r)

Using the formulas given by Yang, q was calculated as a function of electron energy for 300 mg/cm² layers of aluminium and gold. It is seen in fig. 4 which resulted from these calculations that the electron energy has to be several MeV in order to reduce the correction necessary for multiple scattering to a few percent for this absorber thickness even for light elements. It is also seen from the diagram that the fraction of energy expended for bremsstrahlung production (r) increases rapidly with energy. The calculation has been made according to Bethe's and Ashkin's review[3]) (p. 264 ff) using the bremsstrahlung theory of Bethe and Heitler.

It is seen (cf. fig. 4) that a too high electron energy involves too much bremsstrahlung and too low energy gives too large "Umwegfactors". A compromise between these two unfavourable influences on the precision of the energy loss measurements is seen to involve the selection of the energy region around a few MeV as the optimum one. In particular it is seen that it is difficult to avoid large bremsstrahlung losses for heavy elements even at low energies. The point concerning bremsstrahlung is also reflected by the fact that Nelms[29]) only extends her detailed tables on energy loss data of electrons up to the level corresponding to 5% energy loss due to bremsstrahlung. Hence these tables cover energies up to some MeV for heavy elements and up to 10 MeV for the lightest elements.

This discussion should be applicable to average energy loss measurements. If one resorts to most probable energy loss studies, the electrons having suffered large energy losses due to bremsstrahlung will affect the low-energy side of the energy loss spectrum without influencing the position of the maximum appreciably. The bremsstrahlung production will therefore not influence the most probable energy loss determinations. In fact, Hudson[12]) succeeded in studying such properties for 150 MeV electrons in elements of atomic number up to 13.

Because average energy loss studies are not dependent on straggling theories[29]), it was decided to select the energy region so that average energy loss measurements could be made. The discussion which follows is of course a very rough one but the selection of the region 2–5 MeV corresponds very well to the machine available and motivated improvements on it. Another point is that the experiments can be connected with studies on beta- and gamma radioactivity, the energy region of which is the same for many cases. A third point of experimental importance is that the energy region selected is the so-called minimum ionizing region, i.e. the energy loss per unit thickness does not change very much with energy (see for

[11]) C. N. Yang, Phys. Rev. **84** (1951) 529.
[12]) A. M. Hudson, Phys. Rev. **105** (1957) 1.

instance refs.[7]) and [29]). Thus corrections due to the finite thickness of the absorber should be small and, moreover, the well-established ionization chamber techniques can be applied without large corrections. (These points will be explained in more detail in a subsequent paper on the evaluation of the measurements[17]).)

2.3. CHOICE OF ELECTRON SOURCE

The requirements for an ideal electron source for accurate energy loss studies are, besides the desired energy region (here 2–5 MeV): a high degree of energy homogeneity, sufficient intensity, low background (of electromagnetic radiation), energy stability, intensity stability, parallel radiation pencil and low cost.

The demand for a narrow energy distribution is critical and might be formulated (cf.[14])) such that the half-width of the distribution should be small in relation to $\Delta E_p - E_{\frac{1}{2}}$ (cf. fig. 2) and very small in comparison with the apparent half-width, Γ, of the energy loss spectrum. Beta radiation and accelerators are the possible alternatives. In the former case, one can either use a spectral selection of a narrow band from a continuous electron energy distribution or employ conversion electrons produced by gamma transitions. Both possibilities seem to be less attractive than the use of accelerators. There are very few beta emitting nuclides of high energy (2–5 MeV) and with a long half-life. The intensity of course is smaller the higher the energy demanded. Internal conversion gives a low intensity at high energy but external conversion in a thin, heavy converter might be considered. The spectrum will, however, always contain more than one line (e.g. K- and L-lines) and, in addition, a continuum at some distance due to Compton electrons. The situation can be improved by means of spectral selection before the absorber zone. The point of intensity would obviously favour the accelerators.

Among the accelerators conceivable, viz. van de Graaff machines, Cockroft-Walton machines, linear accelerators, betatrons and synchrotrons, many would be possible if the energy distribution is narrow enough and the stability sufficient. Commercial machines are very expensive and some require large amounts of space. Betatrons have been used previously for electron energy loss studies[13–15]) and possess the merits of compactness and cheapness. Our laboratory was fortunate enough to be offered in 1952 a 5 MeV betatron. It will be shown in another paper by the present author that the requirements on the machine have been fulfilled to a large extent[17]). It should be added that other investigators have used as electron source a linear accelerator[12]), continuous beta radiation with energy selection[18,50]) and internal conversion electrons[19,20,6]). (The last reference reviews several papers describing this point.)

3. The Betatron

The 5 MeV betatron used here as a monoenergetic electron source was designed and constructed by Wernholm and Smårs at the Department of Electronics in this Institute. In the beginning, it was made to produce X-rays by orbit expansion on to a tungsten target. Later on, it was equipped with a means for bringing the electron beam outside the machine (Smårs).

A detailed description of the machine with its auxiliary circuits will be published by Smårs and Wernholm[16]). Here, only some pertinent points necessary for the present article will be given. The main data for the betatron are:

Equilibrium orbit radius	8.2 cm
Peak magnetic flux density in orbit	2500 gauss
Field exponent	$n = 0.75$
Injection voltage	25 kV (pulsed)
Number of bursts per second	50
Tube material: pyrex glass covered with a conductive coating (SnO_2 or Pt)	
Intensity of external beam normally	10^8 electrons/sec.

[13]) W. Paul, H. Reich, Z. f. Physik **127** (1950) 429.

[14a]) A. E. Goldwasser, F. E. Mills and A. O. Hanson, Phys. Rev. **88** (1952) 1137; [b]) E. L. Goldwasser, F. E. Mills and T. R. Robillard, Phys. Rev. **98** (1955) 1763; [c]) H. E. Hall, A. O. Hanson and D. Jamnik, Phys. Rev. **115** (1959) 633.

[15]) B. Ziegler, Z. Physik **151** (1958) 556.

[16]) E. Smårs and O. Wernholm, A 5 MeV betatron (to be published).

[17]) T. Westermark, Electron energy distribution and energy stability of the electron beam from a 5 MeV betatron, Nucl. Instr. and Meth. (to be published).

[18]) J. A. McDonell, M. A. Hanson and P. R. Wilson, Austral. J. Physics **8** (1955) 98.

The extraction of electrons in this betatron is performed by rapidly moving the orbit, in its own plane, through a distance of several centimeters[16]). This is made at a predetermined flux density, thus yielding electrons of a certain momentum (irrespective of changes in the guiding field flux curve, as to form, amplitude etc.).

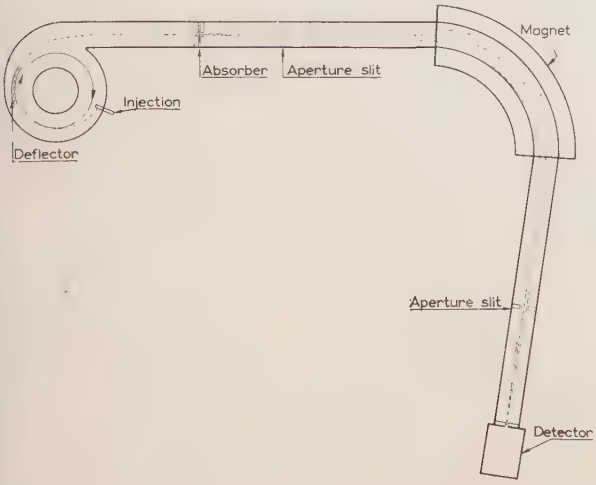

Fig. 5. Diagram of betatron together with spectrometer. Electrons are pulse-wise injected into the betatron orbit (radius about 8 cm). Due to an ejection pulse at a predetermined magnetic flux density, the orbit is moved in the direction indicated so that the beam enters the deflector and is guided out through the side arm of the doughnut tube. After passing the absorbers (if present), a collimated part of the beam enters the spectrometer and is focused on the exit slit where a detector is placed.

The electrons disturbed in this manner then enter a deflection condenser with about 25 kV applied. By means of this, they will be guided out through a side arm of the betatron tube as is shown very schematically in fig. 5. This arm is provided with a thin window transmitting the fast electrons or is alternatively connected to the spectrometer described below so that the two vacuum systems will be combined. The machine is placed in a conventional laboratory (4.5 × 6.4 meters). The radiation hazards are not large due to the low intensity but it is necessary that operation should be made from a control table about 3 m from the betatron tube.

[19]) J. J. L. Chen and S. D. Warshaw, Phys. Rev. **84** (1951) 355.

[20]) P. White and G. Millington, Proc. Roy. Soc., Lond. **120** (1928) 701.

4. Choice of Energy Resolution Device

Many energy resolution devices have been used in previous studies on the energy losses of fast charged particles, e.g. magnetic spectrometers, electrostatic spectrometers, scintillation detectors and Čerenkov-detectors. The best resolution so far is apparently that obtained in the electrostatic spectrometer of Birkhoff and Blackstock[21]), viz. a resolution $\Delta E/E_0$ of 1/100000 for 100 keV electrons, a remarkable figure. Their ingenious method, involving the use of the accelerating potential once again before the spectrometer, does not seem to be applicable to accelerators such as betatrons. The magnetic spectrometer is capable of giving a resolution of the order of 1/1000 or better and its suitability for the present purpose can hardly be questioned. This method was accordingly selected. Among the various types available (for reviews see[22]) and[23])), the sector type instruments were considered suitable here because a beam of, in in the first approximation, parallel electrons was available. A description of the spectrometer will be given in the next section.

5. The Magnetic Spectrometer – Design and Construction

5.1. DESIGN

An important question in the design of a magnetic spectrometer is the judgement of the double-focusing arrangement versus the single focusing one. The former has several merits including higher luminosity, twice the dispersion and hence higher resolution at a given orbit radius. The pole shoes have been given a special shape, which is a complication in construction. Because of the superiority of the double-focusing spectrometer, this type was, however, chosen.

[21]) A. W. Blackstock, R. D. Birkhoff and M. Slater, Rev. Sci. Instr. **26** (1955) 274.

[22]) K. Siegbahn, in Beta- and Gamma-Ray Spectroscopy (North Holland Publishing Company, Amsterdam 1955) Ch. III.

[23]) T. R. Gerholm, Beta-Ray Spectroscopes, in Handbuch der Physik, Vol. **33** (Springer-Verlag, Berlin, 1956) p. 608.

[24]) N. Svartholm and K. Siegbahn, Arkiv f. Mat. Astr. Fys. **33A** (1946) 21.

[25]) N. Svartholm, Ark. f. Fysik **2** (1950) 115–118.

The design was facilitated by studying the descriptions or theories by Svartholm and K. Siegbahn[24]), Svartholm[25,30]), Mileikowsky[28]), Judd[31]), Arbman and Svartholm[51]) and others. The spectrometer should cover the electron energy 0.1–5 MeV or even wider. The following main data were selected:

Deflection angle	90°
Orbit radius (r_0)	250 mm
Magnetic flux density	0–1200 gauss
Pole gap ($2b$)	50 mm
Pole width	150 mm

The condition for double-focusing is, according to Svartholm and Siegbahn[24]), that the field should vary as $1/\sqrt{r}$. Using the conical approximation suggested by Svartholm[25]) and used by Mileikowsky[26]), we find that

$$H_z(r) = H_z(r_0)\left[1 - n \cdot \frac{r - r_0}{r_0}\right] \tag{2}$$

where

$$n = \frac{r_0 \tan \alpha}{b} = 0.5\,. \tag{3}$$

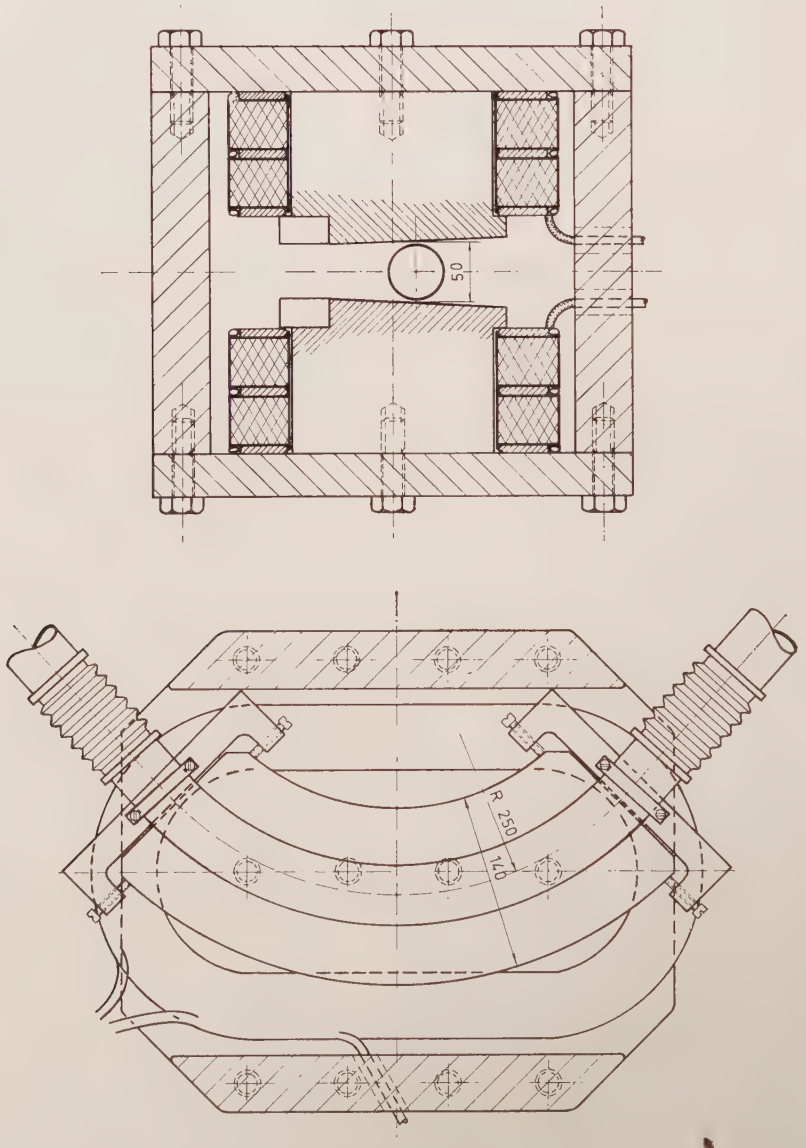

Fig. 6. Design of spectrometer magnet, including mounting of spectrometer tube. (The design has largely been made by the ASEA Company.)

(H_z is the component of the magnetic flux density perpendicular to the plane of the electron orbit. The index refers to the radial position.)

With the above values for r_0 and b, we obtain $\alpha = 2.86$.

Using the above main data, the magnet could then be designed. This was carried out by Dr. L. Dreyfus, ASEA Company. The final design is shown by means of the fig. 6. Care was taken in the design to achieve a good homogeneity of the flux.

5.2. CONSTRUCTION OF MAGNET

The material should preferably be a soft iron with as low coercive force as possible and give at least 3500 gauss at 1 At/cm (Dreyfus). A soft iron material, type SBA-5A, offered by the Surahammar Company almost completely fulfilled the requirements after suitable heat treatment. Test pieces of the material from the ingots used were tested by ASEA. $B = 3500$ gauss was found at 1.2 At/cm. This is close to the requirement set.

The machining was performed by AB Atlas Copco, Stockholm. Dr. C. Mileikowsky's experience[26]) has been most valuable throughout the construction work. In fact, the difficult machining of the pole shoes was made in the same manner as in Mileikowsky's case by putting the ingots pair-wise opposite one another in a large lathe. In this manner, any errors will be symmetrical. The mechanical work was even performed by the same personnel.

Accurate measurements of the results of the pole shoe machining showed that the deviation from linearity along a radius was less than 0.01 mm. Thus it is seen that the resulting precision is even better than the tolerance required which was $\pm$ 0.05 mm. The angle was also found to be accurate.

5.3. THE COILS

The two coils for magnetizing consisted of 12 layers times 16 turns of 3.6 $\times$ 3.2 mm copper wire. This gave a resistance of about 0.8 ohms. The coils which are connected in series are fed with currents up to 10 amp from a large capacity storage battery. The coils are provided with water cooling facilities for work with large currents (see below).

5.4. PERFORMANCE OF MAGNET

The performance of the magnet has been studied mainly by means of the spectrometric data (see below). A few investigations were performed to get an idea of the magnetic data. A less accurate ($\pm$ 3%) but very handy direct-reading gaussmeter based on the Hall effect was used (Dynalabs D 79 Gaussmeter). The flux density at a point close to the equilibrium orbit as a function of magnetizing current is shown in fig. 7. Within the accuracy available, the curve is straight in the portion 0–200 gauss but then curves slightly upwards. It was also shown that no cooling was necessary when currents below 6 A were used. This statement was found to hold true for current changes less than 0.2%.

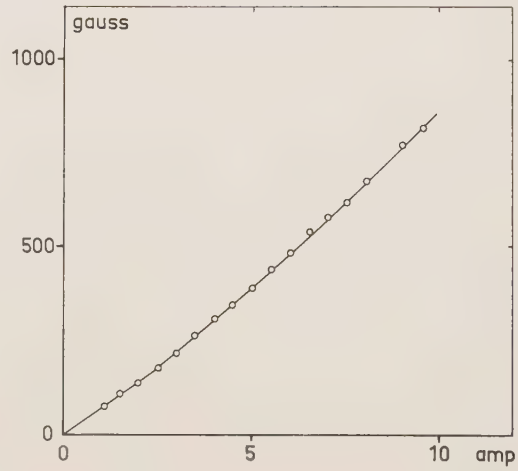

Fig. 7. Magnetic flux density near orbit radius of the spectrometer as a function of coil current. Data taken with Dynalab D-79 gaussmeter which has a stated precision of $\pm$ 3%.

At a fixed coil current, the flux density was measured in the radial direction. A semi-log plot of the data gives a field exponent (n) of 0.54 $\pm$ 0.04 which is near the expected figure within this rather limited accuracy.

The fringing field was also studied. It was found to reach half the flux density between the

[26]) C. Mileikowsky, Ark. f. Fysik **4**, Nr. 16 (1952) 337–346; ibid **7**, Nr 3 (1953) 33–46.

pole shoes after about 1.8 centimeters (or 0.7b). The boundary surfaces are plane and thus no efforts have been necessary to modify them to some curvature in order to achieve better focusing — a thing which is possible, as is well-known.

5.5. THE SPECTROMETER TUBE

A copper tube with 45 mm internal diameter was filled with sand and heated in the workshop with welding flames on a tree fixture in order to get the correct curvature. As is clear from fig. 6, the spectrometer tube is fixed in the horizontal plane of symmetry of the magnet. This was performed by means of a brass construction.

A vertical tube from the bent spectrometer tube leads to the vacuum system. Two slits define the electron beam within the tube. The entrance slit width can be adjusted in the range 0.5–6 mm. The exit slit is symmetrical to the entrance slit and is of similar design. The aperture slits are placed at a distance of 245 mm from the boundaries of the magnet. They can be adjusted to a 5×5, 7.5×7.5 or 10×10 mm square opening.

At the position of the aperture slit, the tube is interrupted by means of flanges which are fastened together by means of rubber O-rings.

5.6. THE VACUUM SYSTEM

Fig. 5 gives some idea of the whole design.

The spectrometer tube is evacuated by means of a fore-pump and an oil diffusion high-vacuum pump (capacity $\sim$ 70 l/sec). A Pirani gauge serves for low vacuum and a Penning vacuumeter for high vacuum. The usual vacuum is 10^{-5} mm. This would correspond to an equivalent absorber that is completely negligible from the energy loss point of view when dealing with electrons in the MeV region.

5.7. THE SPECTROMETER STAND

The magnet and spectrometer are mounted on a table constructed using Dexion profiles (cf. fig. 8). The vacuum equipment is placed on a shelf below the spectrometer. The table is provided with four wheels of rugged construction. Thus the whole table can be adjusted relative to the betatron stand and then fixed to it by screws. The magnet itself is mounted on a movable stand on the table. This stand is of heavy construction and permits, by means of four screws, adjustments of the magnet and spectrometer tube in order to take into account deviations of the betatron electron beam from the horizontal.

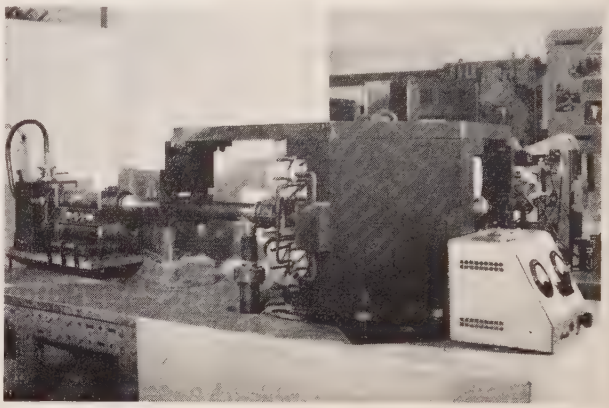

Fig. 8. View of the spectrometer unit.

The detectors used at the exit end of the spectrometer will be described below.

6. The Focusing Properties of the Spectrometer

The focusing properties of the spectrometer described sbove were studied with internal conversion electrons from Cs^{137}–Ba^{137} sources and the thoron deposit. Some studies were made also by means of external conversion electrons. The results will be discussed in terms of the existing theory of spectrometers of this kind.

6.1. CALCULATION OF THE FOCUSING PROPERTIES

Svartholm[30]) and Judd[31]) have given theoretical formulas for the conical sector field spectrometer used here. Mileikowsky[26]) has compared his spectrometer with these results. These papers apply to the case where sources and image are

[27]) H. Slätis, Ark. f. Fysik **6** (1953) 415.
[28]) G. Lindström, Ark. f. Fysik **4** (1951) 1.
[29]) A. T. Nelms, Energy Loss and Range of Electrons and Positrons, Nat. Bur. Stand. a. Circular 577 (1956), b. Supplement to the same (1958).
[30]) N. Svartholm, Ark. f. Fysik **2**, Nr. 20 (1950) 195.
[31]) D. L. Judd, Rev. Sci. Instr. **21** (1950) 213.

situated outside the magnetic sector field. Siegbahn and Edvarson[32]) have compared their precision spectrometer with the theory. In their case, both source and image are situated inside the field. Both groups of papers are of interest for the present case. The theory and the use of it for experimental comparison are so clearly given in the papers that only brief accounts will be presented below when the theory is used.

6.2. THE DISPERSION

The dispersion (D) was measured directly by studying the movement in the image plane of the internal conversion line of Ba^{137} (from a Cs^{137} — Ba^{137} source).

D is given by

$$D = \frac{\delta s}{r_0} \Big/ \frac{\delta p}{p} \qquad (4)$$

where $\delta p/p$ is the relative change in momentum and δs the corresponding radial displacement of the image perpendicular to the optical axis.

The result obtained was $D = 3.9 \pm 0.2$. The accuracy is not very high but shows without doubt that the figure is close to $D = 4$, or that characterizing double-focusing.

Fig. 9. Focusing at the detector plane on a photographic X-ray film of K-conversion electrons from Cs^{137} — Ba^{137} with and without 5 kV extra acceleration voltage. The middle sections of the sources are masked. The photograph shows, despite the only fair contrast, that two spots are produced at each electron energy. Thus double focusing is obtained. Further the unit is seen to resolve the two energies which are 0.5 % apart on the momentum scale. Dispersion data have been evaluated by similar studies.

6.3. FURTHER PROOFS OF DOUBLE-FOCUSING

In another experiment, the middle part of the entrance slit was covered, thus forming two openings situated one above the other. The exposure of a photographic film in the detector plane by means of Ba^{137} internal conversion electron showed the two openings reasonably well pictured (fig. 9). This shows directly that the apparatus is double-focusing. Similar results were obtained with betatron electrons.—A further indication is presented in fig. 10 showing that the intensity has a clear maximum for varying angles of indication in relation to the plane of the orbit (at constant radial position). From the same diagram it is seen that the half-width does not change appreciably, which seems to be in accordance with what can be expected.

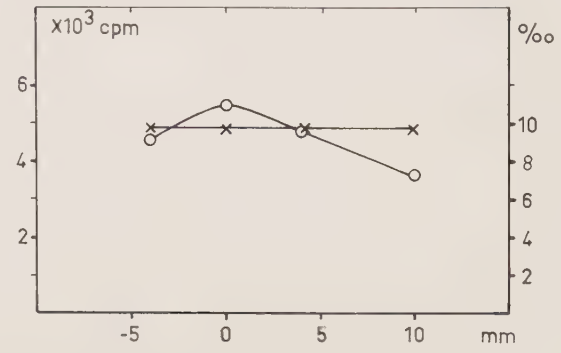

Fig. 10. Intensity and half-width of the Ba^{137} K-line for movements in the (vertical) plane perpendicular the orbit plane.

6.4. AN ELECTROSTATIC METHOD FOR MEASURING HALF-WIDTHS AND ITS APPLICATIONS TO ThB AND Cs^{137} SOURCES

An electrostatic technique has been used to facilitate the study of line-widths[42]). The radiation source was electrically insulated and connected to a variable high tension generator, the output of which was measured (fig. 11). The method is based upon an idea given by Rutherford, Wynn-Williams, Lewis and Bowden[35]) who

[32]) K. Siegbahn and K. Edvarsson, Nucl. Phys. **1** (1956) 137.

[33]) K. Siegbahn, Appl. Sci. Res. B **4** (1954) 25.

[34]) V. M. Kelman, V. A. Romanov, R. V. Metskhvarishvili and Y. A. Kolyunov, Nucl. Phys. **2** (1956/57) 395.

[35a]) E. Rutherford, Wynn-Williams, W. B. Lewis and B. V. Bowden, Proc. Roy. Soc. A **139** (1933) 617; [b]) W. B. Lewis and B. V. Bowden, ibid. **145** (1934) 235.

used it for measuring the differences in energy of alpha particle groups. In 1954, K. Siegbahn suggested[33]) that the technique could be used for accurate h/e determinations. During our work, the outstanding results by Kelman *et al.*[34]) for adjacent conversion electron lines were published.

Using the electrostatic technique, internal conversion lines were studied for various spectrometer parameters. The method yields the line widths directly in electron volts and is very practical, viz. no knowledge of elementary constants or calibrations is necessary. The magnetic flux density is kept constant during each experiment and thus the electrons actually recorded by the detector have the same energy. Thus, the method is in principle free from any change in the focusing properties or other changes due to change of energy and, moreover, the detection efficiency is identical.

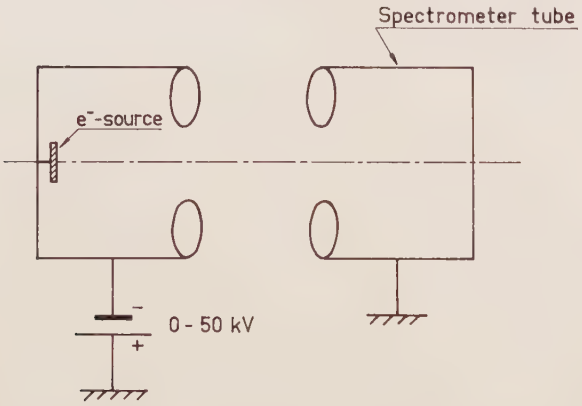

Fig. 11.
Principle of the electrostatic method for measuring half-widths and energy differences of electron conversion lines.

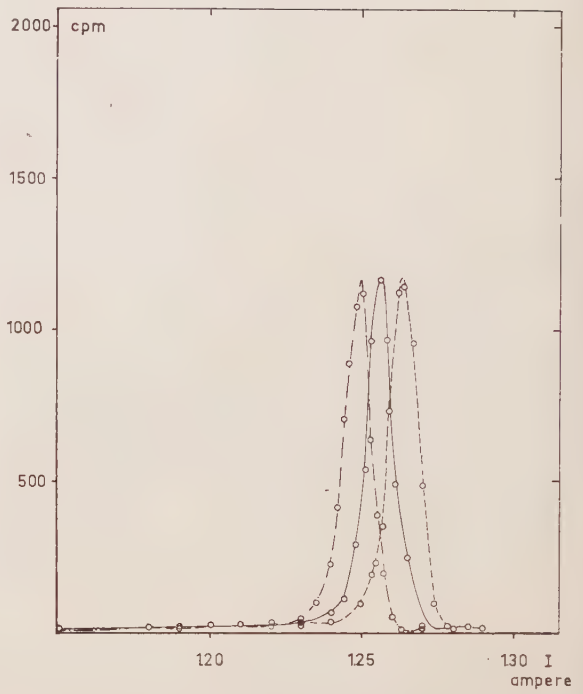

Fig. 12. Movement of the Ba^{137}: K conversion line by means of the electrostatic method illustrated in figs. 9 and 11.

Fig. 12 shows the K-conversion line of Ba^{137} surrounded by those lines obtained by applying + or − 5 kilovolt to the source. The lines were found to be identical within experimental errors as far as height, half-width, base-width etc are concerned. Thus the validity of the electro-statical method under these conditions is proved.

Fig. 13 shows a line studied by the electrostatic technique. The Cs^{137}–Ba^{137} source was 0.46 mg/cm² in this case. The width was found to be 1830 eV or 0.22% (the momentum scale). The

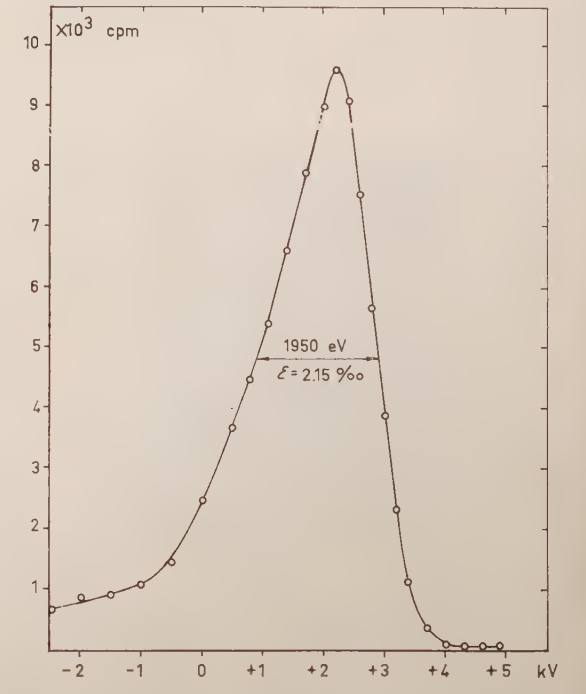

Fig. 13. Ba^{137} K conversion line as studied by the electrostatic technique. The absolute half-width is obtained directly in electron volts. ε is relative half-width expressed in mentomum scale.

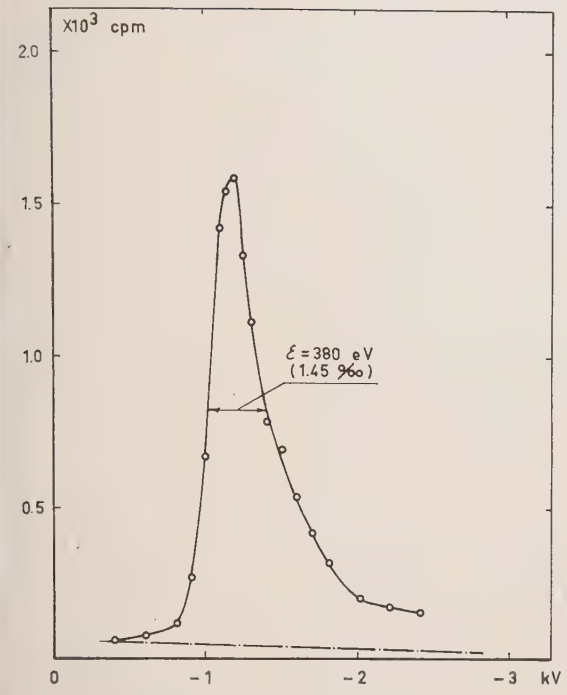

Fig. 14. The ThF line with the electrostatic technique. In this figure, the high energy side is on left (corresponds to less negative voltage). The source was a 0.2 mm Pt-wire which had been exposed to thoron gas in a conventional way. Exit slit width 1 mm. Detector: 1 × 12 mm anthracene. No matter between source and detector. (Relative half-width on momentum scale indicated.)

asymmetry is probably due to self-absorption (Landau distribution) but might partly be due to the spectrometer itself. It was noted during these experiments that the energy difference between the K and L lines (32 keV) or L and M (~ 4 keV) is apparently easy to measure thus confirming the expectation of K. Siegbahn[33]).

The F line from the thoron active deposit was studied using platinum wires of 0.1 mm diameter as sources and by employing the conventional preparation technique. The line width obtained was 380 eV (see fig. 14). It should be noted that the line is asymmetrical despite the minute amount of material deposited. The width found is 1.45‰ (momentum scale).

These results might be compared with those of Siegbahn and Edvarson obtained using an iron-free spectrometer of very high resolution[32]). They got 126 eV for the ThF line and noted that it was asymmetrical. By taking the properties of the high-energy side only, they arrived at 101 eV for the half-width. If the same procedure is used for our results, we get a somewhat narrower half-width (see below). No reason for the asymmetry was forthcoming from our studies.

A possible but yet speculative explanation for some of the asymmetry of the lines from the thoron deposit may be the electrostatic properties of the surface of the wire where the ThA-ions are deposited as positive ions. It has been shown by autoradiography[36]) that plane electrodes containing different metal "islands" are covered, during deposition, with different amounts of activity according to the respective work functions. Although the conditions of the deposition are never very well-defined (e.g. moist air being present), Jech has shown[37]) that the deposition method can be used to measure relative electrostatic potentials between metals. Further, Yamamoto[38]) has shown that alkali treatment of iron electrodes gives a much higher deposition on the oxide areas. Taking these results into account, we might imagine the deposition of ions to occur non-uniformly either due to impurities (cf. Yamamoto[38])) or due to the work function of the deposited activity being different (higher) from that of the wire metal. Thus self-absorption and hence "self-straggling" might be caused in this way. If the explanation is right, a correct choice of wire material might lead to the elimination of the effect. In a recent paper, Karlsson and Siegbahn report comparisons with deposition[43]) experiments using tungsten wires and aluminium foils. In the latter case, the low energy tail is to a very large extent eliminated, a result which the authors attribute to reduced back-scattering. This explanation is plausible but one cannot exclude without further experiments the possibility that part of the change may be due to the electrostatic effect discussed above.

[36]) T. Westermark and L.-G. Erwall, Nature **169** (1952) 703.
[37]) C. Jech and M. Jagrova, Cs. Cas. Fys. **8** (1958) 206.
[38]) D. Yamamoto and T. Goto, Naturwiss. **46** (1959) 559.

6.5. THE ELECTRON-OPTICAL PROPERTIES OF THE SPECTROMETER

The half-width was studied as a function of the distance, detector-pole shoe edge (cf. fig. 15). As is seen, a very flat minimum was found, i.e.

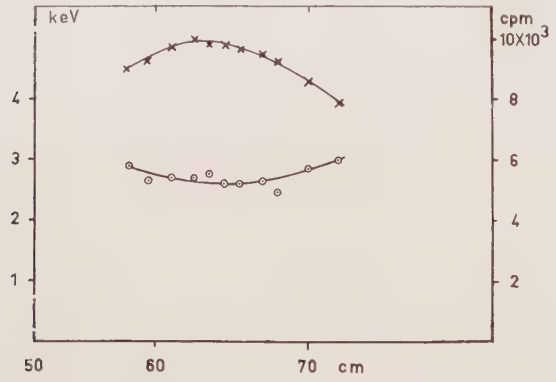

Fig. 15. Half-width of the Ba^{137} K conversion line in keV as measured with the electrostatic technique as a function of distance, pole shoe boundary-exit slit.

the focus is not very sensitive to the distance in question. By using the Al results, the conditions of symmetrical radiation paths were found experimentally and proved to correspond to a focal distance of 650 mm (counted from the pole shoe edge). According to Judd's formulas which use the thick lens analogy, we would expect 540 mm. The difference is probably due to the influence of the fringing fields. (The initial experiments were made without any knowledge of the actual focus. By means of Judd's formulas and further experiments, it was possible to reach systematically the symmetrical case in which the source and image distances relative to the magnet are equal.) The flatness of the half-width minimum probably explains why the electrostatic technique succeeds so well in this very "narrow" geometry. We should theoretically expect some change in the source point of the electrons upon applying a voltage to the source. Hence we should also expect a movement of the image point. This effect has been discussed in some detail by K. Siegbahn in connection with his suggestion of h/e-determinations[33]) because, in many other types of spectrometers, the effect has to be seriously considered. In the present case, we see that even a movement of 1 cm would be difficult to detect at all. A similar discussion might hold true for Kelman's spectrometer[34]) because this is also of sector type with a very small angular electron spread. The relative insensitivity with respect to the source position facilitates the subsequent electron energy loss studies since little care is necessary to place the source in an exact position. A change of a few millimeters or even one centimeter will not affect the results at all.

The fringing fields on both sides of the magnet must *a priori* bend the beam to some extent (compare Mileikowsky's work[26]). In order to be able to study this effect separately, both spectrometer arms were connected by bellows so that the arms can be bent. The optimum half-width was found to occur at about 95° (see fig. 16) thus exceeding the design angle 90°. Also here, care was taken to strive for symmetrical conditions but for practical reasons the final adjustment was slightly unsymmetrical (the difference being only 2°). This result might be compared with that of Mileikowsky[26]) who got an optimum at 192° as compared with 180° in the design.

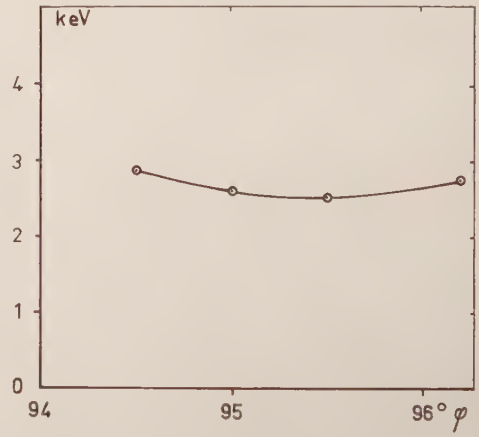

Fig. 16. Ba^{137} K conversion line half-width in keV (the electrostatic technique) as a function of deflection angle. It is seen that the optimum is displaced from the nominal 90° to about 95.3°, apparently due to deflection in the fringing fields.

Mileikowsky ascribed this deviation to the bending effect of the fringing field and also made quantitative comparisons. This explanation is no doubt true also in the present case in which a comparable difference was obtained.

The optimum deflection angle, i.e. 96°, was fixed and thereafter the focal distances were studied again but no detectable change had occurred.

It should be noted here that it has been found that parasitic lines occur when the spectrometer is badly adjusted. This might be due to a scattering of the electrons within the spectrometer tube. These lines also occur when the aperture slits are removed. Therefore such slits are introduced not only in the entrance arm but also in the exit one.

Resolution

The resolution obtained experimentally has been compared with that predicted theoretically:

$$\frac{\Delta B_\rho}{B\rho} = \frac{a+s}{Dr_0} + \frac{2}{D3}(\gamma_r^2 + \gamma_z^2)\,. \qquad (5)$$

This formula is derived from Svartholm's theory by inserting $\beta = \frac{1}{4}$ which is applicable for the ideal conical field. The property β is the second order coefficient in the expression of the flux density as a power series in $(r - r_0)/r_0$. (Formula (2) above includes only the first term.) Mileikowsky has used this relation in his discussion[26]) and it should also be applicable here. It is seen that the radial and axial aperture angles (γ_r and γ_z respectively) contribute with equal weight. They were therefore made equal. a and s are entrance and exit slit widths respectively. D is put equal to 4 (cf. above).

We have proceeded in nearly the same manner as Siegbahn-Edvarson[32]). Tables 1 and 2 summarize the results. The agreement is reasonably good. Some improvement is got when using the method of Siegbahn and Edvarson in which only the high energy side is analysed. The difference may also be ascribed to the aberration in the fringing field which is passed by the particles at about a 3° deviation from the normal. The residual error is about 0.3‰ which compares well with the corresponding error 0.2 — 0.3‰ in the spectrometer discussed by Mileikowsky[26])

Table 1

Comparison of expected and found half-widths of the ThF-line (illustrated in fig. 14)
(all widths are expressed in momentum scale)

	Base width (‰)
Entrance slit 0.2 mm (Pt-wire diameter)	0.2
Detector, exit slit	1.0
Natural line-width[27,28] (twice 70 eV)	0.54
Spherical aberration	0.21
Base width sum	1.95
Half-width, assumed to be half base width	0.98
Experimental half-width	1.45
Difference	0.47

If the experimental half-width is corrected according to Siegbahn and Edvarsson [32]), viz. by taking only the high-energy side, 1.27% is got—i.e. a 0.29‰ difference from the theoretical value.

Table 2

Expected and found half-widths for Cs^{137}–Ba^{137} K-conversion line. (Illustrated in fig. 13)

	Base width (‰)
Source	1.5
Detector	1.0
Spherical aberration	0.21
Straggling in source and cover	1.10
Base width	3.81
Expected half-width	1.90
Experimental	2.15
Difference	0.25

The estimate of the straggling requires an explanation: The source was 0.46 mg/cm² and the cover 0.53 mg/cm² mica, or a total of 0.99 mg/cm² which is taken as aluminium for simplicity. The property S_0 [14a]) is then 0.07 keV for this thickness (S_0 is $= 2\pi e^4 n t/m_0 c^2 \beta^2$). The half-width of the energy loss cirve is, according to Landau's theory, $3.98\,S_0$ [14a]). This was confirmed at 15.6 MeV[14a]) but it is definitely broader at lower energies and for thinner absorbers. Blunck and Leisegang[49]) by refining the Landau theory could bring Paul and Reich's results[13]) into agreement with their theory at least for low Z absorbers. The width was found to be 50% larger than the Landau predictions at 2.8 MeV. At 206 keV (the classical White-Millinton[20]) experiments), it was 80% larger than the Landau width. In the present case, the energy is 625 keV and so 1.7 times the Landau width might be a reasonable but rough guess. We therefore arrive at a half-width of $0.074 \times 3.98 \times 1.70 = 500$ eV. Then twice this amount is to be taken to get the base width, which expressed on the momentum scale is 1.10 ‰.

and Pauli[39]). The explanation given here is due to K-G. Malmfors. When the electron path is situated wholly within the magnetic field as in the case of Siegbahn-Edvarson, the effect does not exist and the experiments and calculations agree much better[32]).

The calculation method is supposed to be adequate as far as the base width is concerned. The assumption that the line shape is triangular and hence the half-width equal to half the base width is, however, an approximation. An exact treatment would require a troublesome folding procedure and, because of this and the apparent success[32,39]), the approximation was judged allowable for our purpose.

With regard to the approximations made, the difficulty of assessing the role of the straggling effect (see text of table) and the possible role of aberrations in the fringing field, the results summarized in tables 1 and 2 can be taken to be satisfactory. Thus the performance of the spectrometer is close to what may be expected. The results for the ThF line (cf. fig. 14) may be taken as a good approximation of the window curve. The actual performance may however be better than this for the reasons discussed above (back-scattering, self-straggling and natural line-widths).

6.6. THE SOLID ANGLE

The solid angle is very small in a spectrometer of this type. It is 0.6×10^{-3} sterad or a 0.5×10^{-4} fraction of 4π. A practical idea of this is to state that a source of about 2 millicuries of Cs^{137}–Ba^{137} gave about 10000 counts/min of the K-peak using the spectrometer data given above. (The small solid angle is of no great inconvenience as far as the intended use for a directed betatron electron beam in concerned.)

6.7. DETECTORS

Several detectors have been used including a simple GM-counter of mica end window type (1.83–3 mg/cm^2 windows), GM-tubes in a coincidence pair, ionization chambers, scintillation detectors and photographic film.

In the case of the GM-counters and ionization chambers, an exit window is necessary. The photographic film has often been placed within the vacuum at the exit slit plane. (Sometimes it has been placed outside the window.) Ilford C X-ray film has been used extensively together with standard procedures. Its use has been shown previously (fig. 8). The scintillation detector has essential merits. No matter is present between the source and the detector. Another advantage is the very low background attainable by using small anthracene or plastic scintillation detectors. We have often used an anthracene crystal with a size of $12 \times 3 \times 1$ mm. In a vertical mounting, the width of 1 mm will determine at the same time the exit slit width. Such a detector gives only a few pulses/min as background and only slightly more when the betatron is operating. This detector or the corresponding plastic scintillation detector (from Nuclear Enterprises, Canada) in conjunction with a photomultiplier tube and a conventional preamplifier has been used together with a commercial scaler or counting-rate-meter and recorder. Both units are provided with adjustable discriminator levels which are put at appropriate values. The scintillation detector has been used for the above described conversion electron studies, for adjustments and studies of the spectrometer and for energy calibrations.

Because of the pulsed action of the betatron, the detectors giving pulses from individual electrons are limited to a counting rate equal to the frequency of the betatron (50 counts/min) without special precautions. Should individual pulses be resolved within the duty cycles of the betatron, detectors and amplifiers much faster than what corresponds to the betatron pulse (a few microseconds) have to be used. At the time when the choice of detector system had to be decided (1956–57), very few commercial and not many more research applications of such instrumentation existed. For this and other reasons, the ionization chamber was chosen to be the main detector for the betatron electron studies. A more detailed description will be given in a special paper dealing with studies of

[39]) R. T. Pauli, Ark. f. Fysik **10**, Nr 16 (1955) 175.

the betatron electron spectrum[17]). Moreover, in that paper, a recording system for such spectra will also be given.

6.8. SOME SUGGESTIONS FOR LOW ENERGY ELECTRON DETECTION

The energy region studied was from 4 MeV down to, for resolution studies, 148 keV. The electron energy loss studies will be confined to the higher part of this range. However, considerable fundamental interest is connected with low energy electrons and the author has therefore considered how the present spectrometer could be adapted to such studies later on. It might be of interest to make a few suggestions here.

Provided the earth magnetic field is appropriately shielded, the spectrometer should be suitable for studies of electrons down to low energies. The scintillation detector (anthracene) described permits, without extra precautions, the detection of electrons down to 20 keV energy. If small NaI(Tl) crystals are used and precautions taken to avoid effects due to moisture, the limit will probably be halved.

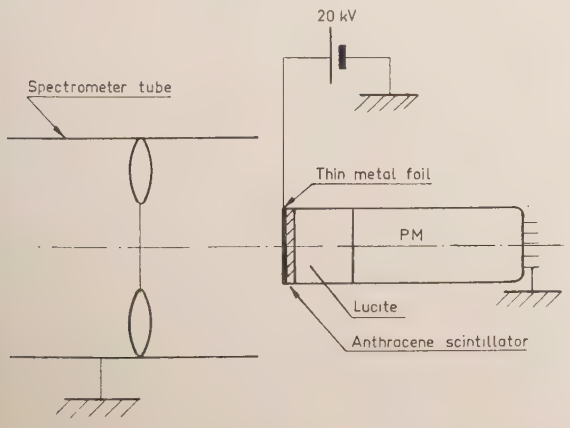

Fig. 17. Suggestion for the detection of electrons of very low energy by after-acceleration. The metal foil should be very thin (0.2 μ Al). The light quide, for example of perspex, takes up the voltage drop due to the auxiliary voltage so that the photocathode can be put at earth potential.

Fig. 17 shows a suggestion for an after-acceleration system permitting the detection of electrons with energies down to very low figures, the limit attainable being probably set by other factors than the one discussed here. After-acceleration has been used before for the case of GM-detectors but some difficulties were encountered[44]). The use of the light guide, which also serves as insulator (as shown in fig. 17), should perhaps eliminate the difficulties.

Some risk of sparking is probably present and some light might be transmitted through the metal foil.

With this after-acceleration set and the use of the electrostatic technique at the source side, the spectrometer might be given a very high resolution, permitting studies of individual energy losses of electrons or the study of Auger electrons from the valence shells.

It should be noted that somewhat similar techniques have been developed for ion detection in mass spectrometers[45]).

7. The Magnetic Spectrometer Applied to Betatron Electron Energy Distribution and Energy Loss Studies

The above-described spectrometer was designed to serve the purpose of energy distribution and energy loss studies on electrons from the betatron mentioned in section 3. It has been shown that the focusing properties agree rather closely with those expected theoretically and are able to give a resolution, $E/\Delta E$, of nearly one thousand. Part of the experimentally found broadening is certainly due to the energy spread in the electron sources themselves as shown above and so the maximum resolution attainable by this spectrometer exceeds the figure mentioned. Of course, it is in practice necessary to operate with certain slit widths to allow for sufficient intensity. But even if such a compromise results in a resolution of $2^0/_{00}$, we have ample means to

[40]) W. Paul and G. Knop (unpublished), referred to in ref.[5]), Fig. 9 of which belongs to this work.

[41]) J. Warner and F. Rohrlich, Phys. Rev. **93** (1954) 406.

[42]) T. Westermark in report to the Swedish Atomic Committee Sept. 30, 1955 (unpublished).

[43]) E. Karlsson and K. Siegbahn, Nucl. Instr. and Meth. **7** (1960) 113.

[44]) H. Slätis, p. 272 in Beta- and Gamma-ray Spectroscopy, ed. K. Siegbahn, publ. place see ref.[5]).

[45]) P. I. Richards and E. E. Hays, Rev. Sci. Instr. **21** (1950) 99; N.R. Daly, ibid. **31** (1960) 264.

investigate the energy distribution of the betatron electrons and the energy loss in thin sheets of matter and thereby make the energy loss small in comparison with the primary energy. This will be illustrated in forthcoming papers. We conclude here by stating that the magnetic spectrometer described possesses excellent properties for the purpose intended and works almost trouble-free.

The description of the calibration of the spectrometer in its adjusted position by means of beta- and gamma radiations will be deferred to a subsequent paper[46]) on methods of energy loss studies. It will be mentioned here, however, that a straight line was obtained over an appreciable $B\rho$-range (1300–1600 gauss cm).

8. Discussion

It should be pointed out that certain improvements and studies of the spectrometer could have been made. The reason why this was not done is that the spectrometer properties are satisfactory for the purpose of studying betatron electrons. We shall, however, mention briefly some of these points for the sake of completeness.

The fringing field of the magnet has been discussed to some extent above. The limiting boundaries are straight and some evidence has been presented that aberration takes place here. It is, however, known that other boundary shapes improve the focusing properties (second order properties). Some theoretical work has been made[47]) but experimental work in this direction is also required if improvements are to be made.

The studies of the exactness of the fit to the conical approximation of Svartholm can certainly be extended. More accurate studies of the radial function of the flux density could give a more exact figure for n and, moreover, β which has not been evaluated here.

Auxiliary electrostatic fields are known to improve the focusing properties as shown by Bergkvist[48]). These ingenious devices could be introduced in the spectrometer described here if desired.

The main design was finished in 1957 and was influenced by the literature known until that time. For various reasons, publication was not possible until now. Some notes on the literature which have appeared since then have, however, been given in connection with this section. Further recent references are no.[52–55]) giving refined design methods.

Acknowledgements

The author is indebted to the Head of the Division, Professor Ole Lamm, for suggesting the problem and for valuable support and good working conditions. He is grateful to Dr. C. Mileikowsky, now at the ASEA Company, Västerås, for many suggestions relating to the spectrometer. Thanks are also due to Dr. J. A. McDonell, Australia, for discussions, especially on detectors, and to Dr. R. Persson, AB Atomenergi, for a discussion on magnet design. Mr. S. Kämpe has contributed very much to the early work and Mr. B. Sjöstrand has had the painstaking duty of operating the equipment and has most valuably assisted with the taking of the experimental data.

[46]) T. Westermark, Measuring techniques for energy loss of 2.8 MeV betatron electrons in matter, Nucl. Instr. and Meth. (to be published); see also T. Westermark: Some measurements of energy loss of 2.8 MeV electrons in light elements and chemical compounds, Nucl. Instr. and Meth. (to be published).

[47]) D. L. Judd and S. A. Bludman, Nucl. **1** (1957) 46.

[48]) K. E. Bergkvist (lecture before the National Committee for Physics Conference, Uppsala 1957).

[49]) O. Blunck and S. Leisegang, Z. f. Physik **128** (1950) 500.

[50]) R. P. Birkhoff, E. E. Hays and S. A. Goudsmit, Phys. Rev. **79** (1950) 199.

[51]) E. Arbman and N. Svartholm, Ark. f. Fysik **10**, Nr 1 (1955) 1.

[52]) G. E. Lee-Whiting and E. A. Taylor, Can. J. Phys. **35** (1957) 1.

[53]) Ewan, Geijer, Graham and Mac Kenzie, Can. J. Phys. **37** (1959) 174.

[54]) H. Daniel, Rev. Sci. Instr. **31** (1960) 249.

[55]) R. L. Burman and A. I. Yavin, Nucl. Instr. and Meth. **7** (1960) 101.

NUCLEAR INSTRUMENTS AND METHODS **10** (1961) 145–163; NORTH-HOLLAND PUBLISHING CO.

ENERGY DISTRIBUTION AND ENERGY STABILITY OF THE ELECTRON BEAM FROM A 5 MeV BETATRON

TORBJÖRN WESTERMARK

Division of Physical Chemistry, The Royal Institute of Technology, Stockholm 70, Sweden

Received 10 September 1960

The adaptation of the Wernholm-Smårs 5 MeV betatron for precise operation is described. Assembly, improvements and normal operation are described as well as a method for recording, by an XY-recorder, the spectrum of the electron line as detected with a magnetic spectrometer and current scanning. The stability of the electron energy was better than $\pm$ 1 keV for 3 hours' operation after introduction of a peaking-strip transformer due to Smårs. The half-width of the electron line was studied as a function of a number of parameters. It is suggested that ejection should be made at large phase angles if the ejection time is finite. The best half-width obtained was 2.6‰ at 2.8 MeV -it was shown to be due partly to the windows used and partly to the spectrometer slits and aberrations. A certain part, about 1 keV, is due to the betatron itself—perhaps caused by the finite ejection time period and betatron oscillations.

1. Introduction

In a previous paper[1]), a magnetic spectrometer has been described which was designed for the purpose of measuring the energy loss properties of electrons from a 5 MeV betatron. This paper will deal with the application of the spectrometer to studies of the betatron electron beam. The emphasis is placed on the stability of the energy of the betatron electrons and on the energy distribution of the beam. The stability and narrow energy width of the electron beam are properties of the utmost importance for successful energy loss measurements. The results will be compared with those of other workers who have studied electron energy losses in this region.

2. Adaptation of the Betatron for Accurate Measurements

2.1. BACKGROUND

A 5 MeV betatron was designed and constructed by O. Wernholm at the Electronics Division of this Institute as early as 1946[17]). It was later improved by E. Smårs and equipped with ejection devices for producing a free external electron beam. Smårs and Wernholm describe the machine in a recent publication[5]). It is a non-biased 50 Hz machine using a pulsed electron injection system and a special ejection system (for operating principles see fig. 5).

The machine was transferred in 1952 to this Division for the purpose of serving as an electron source for extended energy loss studies[1]). Before the accelerator could be used for this purpose, it had to be remounted in its new position in an appropriate manner and all its functions tested and improved to yield a precise operation with respect to energy and intensity in order to serve the intended purpose. Especially, much work had to be done to ensure a narrow energy distribution of the accelerated electrons. During this work we received much advice from Dr. Smårs and Dr. Wernholm. The largest improvement was a new ejection circuit which is described in their paper and the effect of which is described here. Further, we shall summarize pertinent points as to precise and practical operation. In later sections energy stability and energy distribution will be dealt with.

2.2. INSTALLATION

The 5 MeV betatron is a rather small machine with no major radiation hazards. It proved

[1]) T. Westermark, A double-focusing magnetic spectrometer for studies of energy losses in matter of electrons from a 5 MeV betatron, Nucl. Instr. and Meth. (to be published).

possible to install it in an ordinary laboratory of dimensions 4.5 × 6 m. Figs. 1 and 2 give some idea how the installation problems were solved. A new stand for the accelerator is the central part of the various units. Its area is extended so that the load of the betatron itself and the radiation shields are adequately distributed over the floor. The beam is directed opposite from the operator who is sitting at the control table (fig. 3) about 2.5 m from the betatron doughnut tube. The spectrometer unit is placed in the direction of the beam. The electromagnetic radiation produced in the slits etc. is confined to a rather narrow cone and is directed out from the building (the room is on the second floor and so no hazards need be considered). All control cables and signals are connected to the control table where all operation and taking of experimental data take place. Some remote observations of the electron guns and luminescence due to the beam

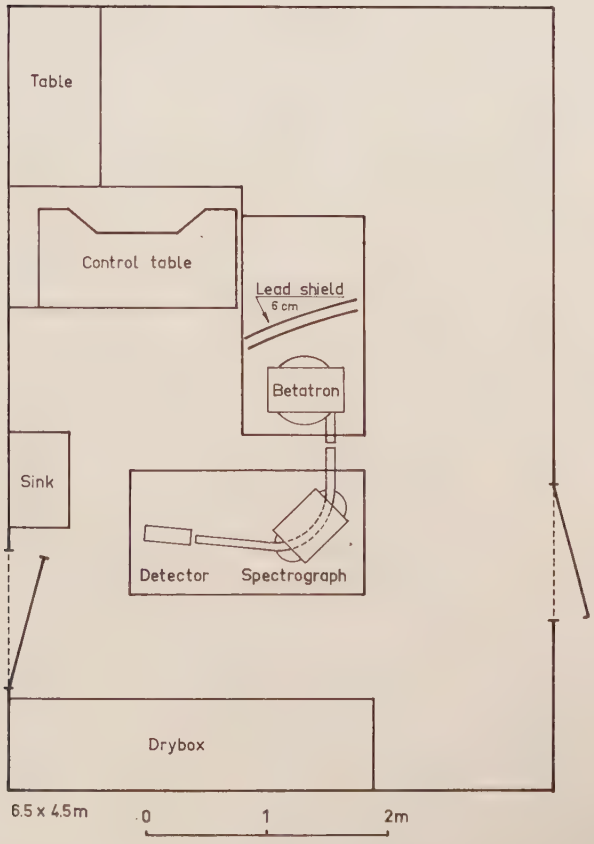

Fig. 1. Plan of installation of betatron with spectrometer for electron energy loss studies.

Fig. 2. View of betatron and spectrometer.

were necessary especially during introductory work. This was mainly done using telescopes and mirrors. Remote mechanical movements were made either by long movable rods or electrical syngone elements.

Some details may be of interest. The betatron magnet and all mechanical pumps are equipped with rubber elements to damp vibrations and reduce the noise level in the room. The betatron stand is made in the form of a table constructed by "Dexion" light-metal profiles. Units which have to be near the betatron are put in the interior of this stand, i.e. below the betatron table. Accordingly the vacuum system (a Metropolitan-Vickers fore-pump and an Edwards oil diffusion pump, Pirani and Penning vacuummeters) is placed here, as well as a new 70 kV pulse transformer for injection, the chassis for the injection and ejection circuitry and the large resonance condenser for the A.C. currents for operating the betatron magnet. The new peaking-strip ejection unit with its direct current stabilizer was also put here. The sides of the stands are closed with plywood sheets to reduce noise.

Details of the connection of the spectrometer table to the betatron stand are described in the previous paper[1]).

The control table (cf. fig. 3) includes all the controls for the machinery, e.g. contacts and

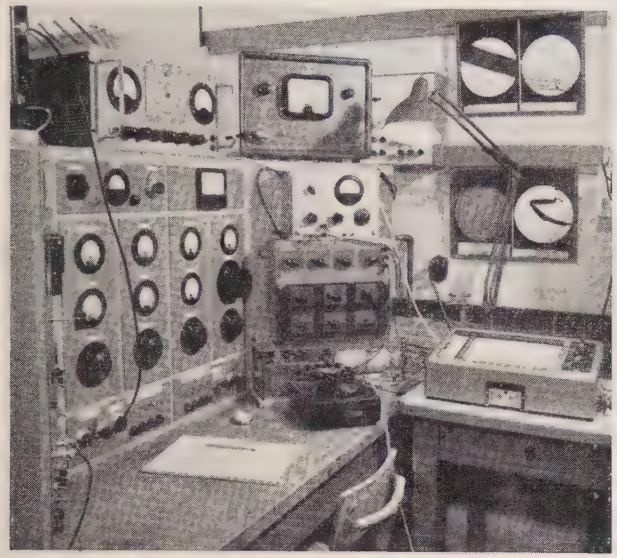

Fig. 3. The control table. At the right current varying devices and the XY-recorder.

controls (mainly by variable transformers, "variacs") for the 50 Hz A.C. current, injection device (phase, glow wire voltage of electron gun, emission control, mechanical position of electron gun), ejection phase (by accurate many-turns ganged precision potentiometer), current pulse amplitude, deflector voltage (by variac on primary side of H.T. transformer) and deflector position. Moreover, the vacuum is readable from special instruments.

The right hand side of the control table includes spectrometer magnet current instrument, regulators and potentiometer with Gorell motor and XY-recorder (see below).

Other instruments such as output recorder, vibration-reed-electrometers (see below) and counting rate-meter are also placed here.

In the following, some further points will be described.

2.3. ELECTRON GUNS

In the beginning, electron guns of the type described by Wernholm[16]) were used. This type has a tungsten wire and molybdenum anodes and can work reliably for a long time. Nevertheless, improvements are possible. Mr. G. Hansson of the Physics Department, Lund University, has constructed a modified type with easily exchangeable wires and with a much longer shaft ($\sim$ 10 cm) which improves the breakdown properties of the unit. Thanks to Mr. Hansson we were fortunate enough to instal such guns. We have not operated the guns with a higher pulse voltage than 45 kV although the intensity increases steadily with voltage. The risk of getting breakdowns, which disturb the records seriously, is rapidly increased at higher voltages.—The region near the electron guns is cooled by tap water flowing through a PVC tube. Electron gun failure has been an important hinderance and much work had to be devoted to it.

2.4. THE DOUGHNUT TUBE

The original Smårs-Wernholm doughnut tube made from Pyrex glass was provided with a small side arm with a 0.2 mm aluminium window for the beam exit.

It was not possible to put the spectrometer entrance end and hence the absorber position and output monitor near the exit arm of the betatron tube. The space between the two betatron coils was too limited and, moreover, a rather strong stray magnetic field is present here. For these reasons a wholly new betatron tube was designed (cf. fig. 4). The exit arm was appreciably lengthened in the new tube and other improvements were also introduced such as better space for the deflector and vacuum pump exit.

The new tube was provided with a thin tin dioxide layer of appropriate resistance[5]) (1000–2000 ohms as measured between two opposite points).

2.5. CHANGES OF COMPONENTS

Several components in the early design had to be changed. Many resistors and condensers were replaced with units rated for much higher powers in order to improve the stability and reduce thermal drift.

2.6. NEW EJECTION CIRCUIT

A new ejection circuit had to be installed to improve the energy stability. It is described in detail by Smårs and Wernholm[5]) and also later on in this paper.

Fig. 4. Photograph of the new doughnut tube with extended exit leg. The electron gun shown is of G. Hansson's design.

2.7. RADIATION HAZARDS

The output of this betatron is rather low. When operated as X-ray generator during an early period, the equivalent Co^{60} source strength never exceeded one curie. Operated as electron generator the beam output is $10^8 - 10^9$ fast electrons/sec. During operation, the room is closed to visitors and the operator is stationed near the control table. The operator wears a film dosimeter and a pocket dosimeter. Normally the film dosimeter record gives less than 50 mrad per month even when the machine is operated almost daily. An extra film dosimeter has been placed in a fixed position ca. 1 meter closer to the betatron tube. It normally shows less than 50 mrad/month.

In a few instances, persons have approached the exit end of the betatron tube to watch fluorescence or to view the orbit itself (luminous at bad vacuum). This occurs when a new tube is installed or at any major changes. In such instances, which have to be kept short, the worker has to wear a shielded hood with thick perspex in front of the face and dose-rate-meter for both gamma and fast electron radiation. Sitting behind a large 25 mm perspex plate when viewing the tube has proved possible. During normal operation, therefore, only minor hazards exist.

When calibrating the spectrometer with gamma emitting nuclides, heavy lead shielding was necessary. Several hundreds of millicuries of nuclides such as Na^{24}, La^{140} and Au^{198} had to be used because of the small solid angle accepted by the spectrometer.

2.8. NORMAL OPERATION

During normal operation, the procedure used is as follows. The vacuum pumps are started in the morning and have to yield at least better than 10^{-5} mm before the betatron can operate. Normal vacuum is 2.4×10^{-6} mm and is produced in 2–3 h. The spectrometer current is most often put on in the morning at the value to be used during the experiments. This appreciably reduces the current drift due to warming-up of the spectrometer coils. Current source is a 8 volt, 320 Ah-lead storage battery (from Jungner AB). All glow-currents for the tubes etc. are put on in the morning.

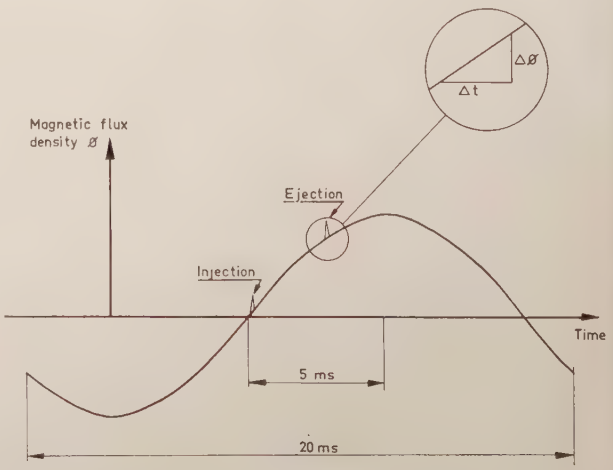

Fig. 5. Schematic picture of injection and ejection time of the betatron. The "magnified "sketch is intended to illustrate the derivation of formulas (1)–(5) (see text).

Actual operation can start at noon. The operator first starts the main 50 Hz A.C. voltage for the betatron coils. Starting from zero, the voltage is increased by means of a variac up to the amplitude wanted. An appropriate deflection voltage and ejection pulse voltage are actuated and the energy control of the biased peaking-strip transformer is set at the figure wanted. The injection is started by actuating the glow current of the electron gun and applying the pulsed high voltage up to a safe but sufficient value. The correct injection phase position is then found (by experience or using an X-ray detector outside the orbit). The peak amplitude of the ejection coils is then varied until a beam is obtained outside the betatron. This is detected with an ionization chamber placed just outside the betatron exit window and a Speedomax recorder (the unit is described in the next section).

Under normal operation, the operator knows, after making a few trials, the right parameters to reach at this point. He then starts to optimize the intensity by fine adjustment of (above all) injection phase angle and also ejection peak current by keeping the AC peak amplitude, injection voltage, deflection voltage, energy control and mechanical position of electron gun and deflector constant. After some time, 5–30 min, a stable and sufficiently high output is obtained. The constancy of the output is judged from the recorder. Experiments such as primary beam studies or energy loss studies can then be begun by connecting up the corresponding equipment such as devices for varying spectrometer current, spectrometer output recorders etc. Thus no further warm-up period is necessary to reach energy and intensity stability (cf. below).

The operation of the machine is, as seen, rather complicated and requires much skill, experience and patience. Further requirements for a good energy loss experiment which it is worthwhile to evaluate will be given in a subsequent paper[4]).

[4]) T. Westermark, Measuring techniques for energy loss studies of 2.8 MeV betatron electrons in matter, Nucl. Instr. and Meth. (to be published).

3. Method of Recording the Betatron Electron Energy Spectrum

3.1. ALIGNMENT OF THE BETATRON ELECTRON BEAM

The spectrometer previously described[1]) was shown to possess a resolution corresponding to a spread of about 0.1–0.2% (momentum scale) depending largely on the slit widths used. It had, for the studies to be described below, to be aligned to the betatron electron beam so that this beam passed straight through the entrance slit of the spectrometer. This difficult work was facilitated by the use of X-ray films to trace the beam in space and within the spectrometer tube. The spectrometer stand is movable on four wheels. After course adjustments, this stand was fastened to the betatron stand which is not movable. This was performed using some special screws. The final adjustments relative to the betatron stand were made by small but precise movements of some strong adjustment screws supporting the heavy stand for the spectrometer magnet (hereby only the spectrometer is moved and not its stand) until the maximum intensity from the betatron electrons was obtained through the spectrometer. At this point, the half-width of the betatron electron distribution (to be discussed below) had a minimum. The screws were fixed and never thereafter moved. The construction is strong enough to eliminate any vibration and movements of the spectrometer relative to the betatron. This was confirmed by the fact that the properties of the beam, e.g. half-width and intensity of the transmitted beam relative to the intensity of the beam measured just outside the exit window of the betatron, were reasonably constant. With the various positions found, the whole unit has operated satisfactorily for nearly two years.

3.2. INTENSITY RECORDING OF THE BETATRON BEAM OUTPUT

A 10 mm thin air ionization chamber is placed close to the exit leg of the betatron. The details are explained in fig. 6. The central electrode of the chamber is a wire loop circumscribing the electron beam. It was found that a saturation

collection was obtained at 300 volts. The output of the ionization chamber was fed through a cable of good insulating properties to a high-ohm resistor (of the well known glass-sealed Victoreen type) of 10^9 ohm ($\pm$ 20%) and then to

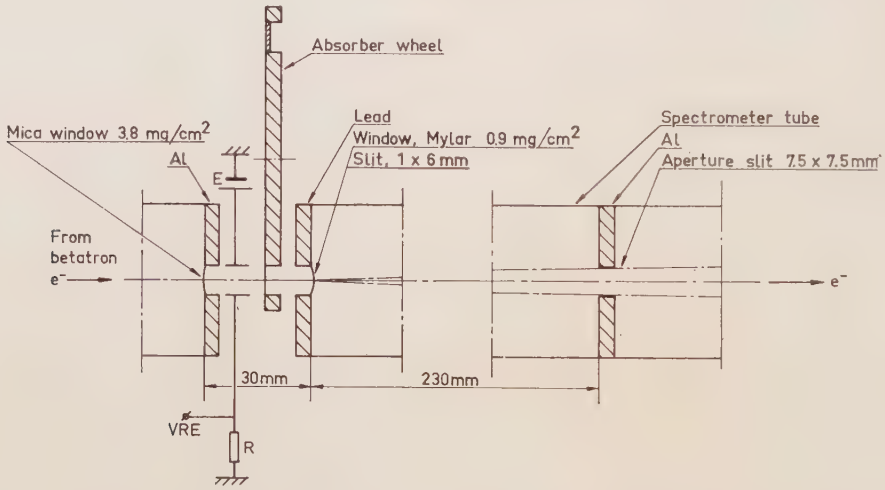

Fig. 6. Sketch of ionization chamber output detector and absorber position just outside betatron exit leg window. Some idea of electron beam limitations for spectrometric studies is also given. The sketch is seen in a horizontal direction and so the entrance slit is seen from the side.

earth. A vibrating-reed electrometer[2]), model 33B from the Electronic Instruments Ltd., Richmond, Surrey, England, was coupled across the resistor and thus measured the output current (cf. fig. 6). The input impedance of the instrument is 10^{13} ohm according to the manufacturer. The following ranges are provided: 10, 30, 100, 300 and 1000 mV. The accuracy varies between $\pm$ 2% on the 10 mV range to $\pm$ 0.3% on the 1000 mV range. The output of the electrometer is fed to a continuously recording Speedomax recorder from Leeds & Northrup Company, USA. This instrument has a 10 mV full deflection in the most sensitive region. By means of precision resistors, the sensitivity could be lowered by the factors 2, 5, 10 and 20. It is thus seen that several combinations of intensity measurements are possible. The 300 mV range of the electrometer is the one normally used. The *RC* time constant is less than the basic time constant of the instrument which is stated to be about 0.25 sec by the manufacturer.

These instruments serve together to record continuously the output of the betatron. This intensity which is of the order of 10^8–10^9 fast electrons/sec (actual ionization current obtained in routine work during 1958–60 was 3–5 $\times$ 10^{-10} amps) seldom enters any measurements or evaluations. It is, however, of fundamental importance in connection with accurate measurements because it shows whether the relative output is constant enough to justify the further treatment of other recordings for measurement purposes to be described below. It is of course sensitive to various types of failures of the betatron. The X-ray contribution in the dose rate recorded in this manner is very low.

3.3. THE DETECTOR OF THE SPECTROMETER OUTPUT

Two identical ionization chambers filled with sulfur hexafluoride serve as detectors for the output of the spectrometer for betatron electron studies. Constructional details are given in fig. 7.

The two outputs are connected in front of the high-ohm resistor (normally 5.1 $\times$ 10^{10} ohm, Victoreen type) and thus the voltage across the latter indicates the difference in current. Thus

[2]) Electronic Instr. Ltd., Richmond, Surrey, England: Operating instructions and service manual of Model 33 B and C Vibrating-reed electrometer.

the X-ray contribution, which was actually small, is automatically substracted.

The voltage across the 5.1 $\times$ 10^{10} ohm resistor is fed to a 33C Vibrating-reed electrometer from the Electronic Instrument Company. This instrument has an input impedance[2]) of 10^{16} ohm, i.e. a thousand times higher than that of the instrument described earlier from the same company. This was necessary because of the much lower currents to be detected at the exit end of the spectrometer.

The time constant here is set by the *RC*-figure which is about 1.5 sec. The vibrator unit of the instrument is separate from the main one. Accordingly, the vibrator is put directly in the vicinity of the twin chambers (cf. fig. 9 of[1])), (the connection between the two chamber outputs being made within $\frac{1}{2}''$ copper tubes serving as electrostatic shielding). The output from the vibrator is fed to the main instrument 3 m away at the control table of the machine. The instrument has the following ranges: 10, 30, 100, 300 and 1000 mV. The accuracy stated is $\pm$ 1% on the higher ranges and $\pm$ 2% on the lower. We have most often used the lower ranges. A lead shield was put between the ionization chambers and the betatron tube to reduce the X-ray flux resulting from electrons colliding with the wall or constructional details within the doughnut tube and from electrons stopped by the slits defining the beam fed to the spectrometer. The lead shield also covered the vibrator unit and the connection to the twin chamber setup.

The voltage coefficient of resistors of the type used is very small[19]) and here 1 V at most is applied to them and any errors of this kind can be neglected. The temperature coefficient is also small.

Some use has been made of scintillation detectors[1]) and simple GM-tubes and a counting-ratemeter. In these cases the intensity had to be limited to a figure much less than the repetition rate of the betatron pulses. The use of the *XY*-recorder was found feasible also in these cases, although statistical fluctuations were not small.

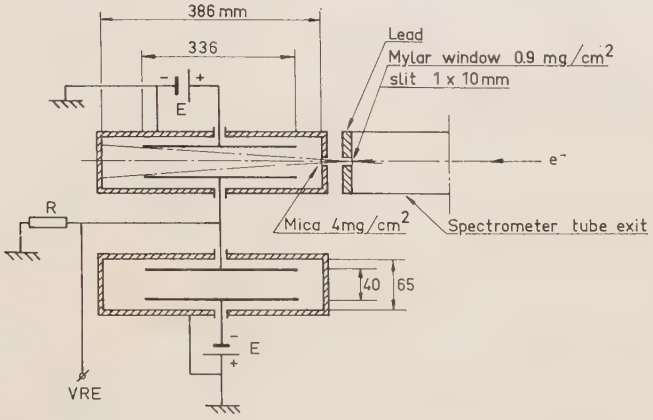

Fig. 7. Ionization chamber detector at exit end of spectrometer.

3.4. CURRENT VARYING DEVICE

The current through the magnet coils of the spectrometer can be varied within a certain range by means of a sliding potentiometer (Mr. B. Sjöstrand made important contributions to this part of the work). Fig. 8 shows the current circuit. The potentiometer was wound using manganin wires on a plastic framework consisting of a movable cylindrical unit 70 mm in diameter and 150 mm long. In this matter we had considerable use of the automizing of a scintillation gamma spectrometer in this laboratory according to work by Mr. K. Ljunggren.) Altogether there are 15 turns in the wire. The unit was then placed in a dust-proof perspex box. This unit is rotated by a variable-speed Gorell motor (type Mg-1000 Timer, Gorell & Gorell,

Haworth N.J., USA). At the end points of the potentiometer, electro-mechanical relays make contact and reverse the motor and thus the contact moves back and forth varying the magnet current over a certain range. The range is determined by the resistor combination chosen (cf. fig. 8).

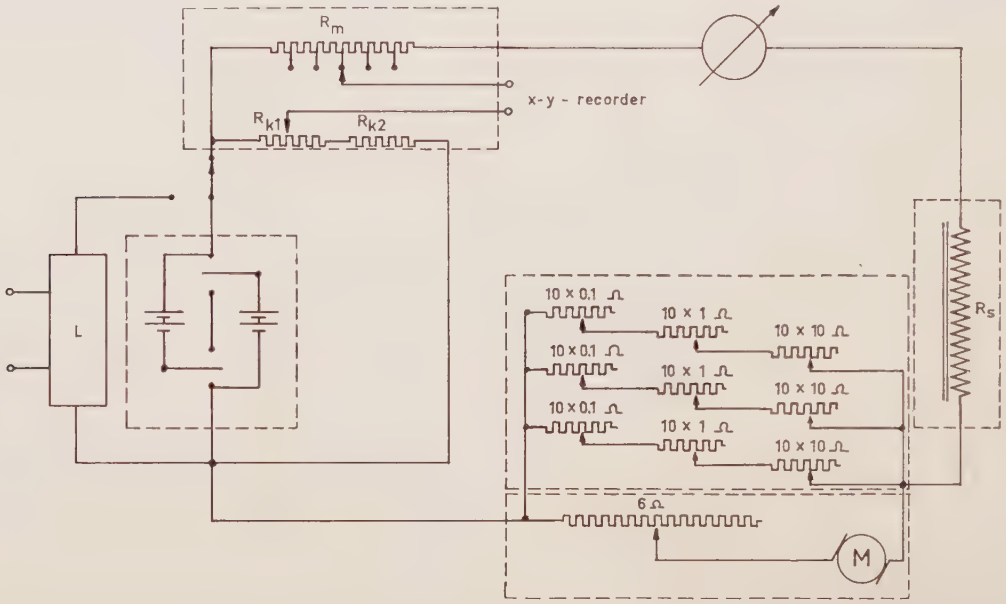

Fig. 8. Feed current system for spectrometer coils including current varying device. Voltage source (left in fig.) is 4 or 8 volt 320 Ah lead storage cells.

The actual velocity of the current scanning is dependent on the position of the contact. It may vary up to a factor of five because of the potentiometric coupling.

3.5. THE *XY*-RECORDER

An *XY*-recorder is used as the main instrument for recording the spectra. The *X*-axis is fed from a manganin resistor as is shown in fig. 8. A simple compensating circuit is used to adjust the zero point.

The recorder is a "Moseley Autograf" instrument from F. L. Mosely Company, Pasadena, California. The ranges are 5, 10, 50, 100, 500 mV and 1, 5, 50, 100 and 500 V on each axis. The zero point can be moved by special potentiometers. The stated accuracy is 0.25% of full scale but after accurate calibrations it may be 0.1%, and the response is described by a stated maximum of 0.5 sec for full scale-travel on each axis[3]).

The *Y*-axis is fed from the output of the vibrating-reed electrometer connected to the twin ionization chambers of the spectrometer output (cf. above).

When the potentiometer contact moves as described above, the intensity distribution is recorded on the *XY*-graph. This is obviously a much more practical way than to record intensity and some property related to the magnetic flux density as a function of time. The subsequent evaluation work would be very large in the latter case.

3.6. RECORDING OF THE PRIMARY LINE

The peaked curve obtained when reading the intensity as a function of magnet current might be termed the primary line. It reflects to a certain approximation the energy distribution of the betatron electrons which may have passed through some thin windows.

Fig. 9 shows an example of a record of this line. We shall often make use of the width at the half-height of the line. In the figure, such a value is presented. It is evaluated in terms of the current and is related to the current at the peak

from our knowledge of the current figure at both end positions of the record. The motor is stopped at these positions and a small pulse is given to the Y-axis so that a vertical mark is got on the record paper. The actual figure for the D.C. current flowing through the coils is read by means of a series-connected 0.2% Siemens moving coil instrument and appropriate shunts. The instrument is provided with a reading mirror and was further provided with a magnifying eye-piece and illumination so that a reading could be made at a relative accuracy better than the stated absolute one. The relative half-width is then evaluated by linear calculation.

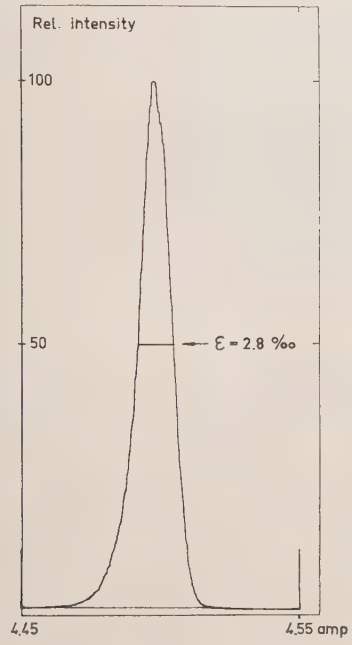

Fig. 9. Example of primary line of unobstructed betatron electron beam at 2.8 MeV as recorded by the magnetic spectrometer and XY-recorder.
(Ordinate intensity in relative scale.)

It is important to ensure that the speed of recording is low enough so that no distortion of the spectra takes place. It was found that both the half-width and the peak intensity can serve as an index for this question. As is shown in fig. 10, these properties change rather fast if a certain recording speed is exceeded. Care has always been taken to choose a speed which is sufficiently slow. In this connection the variable speed due to the design of the current varying device (see above) had of course to be considered. For each new high-ohm resistor figure, we have always taken curves of the type shown in fig. 10 to ensure good recording.

All records are obtained on flat paper of dimensions 21 × 28 cm (size A4). This is a practical feature of this type of recorder since all tracing can be judged at any time and the filing of records is easy.

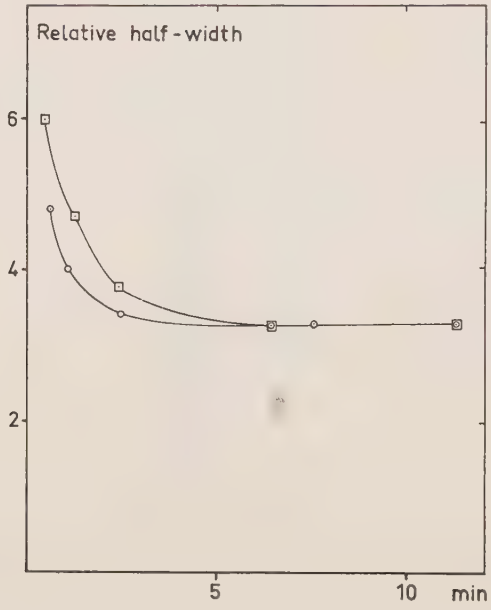

Fig. 10. Effects of scanning speed on half-width and peak height of primary line for two different high-ohm resistor figures. Normal scanning speed is chosen to be well on flat position of the curve.

3.7. PHOTOGRAPHIC METHOD OF RECORDING

Sometimes, a photographic recording of the spectrometer output was practical. To this end, a cylindrical drum of 30 cm diameter was provided with an X-ray film (usually Ilford C X-ray film) in its black paper envelope. The drum was put just outside the spectrometer exit with the slit removed. The fast electrons penetrating the thin window at the end of the spectrometer arm will affect the X-ray film. The drum is rotated by an electric motor so that the film moves about 2–3 cm/min. Thus a picture is got showing not only the beam width at the detector plane but

also its change with time, i.e. the energy stability of the accelerated beam (figs. 11 and 13 below are examples of results obtained using this technique).

4. Stability of the Electron Energy

4.1. GENERAL REQUIREMENTS

For any quantitative measurement using betatron electrons (or X-rays), the requirement for good energy stability is obviously a severe condition. This is at the same time a stringent test of the betatron from the point of view of precision with respect to other accelerators. This question has therefore been studied in some detail using 2.8 MeV electron energy.

It is believed that the injection of the electrons into the orbit of the betatron takes place during a very short time[5]), perhaps a fraction of a microsecond in the present machine. As the injection phase is automatically related to the magnetic flux density in the orbit, corrections for changes in various properties related to the injection are made automatically. This would mean that, at a certain moment after injection, all electrons have to a good approximation the same momentum at the same time. If this discussion is correct, the ejection mechanism is suspected to be responsible for the electron energy and stability as well as spectral distribution.

In the following, investigations of two different devices for ejection will be reported.

4.2. EJECTION DEVICE USING AN INTEGRATOR CIRCUIT

The details of the design have been given in the paper by Smårs and Wernholm[5]). This device has often been used (see ref.[6]) for instance). It might be sufficient to state here that the device consists of a resistor and a capacitor in series with the magnetizing coils. The voltage across the capacitor gives a short pulse when it exceeds a certain value corresponding to a certain integrated flux density which can be changed by biasing the device. Hence the orbit is expanded at a certain momentum which can be exactly predetermined.

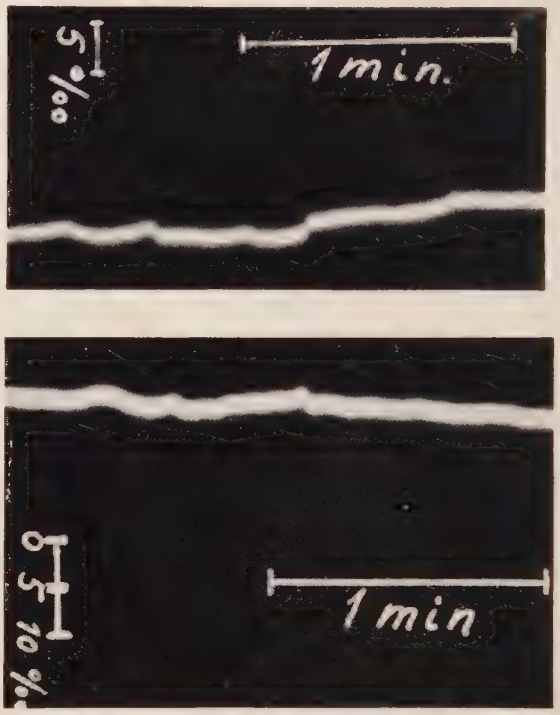

Fig. 11. Energy instability of betatron electrons at 2.8 MeV as demonstrated by exposure of a movable film outside exit slit. Sudden alterations and a slow drift are seen to be present for this ejection device. The base width is apparently only 2‰; a good figure certainly due to the absence of any matter in the path of the electron. It is seen that the base-width is not changed during these changes (Entrance slit 6 mm high).

The electron energy stability using this circuit was studied by means of the photographic recording method (see above). During these studies, the two vacuum systems were connected and accordingly no solid matter at all was present in the path of the betatron electrons in front of the exit window.

Fig. 11 shows that the energy stability is not good at all in this circuit. There are, in addition to a severe drift (usually upwards) of the energy, sudden alterations in energy. It is seen that the width is constant during these changes and so

[3]) The Moseley Autograf, Instruction and operating manual for Model 3 *XY*-recorder, F. L. Moseley Co., Pasadena, Calif., USA.

[5]) E. Smårs and O. Wernholm, A 5 MeV betatron, Nucl. Instr. and Meth. (to be published).

[6]) L. Katz, A. G. McNamara, P. A. Forsyth, R. N. H. Haslam and H. E. Johns, Can. J. Phys. A **28** (1950) 113.

one is forced to assume that some drift and some irregular phenomena were present in the ejection circuit used. This circuit was then abandoned. No efforts were made to discover the real source of the instability.

4.3. THE PEAKING STRIP EJECTION CIRCUIT

Because of the bad behaviour of the older ejection circuit, it was decided to instal another one. Dr. E. Smårs, who had extensive experience from work on a 1200 MeV electron synchrotron at this Institute, designed a peaking-strip circuit which, in principle, had no property that could change with time and is in fact similar to the injection device. The magnetic flux of the peaking-strip transformer is backed with a stable direct current which is variable. The saturation point and hence the magnetic flux density for ejection are accordingly controlled by the setting of this current. The latter has to be stable (better than 0.2%). A stabilizer designed by Smårs was constructed here as well as the peaking-strip transformer. For further details, see ref.[5]) (section 6).

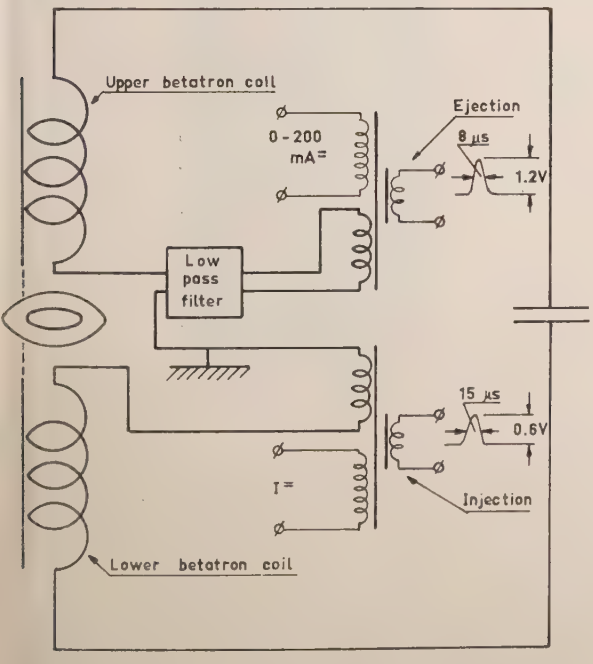

Fig. 12. Scheme of the Smårs' peaking-strip method for ejection control. The figure shows how the low-pass filter had to be introduced to prevent injection pulses from actuating the ejection system.

The whole unit was then installed in the betatron. It was noted that the injection pulses disturbed the new amplifier so that the ejection circuit fired at once. It was found, however, that

Fig. 13. Photographic study of energy stability with the same technique as shown in fig. 11 and text. In this case a new peaking-strip transformer circuit (due to Smårs) was installed and is shown to yield a very good stability ($< 1‰$ in 5 min). Base-width in this case was larger than for fig. 11, but the phase angles were not comparable and, moreover, windows were introduced. (The scale is the same.)

a low-pass filter (Radio interference filter Type 146 from Hopkins Engineering Company, San Fernando, Calif. USA) in series with the output from the transformer removed the disturbing pulses to a considerable extent (cf. fig. 12). By finding a suitable position in relation to the betatron, virtually no disturbance at all was detected. These improved units have been operated without any failure for three years.

The energy stability of the betatron electrons was again studied by means of the photographic method. The result, see fig. 13, showed no change with time at all. This statement means that the stability was better than at least 0.1% over several minutes. No sudden changes were detected at all.

Records of the primary line by the XY-recorder and the above-described techniques

permitted more extensive studies. Fig. 14 shows the results of runs covering about 2 h. The current corresponding to the peak was evaluated from a series of fifteen such records and plotted as a function of time. It is seen that the primary

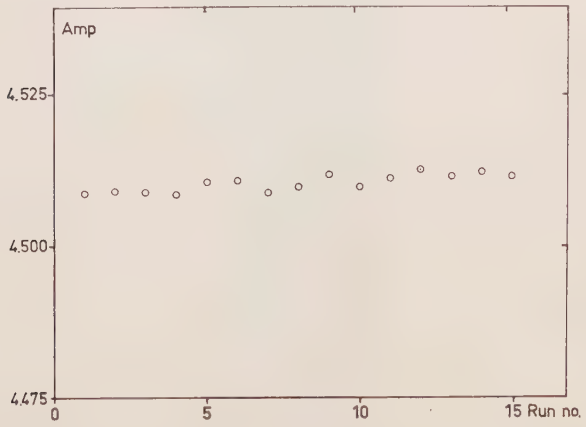

Fig. 14. Peak position of electron energy during several hours' operation. The stability found is seen to be within $\pm 0.3^0/_{00}$ for this period. These stability data include drift of recording circuits and hysteresis effects.

line is recorded at the same X-position on the recorder within $0.3^0/_{00}$. Unless a counteracting drift of the compensating current is assumed, this at the same time tells us that the drift of the whole assembly is negligible and that hysteresis does not affect the position. All records have been taken with an *increase* of the magnet current and with the same scanning range.

5. Energy Distribution

5.1. GENERAL

The above described method for recording the primary line and evaluating the half-width has been used for extensive empirical studies of the influence of various parameters. As will be described below, the half-width partially reflects the energy distribution of the betatron electrons but is partly due to slit widths, spectrometer aberrations and straggling in the foils. The procedure has been simply to vary one parameter at a time and then to inspect purely empirically how it affects the half-width and, in most cases, the intensity. In this manner, some knowledge, although not exhaustive, is gained concerning the energy distribution and secondary influences on it. Except for section 5.7 all studies were made at 2.8 MeV.

5.2. DEPENDENCE ON PHASE ANGLE

Two studies of the dependence of half-width on the phase angle of the ejections were made. The principles can be explained in relation to fig. 5. We shall repeat here the plausible assumption made above that, to a first approximation, the injection process has no appreciable influence on the energy or energy distribution of the accelerated electrons. The ejection might however have some influence and therefore its position in relation to the maximum of the sine curve was varied. The ejection position and hence the energy is uniquely determined by the parameters in the ejection circuits described

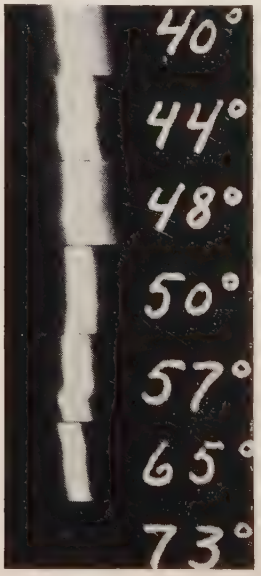

Fig. 15. Photographic study of base width of electron momentum distribution for betatron electrons at 2.8 MeV as a function of phase angle of ejection (other parameters kept constant). The decrease of base width with increasing phase angle is obvious (cf. text). Film pieces are cut from more extensive exposures.

above and by Smårs and Wernholm[5]). One can, however, vary the amplitude of the betatron magnet current and hence the phase angle (i.e. at constant energy setting). For practical reasons, it is difficult to achieve an angle very close to 90°.

One experiment using the photographic method was made when the two vacuum systems were connected and hence no solid matter was present at all in the path of the electrons. The

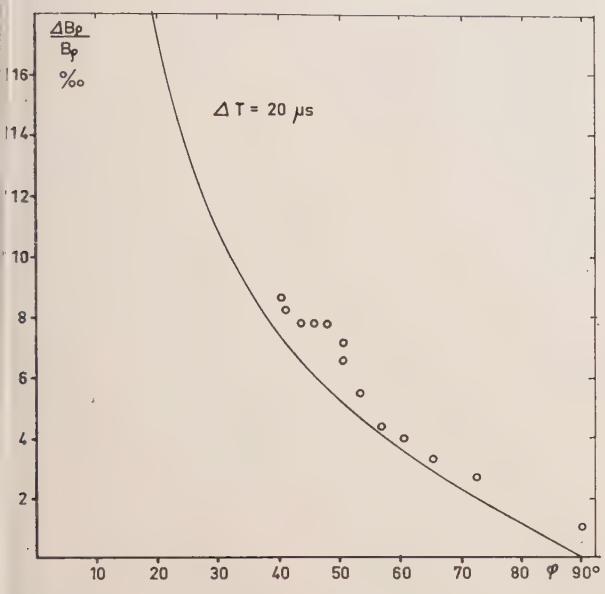

Fig. 16. Base-width of electron momentum distribution as a function of phase angles as found for the experiment shown in fig. 15. The solid curve corresponds to formula (5) with $\Delta t = 20$ μsec. The circle at 90° corresponds to slits used.

amplitude of the betatron A.C. magnet current was varied and the corresponding phase angles were determined by the positions of the injection and ejection pulses on an oscilloscope (Tektronix Type 514D). Fig. 15 shows the results. A decrease in the width is clear from a visual inspection. Rough measurements of the base width yielded the results presented in fig. 16. The decrease is very clear. The weak points in this experiment are that no accurate density-exposure studies were made and that an intensity decrease takes place when moving towards large phase angles. Thus misinterpretations might be possible although the general trend is quite obvious.

A more certain method is to record the primary line electrically with the above described method. This has been done at an instant when the two vacuum systems were disconnected, i.e. two windows and a certain distance of air had to be traversed by the electrons. Moreover, it was made with the peaking-strip ejection circuit and with the final alignment. The dependence on phase angle can thus not be expected to be comparable with the former case described. Moreover, this study was made with the new ejection circuit whereas figs. 15 and 16 refer to the old one. Fig. 17 shows the result. The trend is obvious but, as expected, not as pronounced as before.

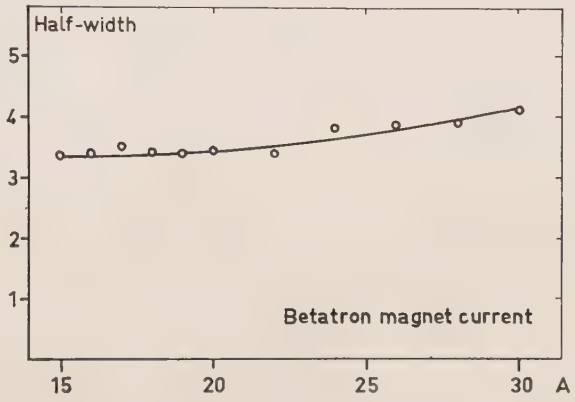

Fig. 17. Half-width at 2.8 MeV found by varying betatron magnet current amplitude (i.e. phase angle) energy setting and other variables kept constant.

5.3. DEPENDENCE ON PHASE-ANGLE (THEORETICAL)

In the present accelerator, there is a certain time distribution for the ejected betatron beam. The high-current pulse from the thyratron-condenser circuit (described by Smårs and Wernholm[5])) has a rise-time of slightly less than 1 μsec but it is found that this does not affect the beam instantaneously. This was demonstrated by the Tektronix oscilloscope which was triggered by the ejection pulse and recorded the pulse from a scintillator-photomultiplier. A photograph covering a certain time reflects the arrival spectrum of the electrons. It was found that the longest time was about 15 μsec whereas the most probable delay was roughly 6 μsec.

This time distribution means that some electrons are ejected at the nominal energy corresponding to the settings but others are delayed and are thus further accelerated gaining a higher energy. In momentum, this may be expressed in the following manner:

The accelerating A.C. flux density is:

$$\Phi = \hat{\Phi} \sin \omega t \tag{1}$$

($\hat{\Phi}$ is the peak amplitude).

At a certain flux density, the ejection circuit is fired and electrons are ejected at a certain momentum

$$B\rho = k\Phi \,. \tag{2}$$

The energy distribution can be represented by

$$\varepsilon = \frac{\Delta\Phi}{\Phi} = \frac{\Delta B\rho}{B\rho} \,. \tag{3}$$

Electrons spending an extra time in the orbit are further accelerated (cf. fig. 5). The extra momentum is got by differentiating (1):

$$\Delta\Phi = \hat{\Phi}\, \omega \cos \omega t \cdot \Delta t \,. \tag{4}$$

Hence

$$\frac{\Delta\Phi}{\Phi} = \frac{\Delta B\rho}{B\rho} = \frac{\hat{\Phi}\, \omega \cos \omega t}{\Phi \sin \omega t} \cdot \Delta t \,. \tag{5}$$

Or

$$\frac{\Delta B\rho}{B\rho} = \frac{2\pi \cdot \Delta t}{T} \cot \varphi \tag{5a}$$

where T is the period and φ is the phase angle of ejection.

In (5a), Δt is referred to the whole width of the time distribution and thus $\Delta B\rho / B\rho$ has the character of a base width. In this sense, it can be connected to the error discussion of the spectrometer (cf. ref.[1])). Of course, other measures of the time distribution might be used, viz. a most probable time and by (5a) a corresponding momentum distribution property can be found.

This formula obviously predicts a very pronounced dependence of the half-width on the phase angle. The solid curve in fig. 16 represents the cot-function when Δt is put at 20 μsec. (T is 20 000 μsec in the betatron used). The good agreement may be somewhat fortuitous with regard to the experimental method employed (see above). Qualitatively the same effect is demonstrated in the more accurate study shown in fig. 17. The dependence on phase angle here is consistent with a Δt of about 3 μsec. No actual measurement has been made of this property. The magnetic field including the fringing field at the ejection moment is supposed to act in a momentum-selecting manner and hence the entrance slit might select a beam of electrons with a narrower time distribution than that of the whole beam.

The actual deduction of (5a) does not seem to have been given before, but the general relationship is no doubt known by other workers. This is clear indirectly from some authors on betatrons. For instance, Keegan[8]) speaks about the ejection "to straddle the peak field of the betatron — the energy spread is reduced to a minimum". Another approach is to strive to minimize the time distribution of the electrons ejected by more modern methods (e.g. ref.[9])). This would decrease the energy distribution.

In a private communication, Dr. D. W. Kerst confirmed that no explicit studies of the energy distribution have been made to his knowledge[20]). He pointed out, however, that ejection at 90° would narrow the energy distribution and that it would be technically feasible to reduce the time to less than 1 μsec. He mentioned that he had made an estimate of the influence of the energy spread of the orbit oscillations. Their contribution would be very small (0.2 $^0/_{00}$ in a case considered). Dr. Kerst also expressed the view that except for the oscillations the electrons at a certain moment have "one and only one momentum". This is in accordance with the view expressed by Smårs and Wernholm[5]) that the injection does not appreciably influence the properties discussed.

We might conclude here that the ejection should be made as late as possible (i.e. large phase angle) to narrow the energy distribution if there is a finite time of ejection. As the intensity decreases when this is carried out, a compromise must always be made. We have often selected 60° as a practical case. (An ejection at 90° as suggested to the author by Dr. Kerst would of course require the peak amplitude to be very well stabilized.)

[7]) E. R. Saunders, A biased peaker strip energy control system for betatrons and synchrotrons, Nat. Bur. Stand. Report 3263.

[8]) T. J. Keegan, Rev. Sci. Instr. **24** (1953) 472.

[9]) C. L. Hammer and A. J. Bureau, Rev. Sci. Instr. **26** (1955) 594–598, K. N. Geller and E. G. Muirhead, Rev. Sci. Instr. **31** (1960) 308.

5.4. DEPENDENCE OF HALF WIDTH ON DEFLECTOR VOLTAGE

The deflector plate (cf. ref.[5])) voltage has an important influence on the operation of the betatron. The deflector steers the electrons moved into the gap between the plates so that an orbit outside the normal betatron orbit is followed. In the ejection instant, the electrons are subjected to a magnetic flux density corresponding to the radial position of the deflector and further to the electrical field strength between the plates. Such a unit is a rough beta spectrometer in itself. Fig. 18 shows that the betatron intensity has a pronounced maximum at a certain deflector voltage. This is in accordance with the above statements and with the view expressed by Ziegler[10]). The half-width is seen to have minimum very near the intensity maximum.

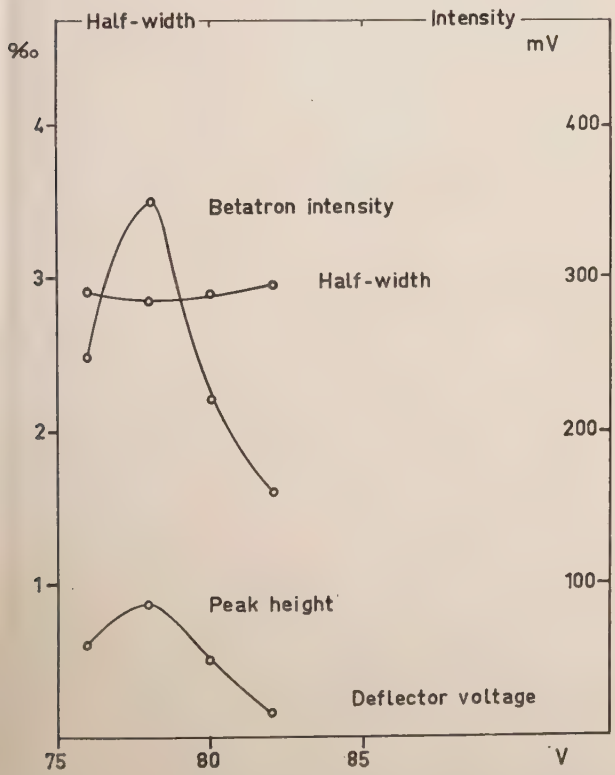

Fig. 18. Half-width and peak intensity as well as output intensity as a function of deflector voltage. The latter is measured on primary side of a 150:1 transformer. To transfer intensity scale to current, the resistor figures 2.5×10^{10} ohm (lower curve, i.e. spectrometer output) and 10^9 ohm ("betatron intensity") have to be used. The behaviour is qualitatively explained by the beta spectrometric action of the deflector and magnetic field.

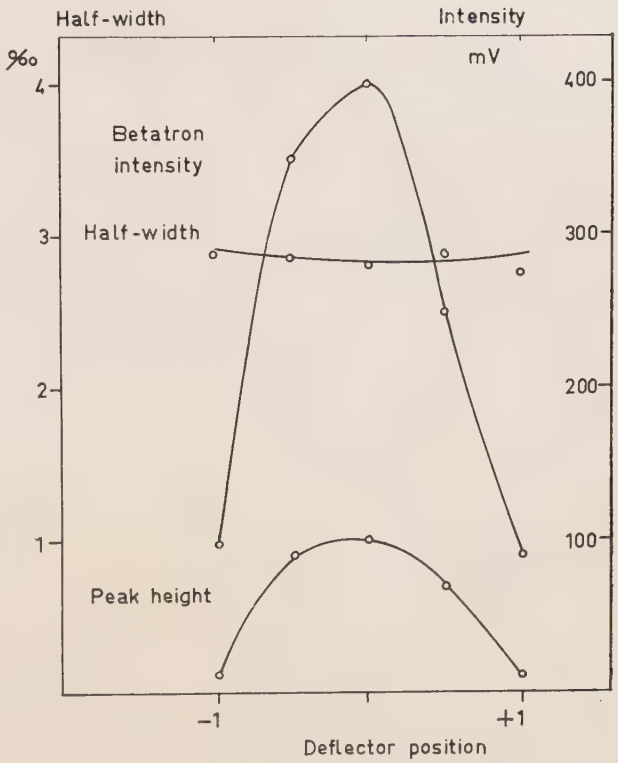

Fig. 19. Influence of deflector position on half-width and intensity of primary line. Scale unit of deflector position means one turn on the axis moving deflector radially.

No further analysis of the deflector mechanism was made. It seems enough for our present purposes to note that the point of maximum intensity for the machine, which is sought as a matter of routine by the operator, yields at the same time the best half-width.

Special studies were also made on the influence of the deflector position. This position is related to the angular movements and serves to admit as much of the orbital electrons as possible. Again as is seen in fig. 19, the result is that the minimum half-width is close to the point of maximum intensity. Thus the operator correctly finds also this point empirically. It may be noted that the deflector position is quite critical. The strong dependence of the intensity and the increase of the half-width might be due to collisions with the metallic material of the deflector plates (glancing collisions and multiple scattering).

[10]) B. Ziegler, Z.f.Phys. **151** (1958) 556.

Fig. 20. Half-width of primary line as a function of ejection voltage. The latter is a relative measure of peak pulse current of ejection loops.

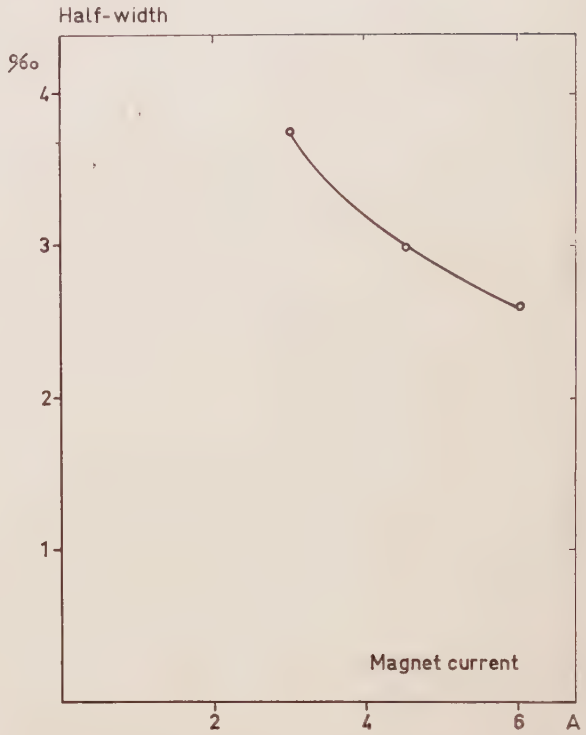

Fig. 21. Half-width of primary line as a function of spectrometer current, 6 amp corresponds to 3.85 MeV, the momentum scale being almost linear with current. The trend is compared with calculated figures (see table 1).

5.5. DEPENDENCE ON EJECTION VOLTAGE

Fig. 20 shows the dependence on the ejection voltage i.e. a property related to the peak current amplitude of the ejection loops. This amplitude determines the lateral movement of the whole orbit. The curve is somewhat irregular but exhibits a minimum (between 140 and 160 V in the figure). The operation is normally made at this minimum position which corresponds to maximum intensity.

5.6. HALF-WIDTH AS A FUNCTION OF ENERGY

The half-width was found to decrease with energy as is seen in fig. 21 where constant phase angle and constant conditions were used. The result will be discussed below.

5.7. HALF-WIDTH AS A FUNCTION OF WINDOW THICKNESS

Fig. 22 shows that the half-width increases with increasing thickness of the aluminium foil interposed in the "source" position between the

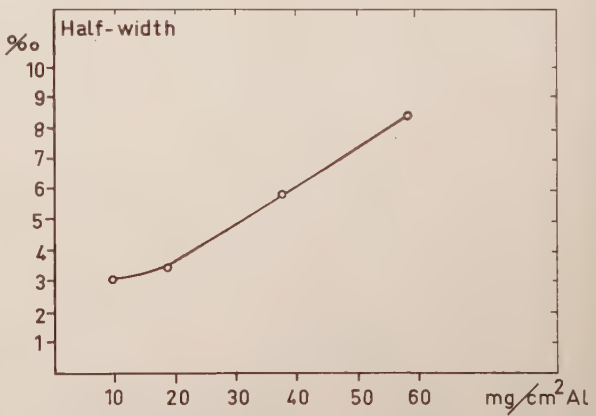

Fig. 22. Half-width as a function of matter thickness in the path of the electron beam.

betatron exit and spectrometer entrance. The result indicates that, as expected, foils and windows contribute to the straggling of the beam. On the other hand, the figure shows that the gain below 10–12 mg/cm² is very small.

The latter point was confirmed by filling the

space between the betatron exit window and the spectrometer entrance window (about 30 mm) with helium instead of air (both at atmospheric pressure). The half-widths found were 3.6‰ (air) and 3.3‰ (helium) or a gain of only 0.3‰. It did not seem worthwhile to use helium because of the extra labour and cost involved and so air was used in all subsequent runs.

5.8. DEPENDENCE OF THE HALF-WIDTH ON SLIT WIDTH

The dependence on slit width can be treated theoretically. Nevertheless it was investigated how the half-width changes for small slit-widths. It is seen from fig. 23 that it tends to the same level as that found for small foil thicknesses. Of course, here a practical compromise has always to be made. As Ziegler[10]) points out, the slit width might not be exactly defined because electrons may penetrate the edge of the slit and by multiple scattering be restored to the beam. We have studied empirically whether the slit material affects the half-width of the primary line.

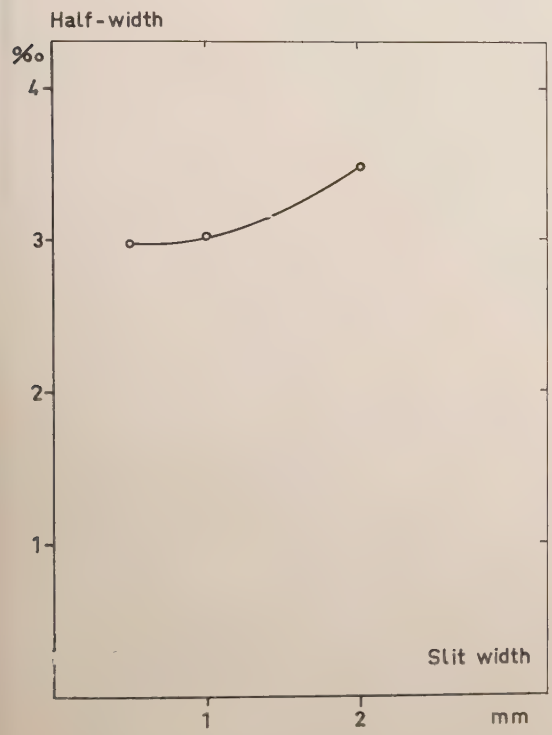

Fig. 23. Half-width as a function of slit widths (sum of entrance and exit slits)

Slits of aluminium and lead with thicknesses corresponding to the range of electrons in question were used. No difference in half-width at all could be detected. (3.50‰ was found in both cases under the particular conditions used in this experiment). In order to save space near the absorber position we have chosen to work with lead slits. It may be noted here that Goldwasser *et al.*[11]) used gold slits with the idea that those electrons colliding with the slit would be scattered out of the beam penetrating the spectrometer.

5.9. FORM OF THE PRIMARY LINE

The primary line shows some asymmetric character which is certainly due to the straggling in the windows and foils (Landau distribution). The form is very roughly triangular. The width at 10% of the peak height is 6.2‰ as compared with 5.2‰ if the triangular form is strictly valid (cf. fig. 9).

5.10. COMPARISON OF HALF-WIDTH WITH THEORY

The expected half-width can be discussed in the same manner as has been done by Siegbahn and Edvarson[12]) and in a previous paper by the present author[1]). From this discussion we might thus infer, approximately, the contribution of the betatron itself. The discussion is made in terms of base-width and is summarized in table 1 for three different energies.

The average difference found in table 1 may be taken to be 0.3‰. The dependence on energy might not be real. The magnitude is consistent with $\Delta t = 3$ μsec (eq. (5a)) and 55° phase angle.

This is in fact a very small contribution to the total distribution and is of the order estimated by Kerst[20]) for the contribution of the betatron oscillations. It must be remembered that the estimation of the straggling distribution is difficult indeed. It was made in the same way as in the previous paper by the author[1]) by using the Blunck and Leisegang theory[14]).

[11]) E. L. Goldwasser, F. S. Mills and A. O. Hansen, Phys. Rev. **88** (1952) 1137.

[12]) K. Siegbahn and K. Edvarson, Nuclear Physics **1** (1956) 137.

[13]) W. Paul and H. Reich, Z.f.Phys. **127** (1950) 429.

[14]) O. Blunck and S. Leisegang, Z.f.Phys. **128** (1950) 500.

TABLE 1

Estimation of contributions to the base-width $\Delta B\rho/B\rho$ of the betatron electron energy distribution. (Energy figures are taken from calibration curve given in[4].)

	Spectrometer current and energy		
	3.0 amp $E_0 = 1.75$ MeV	4.45 amp 2.78 MeV	6.0 amp 3.85 MeV
	‰	‰	‰
Slits	2.00	2.00	2.00
Spherical aberration	0.16	0.16	0.16
Aberrations in fringing field[1])	0.50	0.50	0.50
Straggling in the foils	4.12	2.80	2.06
Sum base width	6.78	5.46	4.72
Half of base width	3.39	2.73	2.36
Experiment	3.75	3.0	2.6
Difference	0.36	0.27	0.24

6. Conclusions

It can be concluded that the energy stability is better than $\pm$ 0.3‰ for at least 3–4 hours' operation and without any warming-up period. Further, the half-width of the primary line can be explained in terms of slit widths, spectrometer aberrations, straggling in windows and air gap. A residual energy spread of roughly 0.3‰ might be attributed to the betatron itself and is probably caused by the finite time of the ejection process but perhaps also by betatron oscillations.

In table 2, different workers' data for energy stability and half-width of the primary line are given. Only work intended for energy loss studies is included. Much work on energy stability in the literature is concerned with machines yielding electromagnetic radiation for nuclear reaction studies.

Acknowledgements

The author is indebted to Professor Ole Lamm, Head of The Institute, for his promotion of these studies and good working conditions. Prof. H. Alfvén, Drs. O. Wernholm and E. Smårs, Department of Electronics, are most heartily thanked for the gift of the betatron. The important design and construction work due to the latter persons will be clear from their own paper[5]). Mr. S. Kämpe has made a contribution of several years' difficult work to the rebuilding of the betatron

TABLE 2

	Paul-Reich 1950[13]) †	Goldwasser[11]) *et al.*	Ziegler[10])	Present work (2.8 MeV data)
				‰
Energy stability $\frac{\Delta B\rho}{B\rho}$		< 0.1 %		0.3
Energy stability ΔE(keV)		< 16 keV	10 keV	(1 keV)
Half-width of primary line	18 ‰ (2.8 MeV)			
	31 ‰ (4.5 MeV)	2.53 ‰	5.2 ‰	2.6 ‰
Part attributed to accelerator itself	18 keV 2.8 MeV	15 keV	—	0.3 ‰
	75 keV 4.5 MeV			(1 keV)

† Later the data of this machine have been improved[15]).

after its transfer to the present site. Without his patience and detailed examination of all conceivable components and functions of the accelerator, the final results would hardly have been obtained. Thanks are further due to Mr. B. Sjöstrand who has operated the machine and spectrometer since 1955 and has contributed much to the practical design and taken almost all experimental data reported in this paper. Mr. P. Pedersen has given many valuable contributions concerning electronic construction and measurements. Mr. R. Östling of the Electronics Division has made the very difficult glass-blowing work in a most skilful manner. The author is grateful indeed for correspondence with Dr. D. W. Kerst, now at General Atomic, San Diego, USA and for his kind permission to publish his points on the energy distribution problem.

[15]) H. Frank, Z.f.Naturforschung **12**a (1957) 750.
[16]) O. Wernholm, Ark. f. Fysik **5** (1952) 565–80.
[17]) O. Wernholm, Tekn. Tidskrift **76** (1946) 209.
[18]) T. Westermark, Trans. Instruments and Measurements Conference, Stockholm 1949, p. 308.
[19]) A. B. L. Whittler, Rev. Sci. Instr. **31** (1960) 208.
[20]) D. W. Kerst (personal communication).

NUCLEAR INSTRUMENTS AND METHODS **10** (1961) 164–168; NORTH-HOLLAND PUBLISHING CO.

MULTICHANNEL DETECTOR FOR USE IN PARTICLE SPECTROMETERS†

BENT ELBEK†† and MICHIYUKI NAKAMURA

Lawrence Radiation Laboratory, University of California, Berkeley, California

Received 10 November 1960

A 15-channel scintillation counter has been constructed for use in magnetic spectrometers with extended focal line. It utilizes 15 organic scintillators placed along the focal line. The scintillators are optically coupled in binary code to four photomultiplier tubes. The output pulses from these tubes are electronically converted into standard current pulses (weighted 1, 2, 4, 8) in a common resistor. The resulting voltage pulse is proportional to the position of the scintillator giving the light pulse, and can be displayed on a "kicksorter". The results of an experimental test of the multichannel electron detector are described. Further improvements are expected with use of a fifth multiplier tube in coincidence with the above mentioned tubes.

1. Introduction

Most magnetic spectrometers of the flat type have a focal line along which particles of various momenta are focused with good resolution. The length of the focal line depends on the type of spectrometer. Thus in magnetic spectrographs using photographic-plate detection, the ratio of maximum and minimum momenta focused can be as high as 5. In the various types of double-focusing spectrometers, the momentum range is less, typically of the order of 10% of the average momentum.

It is clear that the time required for taking data with a spectrometer is reduced considerably if information from several counters placed along the focal line can be taken in one run. Also there are advantages in recording as much as possible of a spectrum in one run, particularly when operating in conjunction with an accelerator or when recording particle spectra from rapidly decaying activities.

When placing several counters along a focal line, one encounters problems of space, and the external circuitry gets complicated as soon as more than a few counters are used. This is especially true for the application of scintillation detectors, in which even the smallest phototubes in connection with their light guides are large in comparison with the space available in most spectrometers.

This paper describes a 15-channel scintillation detector in which some of the problems mentioned above are solved by coding the light output of each scintillator into a binary system. The detector was constructed for use in a beta spectrometer of the wedge type[1,2]), but also should be useful for other spectrometers with a focal line or in angular-distribution equipment. The system of binary coding is of course applicable also to arrays of other types of detectors[3]).

2. The Spectrometer

The single-gap wedge spectrometer was of the type introduced by Koefoed-Hansen, Lindhard, and Nielsen[1,2])†. It has a source-to-detector distance of 32 cm which experimentally yields a dispersion D of about 75 cm measured along the focal line. (The dispersion D is defined by the

† This work was done under the auspices of the U.S. Atomic Energy Commission.

†† On leave from the Institute for Theoretical Physics, University of Copenhagen, Copenhagen, Denmark.

††† We are grateful to Dr. O. B. Nielsen for drawings of and information about a similar spectrometer built by him.

[1]) O. Koefoed-Hansen, J. Lindhard and O. B. Nielsen, Mat. Fys. Medd. Dan. Vid. Selsk. **25** No. 16 (1950).

[2]) O. B. Nielsen and O. Koefoed-Hansen, Mat. Fys. Medd. Dan. Vid. Selsk. **29** No. 6 (1955).

[3]) Binary coding of scintillation detectors has also been used in a particle hodoscope: L. W. Alvarez, Rev. Sci. Instr. **31** (1960) 76.

equation $\Delta p/p = \Delta s/D$, where Δp is a small change in the momentum p and Δs the corresponding movement of the image along the focal line.) The scintillator width of 4 mm thus

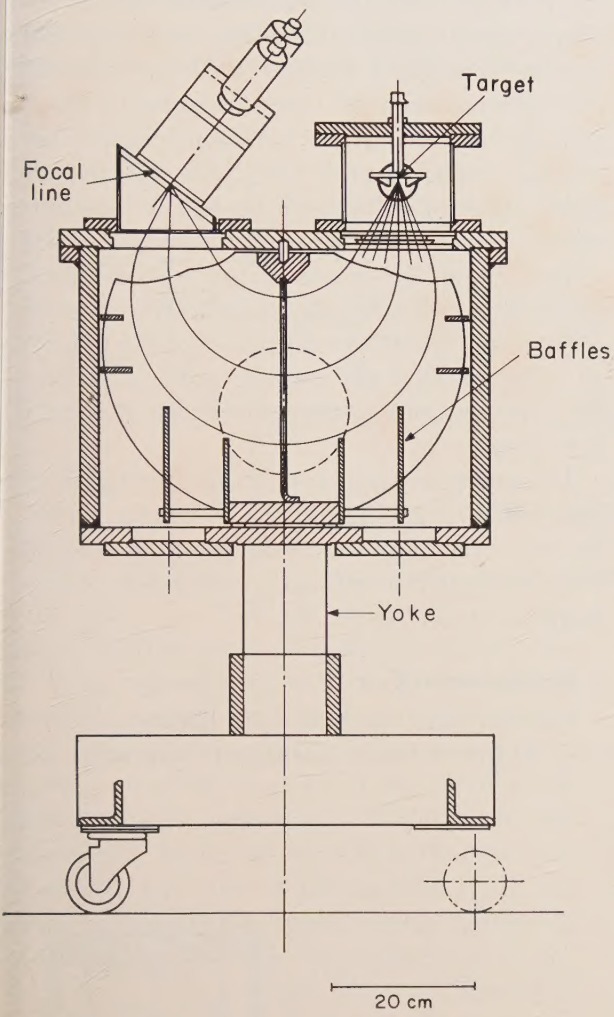

Fig. 1.
Wedge-gap beta spectrometer with multichannel counter.

corresponds to a momentum resolution of about 0.5%. This is somewhat large compared with the resolution of the spectrometer, which is about 1% under typical operating conditions. However, it was felt that the width of the individual scintillators could be reduced by baffles if necessary.

The inclination of the focal line with respect to the wedge axis was found to be about 38 deg. For convenience in construction, the scintillators were kept in air separated from the spectrometer vacuum by a 1 mg/cm² aluminized Mylar foil. Fig. 1 shows the general arrangement of the counter when placed in position on the spectrometer.

3. The Detectors

Organic scintillators were used; plastic in one unit, anthracene in another. The plastic has the advantage of being easy to machine to accurate dimensions, but the light output is smaller than for anthracene. As detection of low-energy electrons was essential for the experiments planned, anthracene was finally preferred. The size of the individual scintillators was 12 by 4 mm with a thickness of 3 mm, corresponding to the range of about 800-keV electrons. Crystals thinner than the range of the electrons gave an undesirable output-pulse spectrum.

Each scintillator was glued onto a light coupler of Lucite (fig. 2) with Epon Resin no. 820.

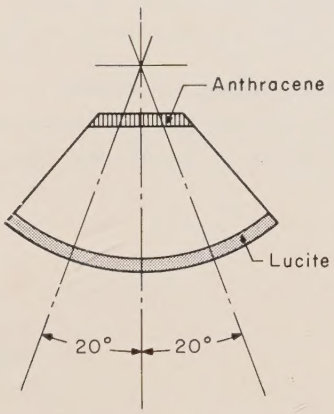

Fig. 2. Scintillator and light coupler.

4. The Code

Fifteen of the light couplers were placed side by side, separated by 0.02-mm aluminum foils. The curved bottom surface of the coupler assembly was aluminized by evaporation in a binary pattern as shown in fig. 3. This partly aluminized surface was then joined with Epon resin to an assembly consisting of four Lucite light pipes (fig. 4) numbered 1, 2, 4, and 8. The binary pattern was carefully aligned with respect to the light guides so that scintillator No. 1

gives light to light guide No. 1; scintillator No. 2 to light guide No. 2; scintillator No. 3 to light guides Nos. 1 and 2; and so on up to scintillator No. 15, which is open to all light guides. Each of the four light guides is optically coupled to an RCA 6655A photomultiplier tube. The tubes were specially selected for low noise.

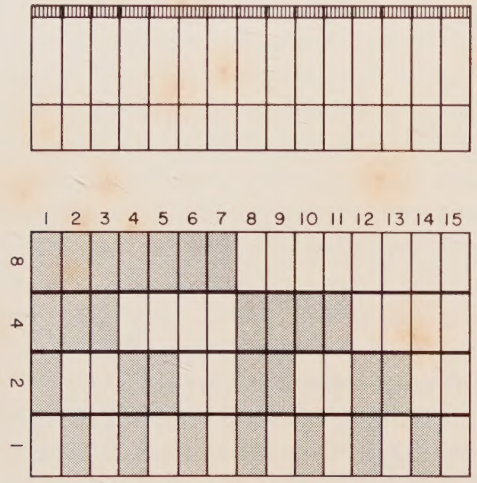

Fig. 3. Binary coding pattern on curved surface of the assembly of 15 lights couplers with scintillators.

5. Digital-to-Analog Conversion

A block diagram of the digital-to-analog converter is shown in fig. 5. The signal from each photomultiplier tube is amplified by a transistor amplifier having a gain of about 500. A simple discriminator cuts away low-energy pulses and noise. A standard one-shot multivibrator trigger circuit standardizes the pulses of the signals. The trigger-circuit signal cuts off the constant current flowing through a common-collector resistor. The currents from the constant-current sources add algebraically in the common resistor. The constant-current source and common-collector-resistor scheme is shown in fig. 6. The constant-current sources are adjusted to currents in the ratio 1:2:4:8, for example 1, 2, 4, and 8 mA. The voltage pulse developed across the common resistor is proportional to the sum of the weighted currents, thus the voltage pulse is proportional to the position of the scintillator giving the light pulse.

An emitter-follower is used for a low-output-impedance driver. The signal is further amplified by a vacuum-tube linear amplifier with an output compatible with our vacuum-tube pulse-height analyzer (Penco PA-4).

6. Experimental Test

The first unit was built with plastic scintillators. It proved the feasibility of the system but

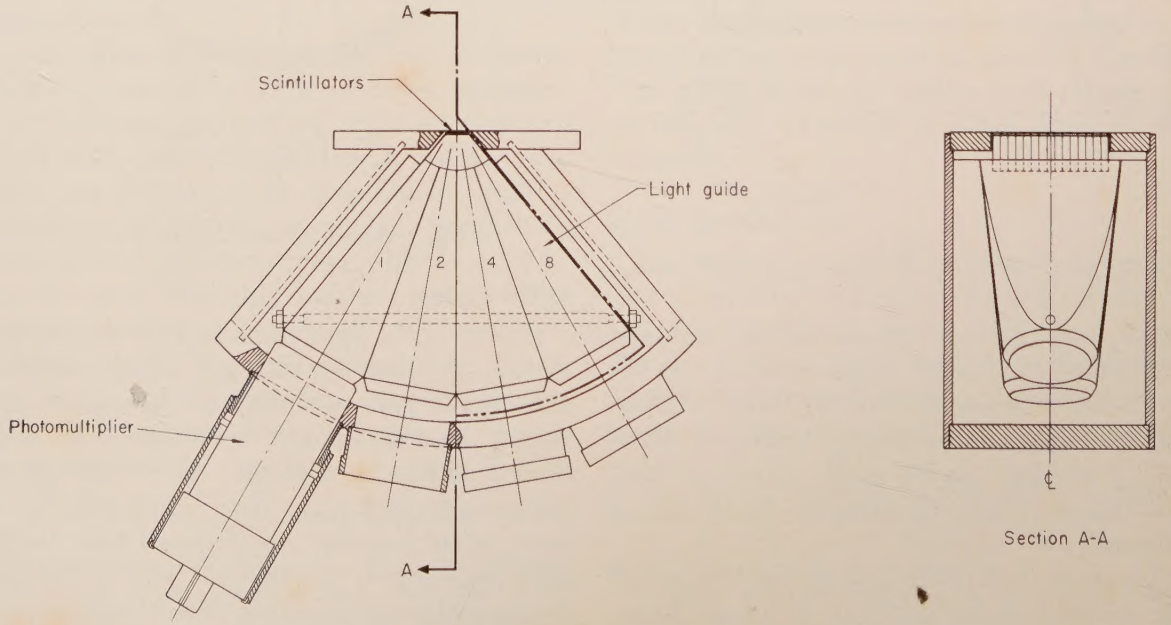

Fig. 4. Complete assembly of the multichannel counter.

so revealed a number of difficulties. As expected, the worst problem was to obtain equal sensitivity in all counters. It was found that the simplest way to check the sensitivity of each channel was to focus the flat maximum of a continuous beta spectrum on the counter by means of the spectrometer. Under these circumstances, the number of electrons per channel does not vary appreciably within the interval of about 8% momentum covered by the counter array, although there was a slight variation in counting rate from one end of the array to the other, probably reflecting a variation in the transmission of the spectrometer. That the variation was not due to the counter itself was proved by turning the counter assembly 180 deg.

Checked in this way, the sensitivity of the channels varied by up to 15% from the average. This result was obtained after some adjustment of the bias and high voltage on the phototubes. The nonuniformity in the counting rate was worst at low electron energies. Below an electron energy of about 200 keV it was difficult to obtain data with weak sources because of an increase of the general noise level. The noise was most prominent in Channels 1, 2, 4, and 8, which required a pulse in only one photomultiplier. Also there was a tendency for these channels to have a somewhat larger efficiency than the rest. This is probably related to the fact that owing to the complicated system of light collection, the pulse-height distribution from a single scintillator has a tail that extends down to zero pulse height with appreciable intensity. The bias on the phototubes therefore causes a certain loss of counts, e.g., 10%. The channels requiring only a single multiplier pulse then have 90% efficiency, those requiring two pulses have 81% efficiency, and so on. This effect was most pronounced for lower electron energies, and was almost absent above 500 keV.

The second unit, equipped with anthracene crystals, showed in general the same effects, but to a much smaller extent. With careful adjustment of the high voltage and the bias on each tube, the individual channels did not vary more than $\pm 5\%$ at an electron energy of 300 keV. Also this unit could work down to an electron

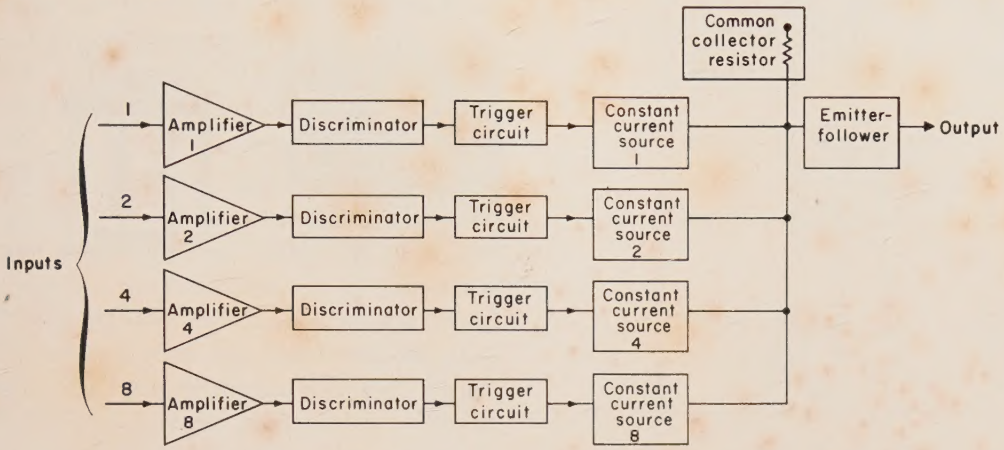

Fig. 5. Block diagram of digital-to-analog converter.

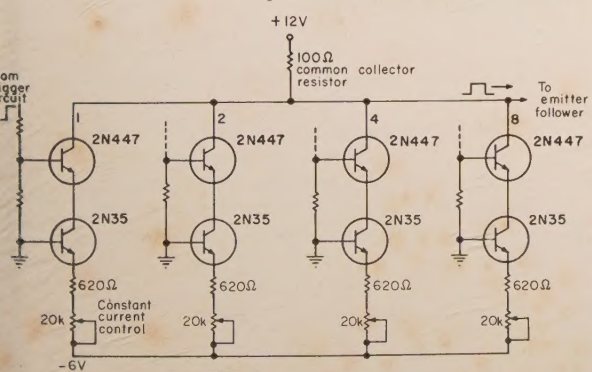

Fig. 6. Constant-current control circuits for adjusting weighted currents in common-collector resistor. The currents turned off in each circuit add algebraically in the common-collector resistor.

energy of about 100 keV without serious noise problems. Fig. 7 shows the Cs^{137} K and L peaks recorded in a single run on this counter.

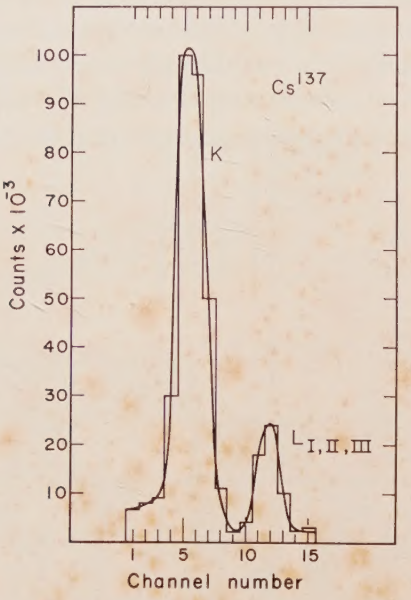

Fig. 7.
K- and L-conversion lines from the 662-keV transition in Cs^{137} recorded in a single run on the multichannel counter.

7. Further Improvements

We expect to be able to cure most of the difficulties encountered with the two units discussed above in a new unit presently under construction. In this device a fifth light guide and photomultiplier are introduced (referred to in the following as the coincidence multiplier). The light guide is placed between light guides 2 and 4 in fig. 3, and is open to all 15 scintillators. The signals from the coincidence multiplier are used to gate the combined signal obtained from the other multipliers. In this way several advantages are obtained:

(a) Tube noise is essentially eliminated by the coincidence requirement.

(b) Pulses produced by scintillations in the Lucite light guides are eliminated. Pulses of this origin may be partly responsible for a large increase in counting rate in Channels 1, 2, 4, and 8 observed when the detector is used in a heavy background of fast neutrons.

(c) In practice only one bias has to be adjusted, namely that on the coincidence multiplier. The biases on the other tubes can be set somewhat lower, with correspondingly smaller losses. As the coincidence channel treats all the pulses in very much the same manner, it is to be hoped that the counting rate will show only small variations from channel to channel.

(d) The detector is very well suited for operation in a fast coincidence setup, e.g., for detection of the beta spectrum in coincidence with alpha particles or gamma rays. A fast coincidence signal is easily derived from the coincidence tube.

Acknowledgements

It is a pleasure to acknowledge several helpful discussion, with Dr. Richard M. Diamond and Dr. John O. Rasmussen.

One of us (B.E.) wishes to acknowledge a Fulbright travel grant.